THERMOCHEMISTRY OF AQUEOUS SODIUM PHOSPHATE INTERACTIONS WITH METAL OXIDES IN HIGH TEMPERATURE WATER

CENTRE FOR NEWFOUNDLAND STUDIES

TOTAL OF 10 PAGES ONLY
MAY BE XEROXED

(Without Author's Permission)

SEAN EDWARD QUINLAN

THERMOCHEMISTRY OF AQUEOUS SODIUM PHOSPHATE INTERACTIONS WITH METAL OXIDES IN HIGH TEMPERATURE WATER

by

Sean Edward Quinlan

A thesis submitted to the

School of Graduate Studies

in partial fulfilment of the

requirements for the degree of

Master of Science

Department of Chemistry
Memorial University of Newfoundland

1996

St. John's Newfoundland

National Library of Canada
Acquisitions and Bibliographic Services Branch
395 Wellington Street
Ottawa, Ontario
K1A 0N4

Bibliothèque nationale du Canada
Direction des acquisitions et des services bibliographiques
395, rue Wellington
Ottawa (Ontario)
K1A 0N4

Your file Votre référence

Our file Notre référence

The author has granted an irrevocable non-exclusive licence allowing the National Library of Canada to reproduce, loan, distribute or sell copies of his/her thesis by any means and in any form or format, making this thesis available to interested persons.

L'auteur a accordé une licence irrévocable et non exclusive permettant à la Bibliothèque nationale du Canada de reproduire, prêter, distribuer ou vendre des copies de sa thèse de quelque manière et sous quelque forme que ce soit pour mettre des exemplaires de cette thèse à la disposition des personnes intéressées.

The author retains ownership of the copyright in his/her thesis. Neither the thesis nor substantial extracts from it may be printed or otherwise reproduced without his/her permission.

L'auteur conserve la propriété du droit d'auteur qui protège sa thèse. Ni la thèse ni des extraits substantiels de celle-ci ne doivent être imprimés ou autrement reproduits sans son autorisation.

ISBN 0-612-17637-1

Canada

To my parents

ABSTRACT

Most fossil-fired electrical power generating stations employ low concentrations of sodium phosphate to control boiler water pH. Sodium phosphate "hideout" has been identified as a cause of major corrosion problems in some stations. The objective of this work was to synthesize the principal iron reaction products, maricite and sodium iron (III) hydroxyphosphate, and to determine thermodynamic data pertinent to their formation in reactions of iron oxides with aqueous sodium phosphate under hydrothermal conditions.

Sodium iron(III) hydroxy phosphate (SIHP), $Na_3Fe(OH)(PO_4)_2 \cdot \frac{1}{2}NaOH$, is believed to be the major iron(III) reaction product causing sodium phosphate hideout. The compound was first reported in the early 1980's, from pressure vessel studies on hideout, and its stoichiometry was inferred from elemental analyses on solid reaction products and hydrothermal solutions during hideout experiments. Maricite, $NaFePO_4$, is the major iron(II) reaction product, and has been found both as a natural mineral and in previous phosphate hideout studies.

All syntheses of these solids were carried out at temperatures no higher than 250°C in 45 mL Parr 4744 Teflon-lined stainless steel reaction vessels. These vessels were modified to allow *in situ* filtration of reaction products at high temperature by simply turning the cells upside-down to drain the solution through a stainless steel mesh. Methods were successfully developed for synthesizing sodium iron(III) hydroxy phosphate from hematite, magnetite and iron phosphate, and maricite from iron powder at 95+% yield in these safe, rugged cells. A novel method for synthesizing maricite by thermally

decomposing the complex of aqueous iron(III) nitrilotriacetic acid at 250°C has also been developed

The crystal structure of SHP was determined and is consistent with observations on boiler corrosion product behavior. The crystal structure of maricite was also determined, and found to be identical to that of the natural mineral.

Solubility studies for SHP were carried out in a modified 450 mL Parr 4562 stirred reaction vessel fabricated from Hastelloy C. To avoid the need to control reduction potential, solubility experiments were carried out in the presence of hematite, according to the following reaction

$$\tfrac{1}{2}Fe_2O_3(s) + 13/3Na^+(aq) + 2HPO_4^{2-}(aq) + \tfrac{1}{3}OH^-(aq) \rightarrow$$
$$NaFe(PO_4)_2\cdot(Na_{4/3}H_{2/3}O)(s) + 5/6H_2O(l).$$

Results were obtained up to 325°C at a sodium/phosphate ratio of 2.5, and up to 260°C at a ratio of 3.0 before severe corrosion reactions terminated the experiments. Kinetic experiments approaching equilibrium from unsaturated and supersaturated conditions at 225°C confirmed that equilibrium had been achieved.

From this and previously reported data for the ionization of phosphoric acid, a thermodynamic database for the formation and release of the main iron (III) species under boiler conditions was developed.

ACKNOWLEDGEMENTS

I would like to thank Dr. Peter Tremaine for all his guidance and patience over the years, both as a graduate and undergraduate student. A more understanding and supportive supervisor would be impossible to find.

I am grateful to Dr. Melbourne Schriver and Dr. Murray Brooker for their help and advice while serving on my supervisory committee. I am also grateful to Dr. Charles Loader for his encouragement throughout my university career.

I would like to thank other members of our lab: Dr. Dmitri Shvedov, Caibin Xiao, Zhongning Wang and Dr. Hugo Bianchi for their useful discussions and advice.

Many people contributed to this work. Without their help, I would probably still be trying to get useful data. ICP ES analyses were done by Chris Finch and Peter Haring of the Newfoundland and Labrador Department of Mines and Energy, and the single crystal X-ray diffraction structures were solved by Dr. John Bridson and David Miller. Maggie Piranian provided training and much assistance with the powder X-ray diffraction. Carolyn Emerson provided training and advice in using the scanning electron microscope. The competent and professional assistance of the M.U.N. Machine Shop, and especially the assistance of Randy Thorne, Paul Martin, and Boyd Parsons was essential to this project. Eugene McNeill of Ontario Hydro Technologies provided assistance and constructive advice. I would also like to thank Carolyn Hawkins for her help with many of the figures in this thesis.

Financial support from NSERC/CEA Industrially Oriented Research Grant Program and a Memorial University Graduate fellowship are gratefully acknowledged. The pressure

vessel equipment used for the work was provided by an NSERC capital equipment grant.

I would also like to thank all my roommates and friends, without whose help and encouragement, I would have finished this project at least a year earlier.

Finally, and most importantly, I would like to thank my parents, Edward and Diane, and my sister, Kelly, for all their support. I love them dearly.

CONTENTS

Section			Page
	ABSTRACT		iii
	ACKNOWLEDGEMENTS		v
	LIST OF FIGURES		ix
	LIST OF TABLES		xii
	LIST OF SYMBOLS		xiii
1.0	INTRODUCTION		1
	1.1	Phosphate Hideout in Steam Generators	1
	1.2	Standard State Properties of Aqueous Species and Solids	3
		1.2.1 Solids	3
		1.2.2 Aqueous Species	6
	1.3	Activity Coefficients in High Temperature Water	8
	1.4	The Na_2O-P_2O_5-H_2O System	13
	1.5	Magnetite-Phosphate Interactions	23
		1.5.1 Hideout Reaction Simulations	23
		1.5.2 Magnetite Reaction Products	24
		1.5.3 Phosphate Hideout in Magnetite Corrosion Product Deposits	27
2.0	EXPERIMENTAL		31
	2.1	Chemicals and Materials	31
	2.2	Apparatus	32
		2.2.1 Teflon-Lined Filtration Cells	32
		2.2.2 Stirred Reaction Vessel	34
	2.3	Analytical Methods	36
		2.3.1 Powder X-Ray Diffraction	36
		2.3.2 Single Crystal X-Ray Diffraction	37
		2.3.3 ICP Emission Spectroscopy	38
		2.3.4 Electron Microscopy	40
	2.4	Synthesis and Characterization of Hideout Reaction Products	40
		2.4.1 Experimental Design	40
		2.4.2 Syntheses of Sodium Iron Hydroxy Phosphate ("SIHP")	42
		2.4.2.1 Iron Phosphate Experiments	42
		2.4.2.2 Hematite Experiments	43
		2.4.2.3 Magnetite Experiments	44
		2.4.3 Syntheses of Maricite	45
		2.4.3.1 Iron Powder Experiments	45
		2.4.3.2 Iron Nitriloacetate (FeNTA) Experiments	45

2.5 Solubility Measurements in the Stirred Reaction Vessel ... 47
2.5.1 Kinetics ... 47
2.5.2 Solubility ... 49
2.5.3 Recovery of the Equilibrium Solid Reaction Product ... 52

3.0 SYNTHESIS OF HIDEOUT REACTION PRODUCTS ... 53
3.1 The Iron (III) Product: "$Na_4FeOH(PO_4)_2 \cdot \frac{1}{2}NaOH$" ... 53
3.2 The Iron (II) Product: $NaFePO_4$ ... 66
3.2.1 The Iron Powder Synthesis ... 66
3.2.2 The FeNTA Reactions ... 69
3.3 The Crystal Structures of the Iron (III) and Iron (II) Products ... 75

4.0 SOLUBILITY ... 83
4.1 Kinetics of Phosphate-Hematite Reaction ... 83
4.2 Solubility of the Iron (III) Product ... 88
4.3 A Thermodynamic Model ... 91
4.3.1 Activity Coefficient Model ... 91
4.3.2 Phosphate Ionization Equilibria ... 92
4.3.3 Equilibrium Constants SIHP ... 101
4.4 Comparison With Data From Other Workers ... 106
4.4.1 Background ... 106
4.4.2 Sodium Iron Hydroxy Phosphate (SIHP) at 360°C ... 110
4.4.3 Maricite at 320 and 360°C ... 110
4.5 Discussion ... 113
4.6 Future Work ... 115

5.0 CONCLUSIONS ... 117

6.0 BIBLIOGRAPHY ... 119

7.0 APPENDIX I: X-RAY DIFFRACTION RESULTS ... 133

8.0 APPENDIX II: THE X-RAY CRYSTAL STRUCTURE OF SODIUM IRON HYDROXY PHOSPHATE (SIHP) AND MARICITE ... 141

9.0 APPENDIX III: KINETIC AND SOLUBILITY DATA FOR SODIUM IRON HYDROXY PHOSPHATE FORMATION EQUILIBRIA WITH HEMATITE ... 160

LIST OF FIGURES

Figure		Page
1.1	Mean activity coefficients for 1:1 electrolytes at various temperatures	10
1.2	Mean activity coefficients for 1:2 electrolytes at various temperatures, and the Debye Huckel limiting law	11
1.3	The solubility and equilibrium phases of disodium phosphate, Na_2HPO_4, as a function of temperature	16
1.4	The solubility and equilibrium phases of trisodium phosphate, Na_3PO_4, as a function of temperature	17
1.5	Two-liquid phase and solid-solution boundaries for aqueous solution mixtures of sodium phosphate salts of mole ratios $1.00 \leq Na/P \leq 3.00$ at 200-400°C	19
1.6	Sodium-phosphate-water phase behavior at 300°C	21
1.7	Solubility of trisodium phosphate in sodium hydroxide solutions	22
1.8	Summary of phosphate hideout reactions with magnetite at 320 and 350°C	29
2.1	Schematic diagram of Parr 45 mL Teflon-lined reaction vessels	33
2.2	Schematic diagram of Parr 450 mL stirred reaction vessel	35
2.3	Experimental design for stirred reaction vessel experiments	50
3.1	Scanning electron micrographs of solid reaction products obtained from iron phosphate and aqueous sodium phosphate (Na/P=2.15) at 250°C for three weeks	58
3.2	Determination of weight percent hematite in Sodium Iron Hydroxy Phosphate (SIHP)	60

3.3	Scanning electron micrographs of solid reaction products obtained from hematite and aqueous sodium phosphate (Na/P 2.5) at 250°C for three weeks	62
3.4	Scanning electron micrographs of solid reaction products obtained from magnetite and aqueous sodium phosphate (Na/P 2.15) at 250°C for three weeks	64
3.5	Scanning electron micrographs of solid reaction products obtained from magnetite and aqueous sodium phosphate (Na/P=2.5) at 320°C for two weeks	67
3.6	Scanning electron micrographs of solid starting materials	68
3.7	Scanning electron micrographs of solid reaction products obtained from iron powder and aqueous sodium phosphate (Na/P=1.0) at 250°C for three weeks	70
3.8	Scanning electron micrographs of solid reaction products obtained from FeNTA and aqueous sodium phosphate (Na/P=2.15) at 250°C for one week	72
3.9	Scanning electron micrographs of solid reaction products obtained from magnetite and aqueous sodium phosphate (Na/P=1.0 and 1.5) at 320°C for three weeks	73
3.10	Scanning electron micrographs of solid reaction products obtained from FeNTA and aqueous sodium phosphate (Na/P=2.15) at 205°C for three weeks	74
3.11	Scanning electron micrographs of solid reaction products obtained from magnetite and aqueous sodium phosphate	77
3.12	Crystal structure of SIHP	79
4.1	Kinetics of precipitation of SIHP at 250°C	84
4.2	Kinetics of precipitation and redissolution of SIHP at 225°C	85
4.3	Solubility of known hideout reaction products	90

4.4	Phosphate ionization equilibria	98
4.5	Comparison of experimental and predicted Q_r for the ionization of $H_2PO_4^{2-}$ (aq)	100
4.6	$\Delta_f G^\circ$(SHP) versus temperature	103
4.7	$\Delta_r G^\circ$ for the formation of SHP from hematite versus temperature	104
4.8	Comparison of log K from previous studies and calculated values using the model developed in this work	109
4.9	Equilibrium activities of aqueous hydrogen, a(H$_2$), for magnetite and various hideout products	114

LIST OF TABLES

Table		Page
3.1	Summary of synthetic runs in Teflon-lined filtration cells	54
3.2	Summary of data from XRD quantitative analysis	61
3.3	ICP-ES elemental analysis of SIHP from different synthetic routes	65
3.4	Positional parameters of SIHP	78
4.1	Standard state properties at 25°C and 1 bar	93
4.2	HKF equation of state coefficients for aqueous species	94
4.3	Maier-Kelley coefficients for heat capacities of solids	95
4.4	Standard state properties of the first ionization reaction of phosphoric acid	96
4.5	Standard state properties of the second ionization reaction of phosphoric acid	97
4.6	Standard state properties of the third ionization reaction of phosphoric acid	98
4.7	Standard state properties of the reaction of hematite and aqueous sodium phosphate to produce SIHP	105
4.8	Standard state properties of the reaction of magnetite and aqueous sodium phosphate to produce SIHP	108
4.9	Solubility data from flow experiments at 320°C at the Alberta Research Council	112

LIST OF SYMBOLS

Symbol		Unit
A	Arrhenius equation fitting parameter	$mol^{2} kg^{2} hr^{-1} m^{-3}$
C_p°	Standard molar heat capacity	$cal\ mol^{-1} K^{-1}$
$\Delta_a C_p^\circ$	Apparent molar heat capacity of formation	$cal\ mol^{-1} K^{-1}$
$\Delta_f C_p^\circ$	Standard molar heat capacity of formation	$cal\ mol^{-1} K^{-1}$
$\Delta_r C_p^\circ$	Standard molar heat capacity of reaction	$cal\ mol^{-1} K^{-1}$
E_a	Energy of activation	$cal\ mol^{-1}$
G°	Standard molar Gibbs energy	$cal\ mol^{-1}$
$\Delta_a G^\circ$	Apparent molar Gibbs energy of formation	$cal\ mol^{-1}$
$\Delta_f G^\circ$	Standard molar Gibbs energy of formation	$cal\ mol^{-1}$
$\Delta_r G^\circ$	Standard molar Gibbs energy of reaction	$cal\ mol^{-1}$
H°	Standard molar enthalpy	$cal\ mol^{-1}$
$\Delta_a H^\circ$	Apparent molar enthalpy of formation	$cal\ mol^{-1}$
$\Delta_f H^\circ$	Standard molar enthalpy of formation	$cal\ mol^{-1}$
$\Delta_r H^\circ$	Standard molar enthalpy of reaction	$cal\ mol^{-1}$
I	Ionic strength	$mol\ kg^{-1}$
K	Equilibrium constant	
P	Pressure	bar
P_r	Reference pressure	bar
Q	Equilibrium quotient	

Q_r	Equilibrium quotient of activity coefficients	
Q_{Born}	Born coefficient for standard molar volume	
R	Molar gas constant	1.9872 cal mol^{-1} K^{-1}
S°	Standard molar entropy	cal mol^{-1}
$\Delta_a S^\circ$	Apparent molar entropy of formation	cal mol^{-1}
$\Delta_f S^\circ$	Standard molar entropy of formation	cal mol^{-1}
$\Delta_r S^\circ$	Standard molar entropy of reaction	cal mol^{-1}
T	Temperature	°C, K
T_r	Reference temperature	25°C, 298.15 K
V°	Standard molar volume	cm^3 mol^{-1}
V_w	Partial molar volume of water in solution	cm^3 mol^{-1}
$\Delta_a V^\circ$	Apparent molar volume	cm^3 mol^{-1}
$\Delta_f V^\circ$	Standard molar volume of formation	cm^3 mol^{-1}
$\Delta_r V^\circ$	Standard molar volume of reaction	cm^3 mol^{-1}
X_{Born}	Born coefficient for standard molar heat capacity	
Z	Ionic charge	
a	Maier-Kelley fitting parameter	cal mol^{-1} K^{-1}
$a(A_i)$	Activity of species A_i	mol kg^{-1}
a_1	HKF fitting parameter for V°	cal mol^{-1} bar^{-1}
a_2	HKF fitting parameter for V°	cal mol^{-1}

a_3	HKF fitting parameter for V°	cal K mol^{-1} bar^{-1}
a_4	HKF fitting parameter for V°	cal K mol^{-1}
a_{ox}	Oxide surface area	m^2
a_w	Activity of water	
b	Maier-Kelley fitting parameter	cal mol^{-1} K^{-2}
c	Maier-Kelley fitting parameter	cal K mol^{-1}
c_1	HKF fitting parameter for C_p°	cal mol^{-1} K^{-1}
c_2	HKF fitting parameter for C_p°	cal K mol^{-1}
cal	Defined calorie (National Institute of Standards and Technology)	4.1840 J
d_{H2O}	Density of water	g cm^{-3}
k	Rate constant	mol^{-2} kg^2 hr^{-1} m^{-2}
m	Molality	mol kg^{-1}
m(PO_4, sat)	Equilibrium phosphate molality	mol kg^{-1}
m(PO_4, t)	Phosphate molality at time, t	mol kg^{-1}
m(PO_4, t=0)	Initial phosphate molality	mol kg^{-1}
n	Regression fitting parameter	
r_e	Effective ionic radius	m
r_{cryst}	Crystallographic ionic radius	m
v_1	HKF fitting parameter for V° at constant pressure	cm^3 mol^{-1}
v_2	HKF fitting parameter for V° at constant temperature	cm^3 K mol^{-1}

θ	HKF solvent dependent parameter for temperature	228 K
γ	Activity coefficient	
γ	Stoichiometric mean activity coefficient	
ε	Dielectric constant of water	
η	Product of physical constants of Born equation	6.9466 J m^{-1} mol^{-1}
ϕ	Osmotic coefficient of water	
ψ	HKF solvent parameter for pressure	2600 bar
ω	Conventional electrostatic Born parameter, $\omega(H^+)=0$	cal mol^{-1}

1.0 INTRODUCTION

1.1 Phosphate Hideout in Steam Generators

Sodium phosphate is added to the feed water of fossil-fired utility boilers at parts-per-million levels to control corrosion and scale. A continuing problem associated with phosphate treatment is "hideout" (Stodola, 1991, 1986), characterized by the retention of phosphate in the boiler during operation at high load, and the subsequent release of phosphate into boiler water under low-load conditions. The uptake and release of phosphate at local sites can be accompanied by large excursions to high and low pH, leading to metal wastage and cracking. Hideout is aggravated in modern, high performance drum-boilers which operate at temperatures up to 360°C.

Before 1995, Electric Power Research Institute (EPRI) guidelines for phosphate chemistry control (Ashoff, 1986) recommended that the ratio of Na/PO_4 in boiler water be maintained in the range 2.2 to 2.8. This method of "congruent" phosphate treatment with "invariant-point control" (Panson et al., 1975) is based on detailed information for the pure sodium-phosphate-water phase diagram (Panson et al., 1975, Taylor et al., 1979, Ravich et al., 1955; Broadbent et al., 1977). Within this range, cyclic precipitation and dissolution of phosphate salts should not cause large excursions in pH. In practice, however, boilers can rarely be operated under congruent chemical conditions (Stodola, 1991, 1986). Accumulating evidence indicates that this occurs because the sodium phosphate interacts with components present in the boiler sludge, particularly magnetite

(Stodola, 1991, 1986; Broadbent et al., 1978; Economy et al , 1975; Conner and Panson, 1983, Jonas, 1985, Balakrishnan, 1977, Straub, 1950; Wetton, 1981). EPRI has now revised its guidelines (Dooley, 1994) to reflect the results of successful operating experience at Ontario Hydro and other utilities with "equilibrium" phosphate treatments and the results of new experimental work (Tremaine et al., 1992, 1993; Ziemniak et al., 1992)

The effect of interactions with metal oxides on sodium phosphate solution chemistry has been studied in some detail by Economy et al. (1975) and Connor and Panson (1983) at temperatures up to 315°C. Their work showed that the reactivity of metal oxides causes very significant deviations from the hideout behaviour associated with the pure sodium-phosphate-water phase diagram. However, modern fossil steam generators operate at temperatures and pressures that approach the critical point of water (373°C and 221 bar). Recent work in our laboratory (Tremaine et al., 1993) has extended the experiments of Connor and Panson up to 360°C for magnetite and three of the major components of sludge, Cu, NiO, and ZnO. The solid products and mechanisms of the magnetite hideout reactions have been identified from experiments in static vessels. The results are consistent with experiments on sludge samples from Ontario Hydro's Nanticoke Generating Station.

The two principal phases involved in phosphate hideout reactions with magnetite are sodium iron (III) hydroxy phosphate, "$Na_4Fe^{III}OH(PO_4)_2 \cdot \frac{1}{3}NaOH$" , and maricite, $NaFe^{II}PO_4$. The structural and thermodynamic properties of these compounds are not well

known. The purpose of this research is to develop methods for synthesizing both compounds, and to measure accurate solubility data for "$Na_3Fe^{III}OH(PO_4)_2 \cdot \frac{1}{3}NaOH$", so that a useful thermodynamic database can be developed

1.2 Standard State Properties of Aqueous Species and Solids

1.2.1 Solids

Equilibrium constants, K, for the formation of solid reaction products may be calculated from the standard Gibbs energies of formation of the solid, aqueous and gaseous reactants and products. The temperature and pressure dependence of the equilibrium constant is described by the standard enthalpies, heat capacities and volumes of formation, according to the following equations

The standard Gibbs energies and enthlapies of formation at high temperature and pressure are defined in terms of the formation of the species or compound from the elements in their reference states at the same temperature and pressure For the hypothetical formation reaction of A_2B from the elements A and B, Gibbs energies and enthalpies of formation at high temperature and pressure are defined as

$$\Delta_f G^o_{A_2B,T,P} = G^o_{A_2B,T,P} - 2G^o_{A,T,P_r} - G^o_{B,T,P_r} \qquad (1.1)$$

$$\Delta_f H^o_{A_2B,T,P} = H^o_{A_2B,T,P} - 2H^o_{A,T,P_r} - H^o_{B,T,P_r} \qquad (1.2)$$

where P_r is the reference pressure, 1 bar. The high temperature values of these properties

are calculated from values at 298.15 K and 1 bar through the heat capacity change of formation $\Delta_f C_{p,f}^{\circ}$ and from the volume change ΔV_{Tr}°:

$$\Delta_f G_{T,P}^{\circ} = \Delta_f G_{T_r,P_r}^{\circ} - \Delta_f S_{T_r,P_r}^{\circ}(T - T_r) + \int_{T_r}^{T} \Delta_f C_p^{\circ} dT - T\int_{T_r}^{T} \Delta_f C_p^{\circ}/T \, dT + \int_{P_r}^{P} \Delta V^{\circ} dP \quad (1.3)$$

Volume is assumed to be constant in Equation (1.3) due to the fact that ionic solids have only slight variation in volume with temperature and pressure, so that very little error is introduced by this assumption.

The heat capacities of solids, liquids, and gases are commonly described by the Maier-Kelley equation (1932)

$$C_p^{\circ} = a + bT - cT^{-2} \quad (1.4)$$

Expressions for the heat capacities and volume functions for aqueous species are more complex. These are described in the following section.

Standard Gibbs free energies and enthalpies of formation are used extensively by chemists; however, the calculation of $\Delta_f G_{T,P}^{\circ}$ requires a knowledge of the heat capacity, entropy, and volume of the elements in their reference states at the temperature and pressure of interest. There may be discontinuities in the properties of the elements at the temperatures where phase changes occur, which make the calculation difficult. Since the properties of the elements cancel in the expressions for balanced reactions, Benson (1968)

and Helgeson et al. (1978) have recommended the use of so-called "apparent" Gibbs energies of formation, $\Delta_a G_{T,P}^\circ$. These are defined in terms of the reactions from compounds at T and P from the elements in their reference states at 298.15K and 1 bar. Thus the definitions of free energies and enthalpies become

$$\Delta_a G^o_{A_2B,T,P} = G^o_{A_2B,T,P} - 2G^o_{A,T_r,P_r} - G^o_{B,T_r,P_r} \qquad (1.5)$$

$$\Delta_a H^o_{A_2B,T,P} = H^o_{A_2B,T,P} - 2H^o_{A,T_r,P_r} - H^o_{B,T_r,P_r} \qquad (1.6)$$

Equations (1.5) and (1.6) can also be written

$$\Delta_a G^o_{A_2B,T,P} = \Delta_f G^o_{A_2B,T_r,P_r} + (G^o_{A_2B,T,P} - G^o_{A_2B,T_r,P_r}) \qquad (1.7)$$

$$\Delta_a H^o_{A_2B,T,P} = \Delta_f H^o_{A_2B,T_r,P_r} + (H^o_{A_2B,T,P} - H^o_{A_2B,T_r,P_r}) \qquad (1.8)$$

The temperature dependence of $\Delta_a G_{T,P}^\circ$ is given by the expression

$$\Delta_a G^o_{T,P} = \Delta_f G^o_{T_r,P_r} - S^o_{T_r,P_r}(T - T_r) + \int_{T_r}^{T} C_p^o dT - T\int_{T_r}^{T} C_p^o/T\, dT + \int_{P_r}^{P} V^o dP \qquad (1.9)$$

Equilibrium constants are related to the Gibbs energies of reaction $\Delta_r G_{T,P}^\circ$ by the

following equations

$$\Delta_r G^o = -RT\ln K \tag{1.10}$$

$$\begin{aligned}\Delta_r G_T^o &= \sum \Delta_a G_T^o\,(products) - \sum \Delta_a G_T^o\,(reactants) \\ &= \sum \Delta_f G_T^o\,(products) - \sum \Delta_f G_T^o\,(reactants)\end{aligned} \tag{1.11}$$

1.2.2 Aqueous Species

By definition, Equations 1.3 and 1.9 require the use of the standard partial molar heat capacity and standard partial molar volume, $C_{p,2}^\circ$ and V_2° for aqueous species. The temperature dependence of standard partial molar properties for aqueous species is controlled by ion-water interactions. These may be modelled by the semi-empirical functions originally proposed by Helgeson, Kirkham and Flowers (1981), the "HKF" equations, as revised by Tanger and Helgeson (1988). At constant pressure,

$$C_{p,2}^o = c_1 + \{\ c_2/(T-\Theta)^2\ \} + \omega T X_{Born} \tag{1.12}$$

$$V_2^o = v_1 + \{\ v_2/(T-\Theta)\ \} - \omega Q_{Born} \tag{1.13}$$

Here, the terms c_1, c_2, v_1 and v_2 are species-dependent fitting parameters, Θ = 228 K is a solvent-dependent parameter. The terms $\omega T X_{Born}$ and ωQ_{Born} are the electrostatic contributions to the standard molar heat capacity and standard molar volume according to the Born equation, in which X_{Born}, Q_{Born} and ω are given by

$$Q_{Born} = \varepsilon^{-1} (\partial \ln \varepsilon / \partial p)_T \qquad (1.14)$$

$$X_{Born} = \varepsilon^{-1} [(\partial^2 \ln \varepsilon / \partial T^2)_p - (\partial \ln \varepsilon / \partial T)_p^2] \qquad (1.15)$$

and

$$\omega = Z^2 \eta / r_e \qquad (1.16)$$

where ε is the static dielectric constant of water, $\eta = 0.9466 \cdot 10^5$ J·m^{-1}·mol^{-1}, Z is ionic charge, and r_e is an effective electrostatic radius of the ion ($r_e = r_{cryst} + 0.94\,Z$ for cations; $r_e = r_{cryst}$ for anions) (Shock and Helgeson, 1988). Values for X_{Born} and Q_{Born} were taken from Helgeson and Kirkham (1976).

Neglecting the pressure dependence of ω, the full expressions to describe the variations in C_p° and V° with temperature and pressure take the form

$$\bar{C}_P^o = c_1 + \frac{c_2}{(T-\Theta)^2} - \frac{2T}{(T-\Theta)^3}\left[a_3(P-P_r) + a_4 \ln \frac{\psi + P}{\psi + P_r}\right] + \omega T X_{Born} \qquad (1.17)$$

$$\bar{V}^o(T,P) = a_1 + \frac{a_2}{\psi + P} + \left(a_3 + \frac{a_4}{\psi + P}\right)\left(\frac{1}{T - \Theta}\right) - \omega Q_{Born} \qquad (1.18)$$

Here a_1, a_2, a_3 and a_4 are species-dependent fitting parameters; ψ is a solvent parameter equal to 2600 bar. Xiao and Tremaine (1994) have made a preliminary assessment of the

application of more detailed semi-continuum solvation models by Abraham and Marcus (1986), Abraham et al. (1983), Goldman and Bates (1972) and others. While not complete, the calculations confirm that standard-state and other terms arising from a rigorous treatment of the solvation cycle are small relative to the contribution of configurational hydration to the empirical terms in Equations 1.7, 1.8 and 1.12 at temperatures well-removed from 25°C.

The equations cited above form the basis for the thermodynamic modelling code Supcrt'92 (Johnson et al., 1992). Supcrt'92 is an interactive Fortran 77 program with a thermodynamic database containing many minerals, gases, and aqueous species. The theoretical basis and its practical implementation for the model in this program have been described by Helgeson and Kirkham (1974, 1976), Helgeson et al. (1978, 1981), Tanger and Helgeson (1988), Shock and Helgeson (1988) and Shock et al. (1992). Equations of state for the thermodynamic properties and dielectric constant of water were taken from Haar et al. (1984).

1.3 Activity Coefficients in High Temperature Water

A model for the activity coefficients of the aqueous species is required to describe solubility equilibria at finite molalities. For example, for the reaction

$$A_2B \rightleftharpoons 2A^{+}(aq) + B^{2-}(aq) \qquad (1.19)$$

$$Q = m(A^{+}, aq)^{2} \cdot m(B^{2-}, aq) / a(A_2B) \qquad (1.20)$$

where Q is the equilibrium quotient, and a (A_2B) is the activity of the solid, which is usually unity.

$$K = m(A^{+}, aq)^{2} \cdot \gamma(A^{+}, aq)^{2} \cdot m(B^{2-}, aq) \cdot \gamma(B^{2-}, aq) / a(A_2B) \qquad (1.21)$$

$$\log K = \log Q + \log [\gamma(A^{+}, aq)^{2} \cdot \gamma(B^{2-}, aq) / a(A_2B)] \qquad (1.22)$$

The activity coefficients reflect the effect of ion-ion interactions. At low temperatures, these are very specific for each ion and relatively complex semi-empirical models are required to describe the activity coefficients and other excess properties (Pitzer, 1991). At temperatures above about 150°C, the long range hydration effects that control the specific nature of ion-ion interactions are weakened, and ions of the same charge display much more consistent behaviour. An example from the detailed experimental work by Holmes and Mesmer (1983) is given in Figures 1.1 and 1.2. Lindsay (1989) and Helgeson (1969) have proposed the use of a "model substance" approach in this region, whereby the activity coefficients at a given ionic strength are assumed to be equal to those of sodium chloride. Lindsay's model is used in the EPRI computer code MULTEQ (Lindsay, 1989) which is used to describe crevice corrosion in high pressure boilers and, for this reason, was considered most appropriate for this study.

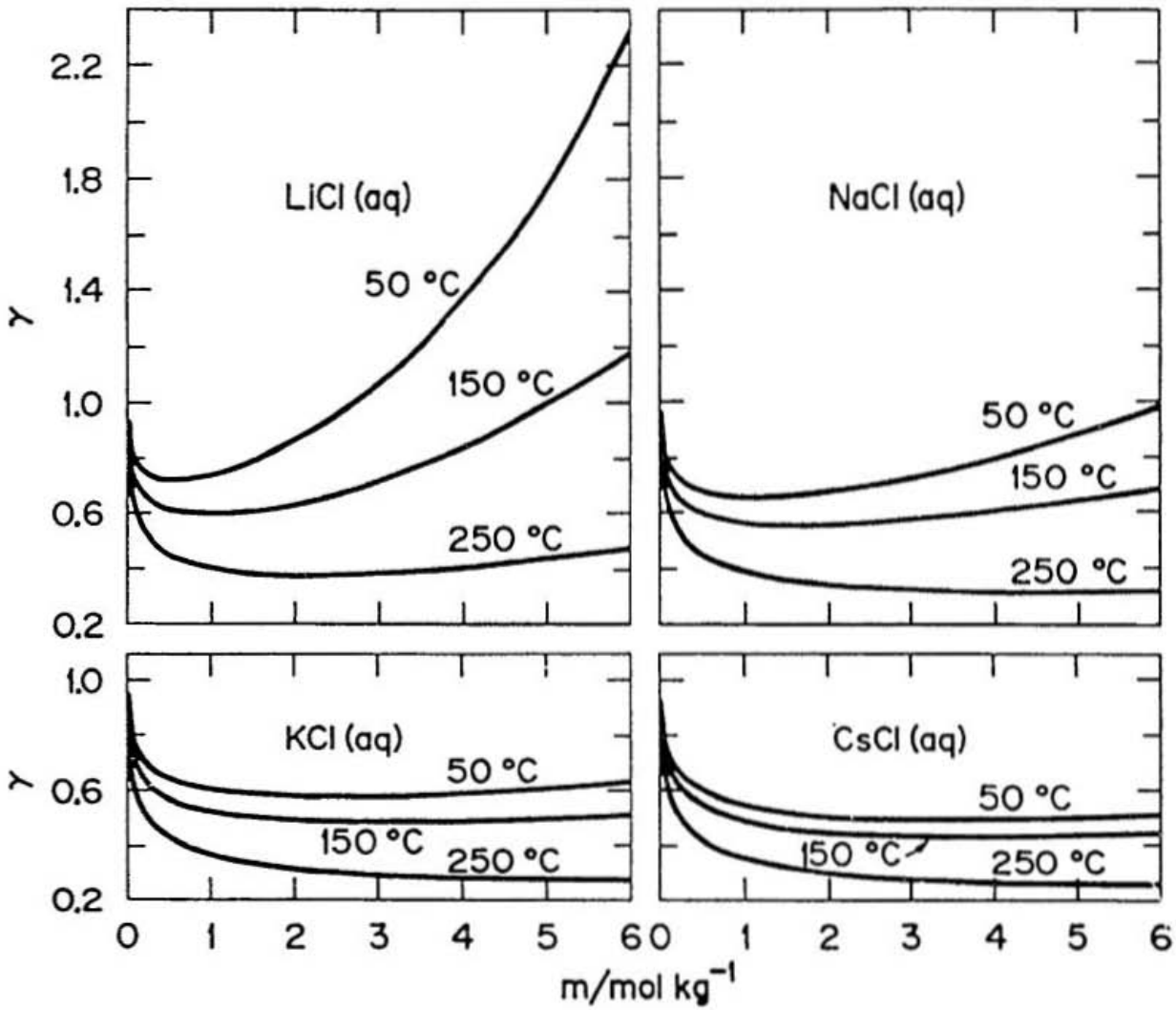


Figure 1.1 Mean activity coefficients for 1:1 electrolytes at various temperatures (Holmes and Mesmer, 1983; Pitzer, 1991)

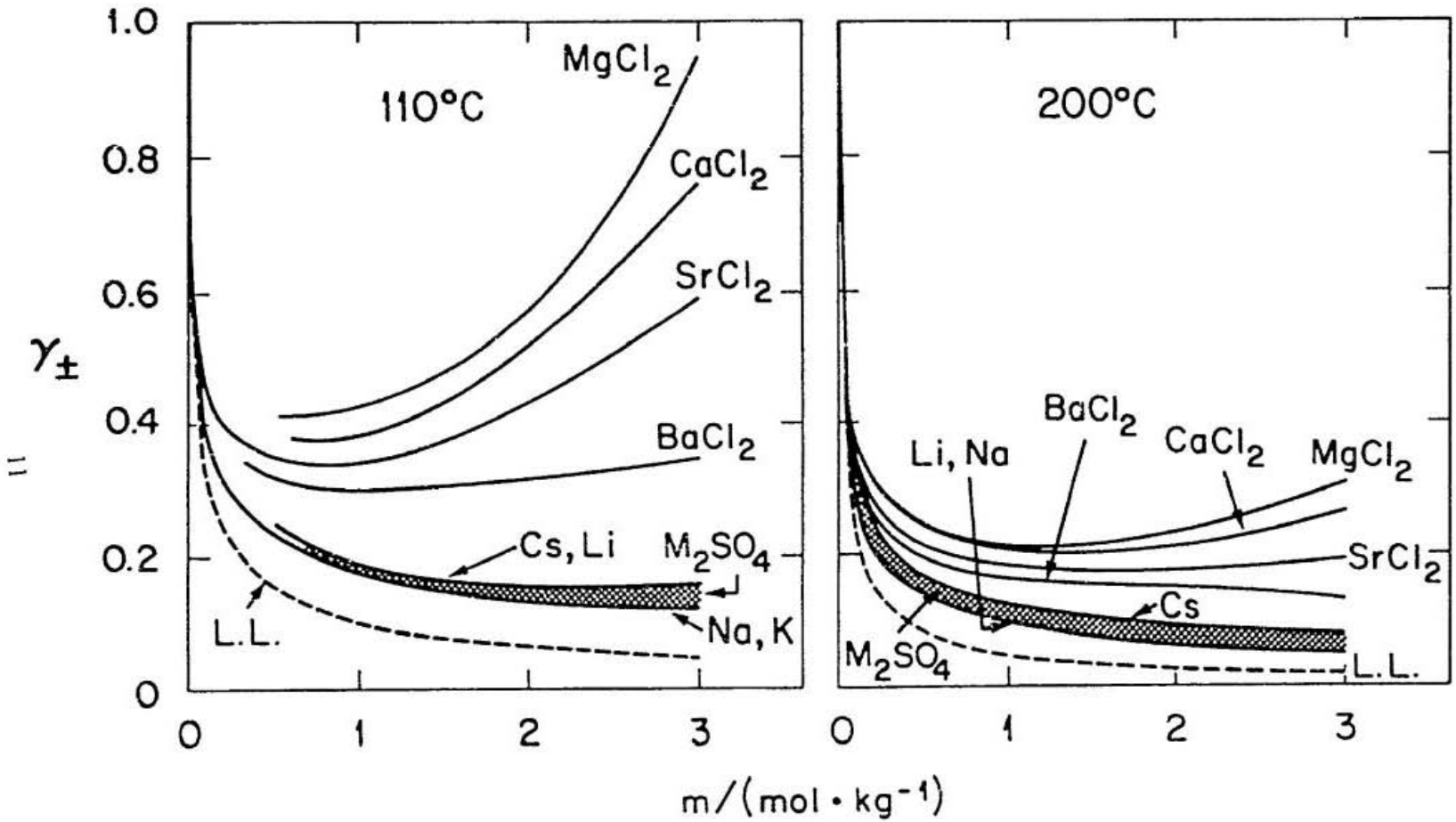


Figure 1.2 Mean activity coefficients for 1.2 electrolytes at various temperatures, and the Debye Huckel limiting law, "LL" (Holmes and Mesmer, 1983, Pitzer, 1991)

The activity coefficient of ions A^{z_A} are assumed to be given by the expression

$$\gamma_{z_A} = [\gamma_{\pm}(NaCl)]^{z_A^2} \tag{1.23}$$

This expression is consistent with the Debye-Hückel limiting law, and is approximately valid in the range 150-325°C (Lindsay, 1989).

From the Gibbs-Duhem equation, the osmotic coefficient of water, ϕ, and the activity of water, a_w may be calculated from

$$\phi - 1 = \frac{1}{\sum_{sol} m_i} \sum_i \int_0^{\sum_{sol} m_i} m_i \left(\frac{d \ln \gamma_i}{d \sum_i m_i} \right)_x d \sum_i m_i \tag{1.24}$$

The term $\Sigma_{sol}\, m_i$ is the total concentration of all dissolved constituents in the solution of interest, and the subscript x on the derivative in the right hand side indicates that the species distribution is held fixed. Each of the integrals in the sum of integrals is evaluated for the range of total concentration from zero to the solution of interest. The activity of water is given by

$$a_w = \exp(-0.018015 \phi \sum_{sol} m_i) \tag{1.25}$$

The result of this expression is the activity of water when the solution is at a total pressure

equal to the vapour pressure of pure water, which is greater than the pressure of water vapour in equilibrium with the solution. The difference in water activity is negligible except in cases of extreme temperatures and concentrations. The correction of this effect may be obtained with the following relationship

$$\left(\frac{\partial \ln a_w}{\partial p}\right)_T = \frac{\overline{V}_w}{RT} \qquad (1.26)$$

in which $\overline{V}_w$ is the partial molar volume of water in the solution

In the original Lindsay model, the activity coefficients for $\gamma_\pm$ (NaCl, aq) were calculated from the Meissner equation (Meissner, 1980) which was found to fit the limited experimental data available at the time. Recently, Archer and Wang (1990) have reported a comprehensive equation of state for the excess properties of NaCl (aq) that is valid up to 325°C. The values for $\gamma_\pm$ (NaCl, aq) and a_w used in our work were taken from the Archer and Wang formulation.

1.4 The Na_2O-P_2O_5-H_2O System

The aqueous chemistry of phosphorus has been reviewed by many authors, including Cotton and Wilkinson (1988), Corbridge (1980), Thilo (1965), and Van Wazer (1958), among others. The main species dealt with in this study are dihydrogen phosphate, $H_2PO_4^-$, hydrogen phosphate, HPO_4^{2-}, and phosphate, PO_4^{3-}, the anions of orthophosphoric acid. These orthophosphates can condense, with removal of water, to

form ions containing more than one phosphorus atom and phosphorus-oxygen-phosphorus bonds. The four most common types of condensed phosphates are: polyphosphates, $[P_nO_{3n+1}]^{(n+2)-}$ (for example, $P_2O_7^{4-}$, pyrophosphate); infinite-chain metaphosphates, $[(PO_3)_n]^{n-}$; cyclic metaphosphates, $[(PO_3)_n]^{n-}$, $n \geq 3$; and ultraphosphates, containing branching units, (for example P_4O_{10}).

The phase diagram for sodium-phosphate-water systems below 100°C is extremely complex (Van Wazer, 1958; Wendrow and Kobe, 1955). At 25°C, there are several multi-hydrated phases of the di- and trisodium salts and two complex salts, $Na_3PO_4 \cdot 12H_2O \cdot ¼NaOH$ and $Na_2HPO_4 \cdot 2NaH_2PO_4 \cdot 2H_2O$. However, as the temperature increases, the hydrated salts quickly become less stable., and at 100°C, only some of the lower hydrated salts remain.

The phase behavior of several condensed phosphates at 30°C has been reported by Griffith and Buxton (1968). At temperatures above 100°, these metastable salts hydrolyse to form orthophosphates (Marshall and Begun, 1989). These salts are thermodynamically unstable, and the hydrolysis reactions become kinetically favourable above 100°C. The solubilities of many phosphates have been reported by Esseltova (1988).

The solubility and aqueous phase behaviour of monosodium phosphate has been measured by Morey (1953) at temperatures up to 620°C. Similar studies on aqueous disodium phosphate have been reported by Broadbent et al. (1977), Panson et al. (1975), Ravich and Shcherbakova (1955) and Wetton (1981) at temperatures up to 350°C.

There are many similarities between the two salts in terms of their behavior. Both

form a series of hydrated compounds and the existence of these hydrates cause their solubilities to increase with temperature. As temperature is increased, the water of hydration are progressively removed until the salts are anhydrous With further increases in temperature, orthophosphates are dehydrated to form pyrophosphate above 300°C and, for the case of monosodium phosphate above 343°C, there is another dehydration to form metaphosphate, $NaPO_3$. The progression from hydrated salts to anhydrous salts to pyrophosphates is shown for disodium phosphate in Figure 1.3 (Broadbent et al., 1977) The actual temperatures of transition are determined by the vapour pressure of the water of hydration relative to that of steam saturated water. These dehydration reactions are reversible (Kiehl and Wallace, 1927) and can be predicted from thermodynamic calculations (Taylor et al., 1979).

The complex salt, $NaH_2PO_4 \cdot Na_2HPO_4$, has been studied by Wetton (1981) and Taylor et al. (1979), and was found to be stable at 300°C It is thought to dissolve congruently, (Taylor et al., 1979; Wendrow and Kobe ,1955) but dehydrates to form $Na_5P_3O_{10}$ and $NaPO_3$ between 300 and 350°C (Wetton, 1981; Edwards and Herzog, 1957).

Figure 1.4 shows the solubility of aqueous trisodium phosphate reported by Schroeder et al. (1937). More recent studies have shown that the saturating phase above 200°C is not the expected trisodium salt, Na_3PO_4, but is a sodium deficient compound, $Na_{2.8}(H_3O)_{0.2}PO_4$. Wendrow and Kobe's (1955) work showed that further uncertainty exists in Schroeder's data because excess NaOH may have been present in the

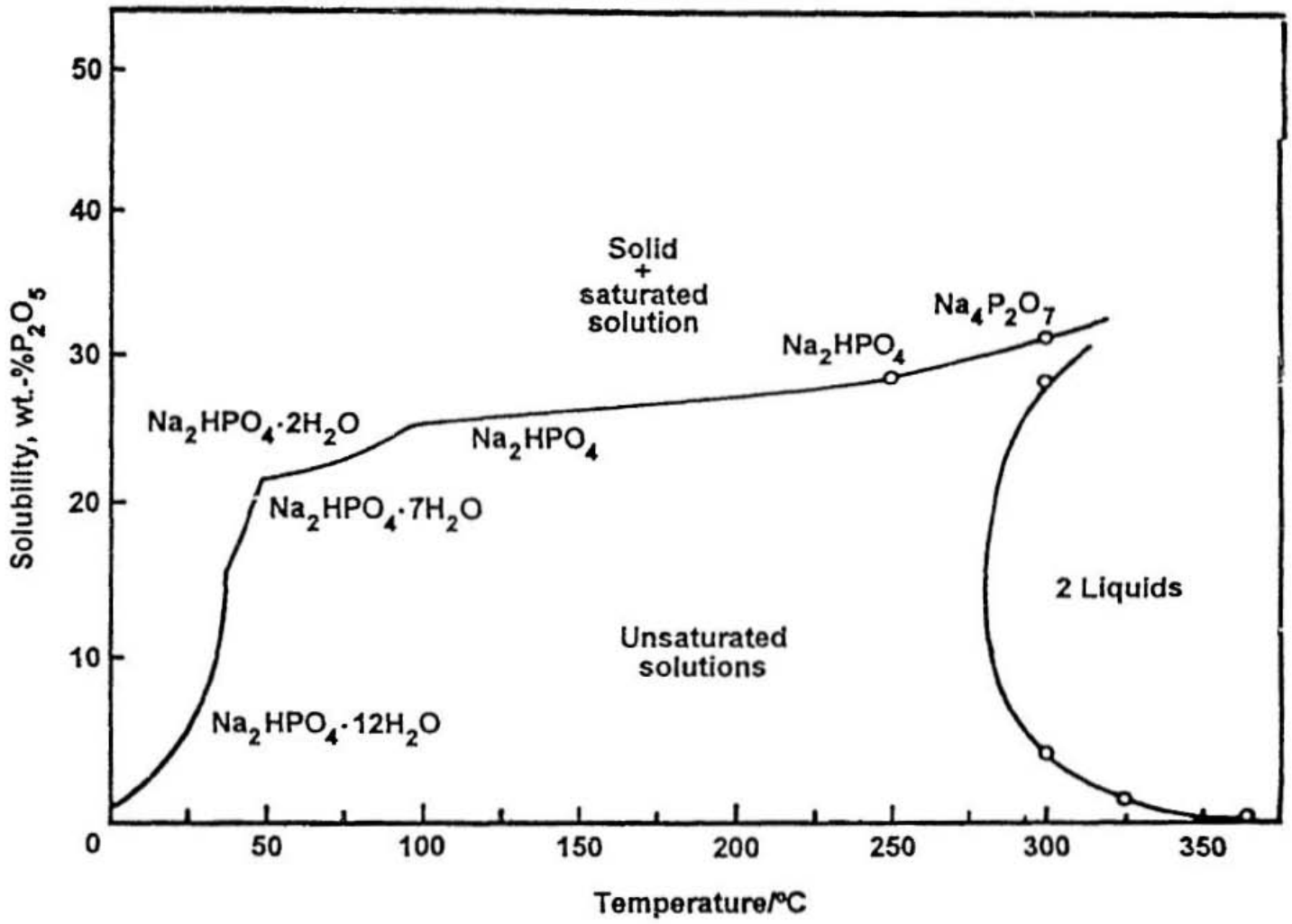


Figure 1.3 The solubility and equilibrium phases of disodium phosphate, Na_2HPO_4 as a function of temperature (Broadbent et al., 1977).

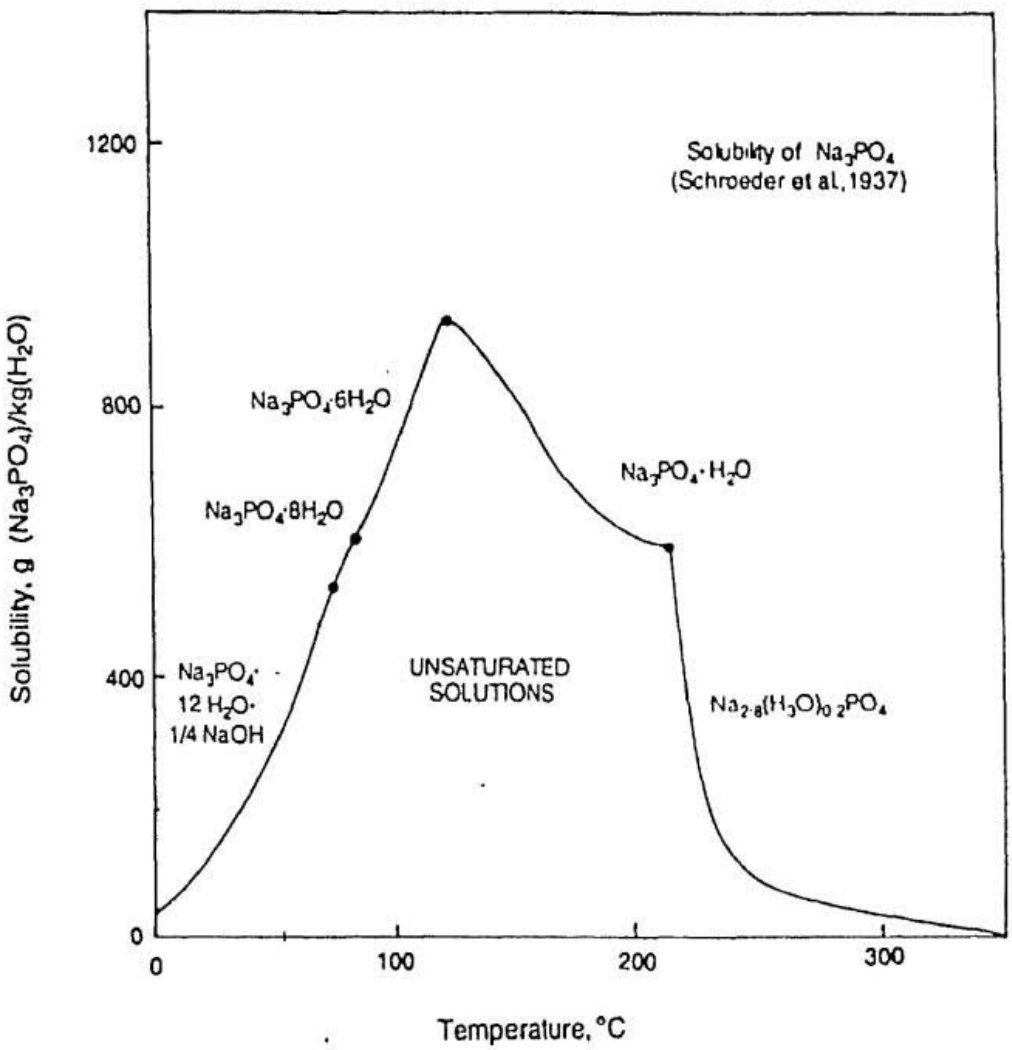


Figure 1.4 The solubility and equilibrium phases of trisodium phosphate, Na_3PO_4, as a function of temperature (Schroeder et al., 1937).

dodecahydrate salt used to prepare the solutions. However, Figure 1.4 does illustrate the sharp decrease in the solubility of trisodium phosphate systems above 120°C that has been reported by later workers (Wetton, 1981; Marshall, 1982; Marshall, 1985; and references cited therein). X-ray diffraction studies by Taylor et al. (1977) and Wetton (1981) showed that the cubic solid solution $Na_{2.8}H_{0.2}PO_4$, is structurally related to cubic Na_3PO_4. This phase is stable up to 350°C and its existence has significant implications for boiler water chemistry control.

A region of liquid-liquid phase separation at temperatures above 275°C in aqueous sodium phosphate systems with Na/PO_4 ratios between 1.0 and 2.1 has been discovered in experimental work by Broadbent et al. (1977) and Marshall (1982). In a study by Marshall and Begun (1989), Raman spectra of the highly concentrated and dilute immiscible liquid phases showed that orthophosphates are the main species present. In Figure 1.5, the boundaries of the two phase region are plotted as a function of temperature, along with the solubilities of Na_2HPO_4 and "Na_3PO_4" from Figures 1.3 and 1.4.

Liquid-liquid phase separation has been observed in potassium phosphate solutions at slightly higher temperatures, and in other systems with very soluble salts of bulky anions (Marshall, 1982 and 1985). This immiscibility phenomenon is apparently due to the decrease in the dielectric constant of water as the temperature approaches the critical point, and the high degree of solute non-ideality. This effect has been qualitatively modelled by Pitzer (1984) with corresponding state theory. Weintgärtner (1989)

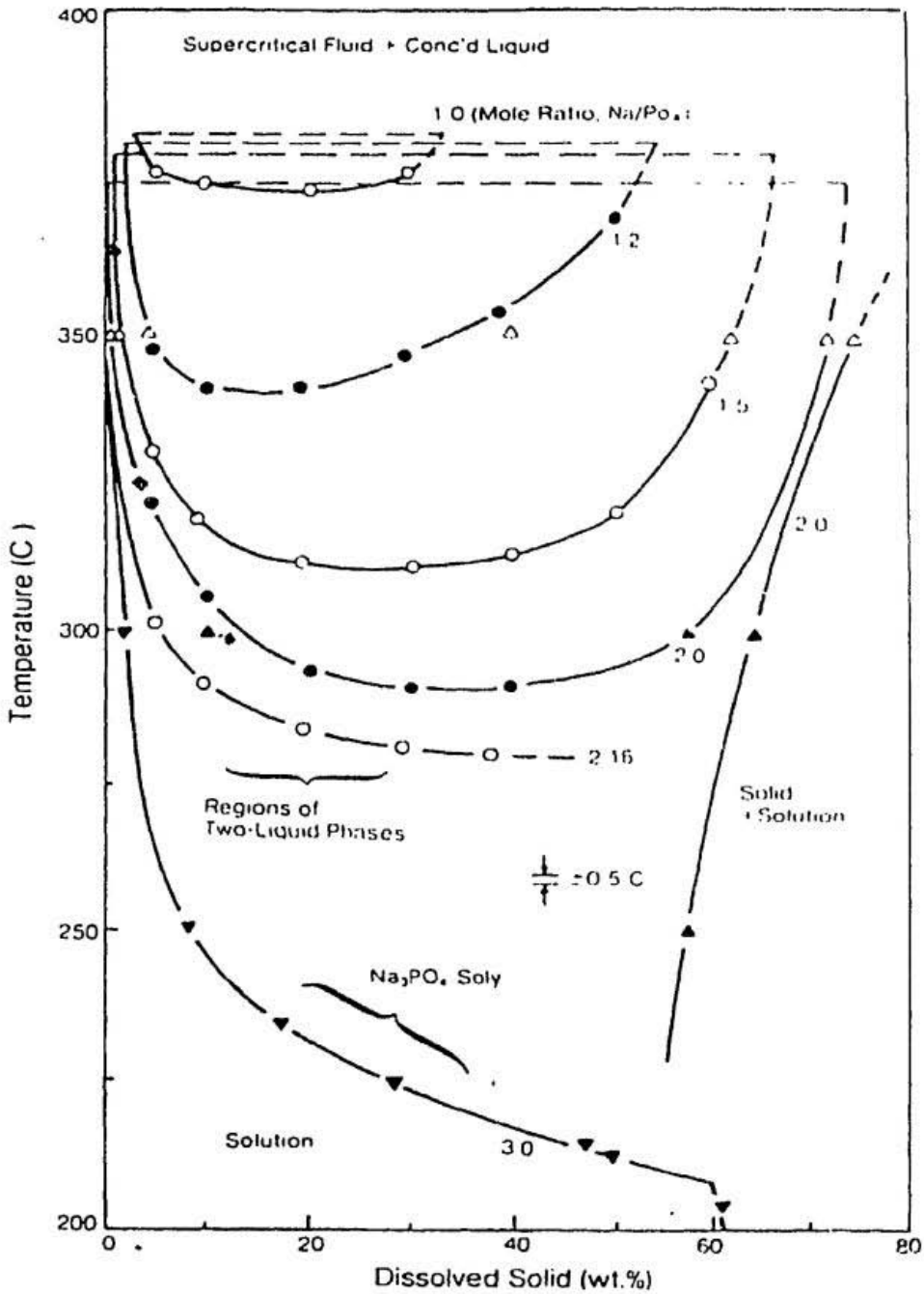


Figure 1.5 Two-liquid phase and solution-solid boundaries for aqueous solution mixtures of sodium phosphate salts of mole ratios, Na/PO_4 from 1.00 to 3.00 at 200-400°C (Marshall, 1982).

successfully applied the Pitzer ion-interaction model to liquid-liquid phase separation in 2-1 electrolytes.

Ravich and Scherbakova (1959) reported that incongruent precipitation of $Na_{2.8}(H_2O)_{0.2}PO_4$ causes excursions to high pH in the Na_3PO_4-H_2O system at sodium phosphate ratios Na/P > 2.8. Marcy and Halstead (1964) confirmed these results and recommended the "congruent phosphate" control practice that is now in widespread use in the power industry. Panson et al. (1975), Broadbent et al. (1977), and Wetton (1981) conducted further solubility studies, extending these measurements to higher temperatures and a wider range of compositions. Taylor et al. (1979) further developed these phase diagrams, and identified equilibrium phases at 300°C by examining solids recovered from dry-out experiments at different solution compositions in powder X-ray diffraction studies. Wetton (1981) recovered and identified equilibrium solids formed at 350°C.

Figure 1.6 presents the ternary phase diagram for the $Na_2O/P_2O_5/H_2O$ system at 300°C. The diagram illustrates the complex sodium phosphates and pyrophosphates that exist under boiler conditions and the region of liquid-liquid phase separation at sodium-phosphate ratios near 2.0. For solutions with $2.2<Na/PO_4<2.7$, evaporating to dryness does not cause excursions to highly acidic or alkaline conditions because they are trapped between the congruent composition at 2.8 and the invariant point at 2.15. Figure 1.7 shows the increase in solubility at $Na/PO_4 > 3.0$ above 300°C, conditions that are very corrosive.

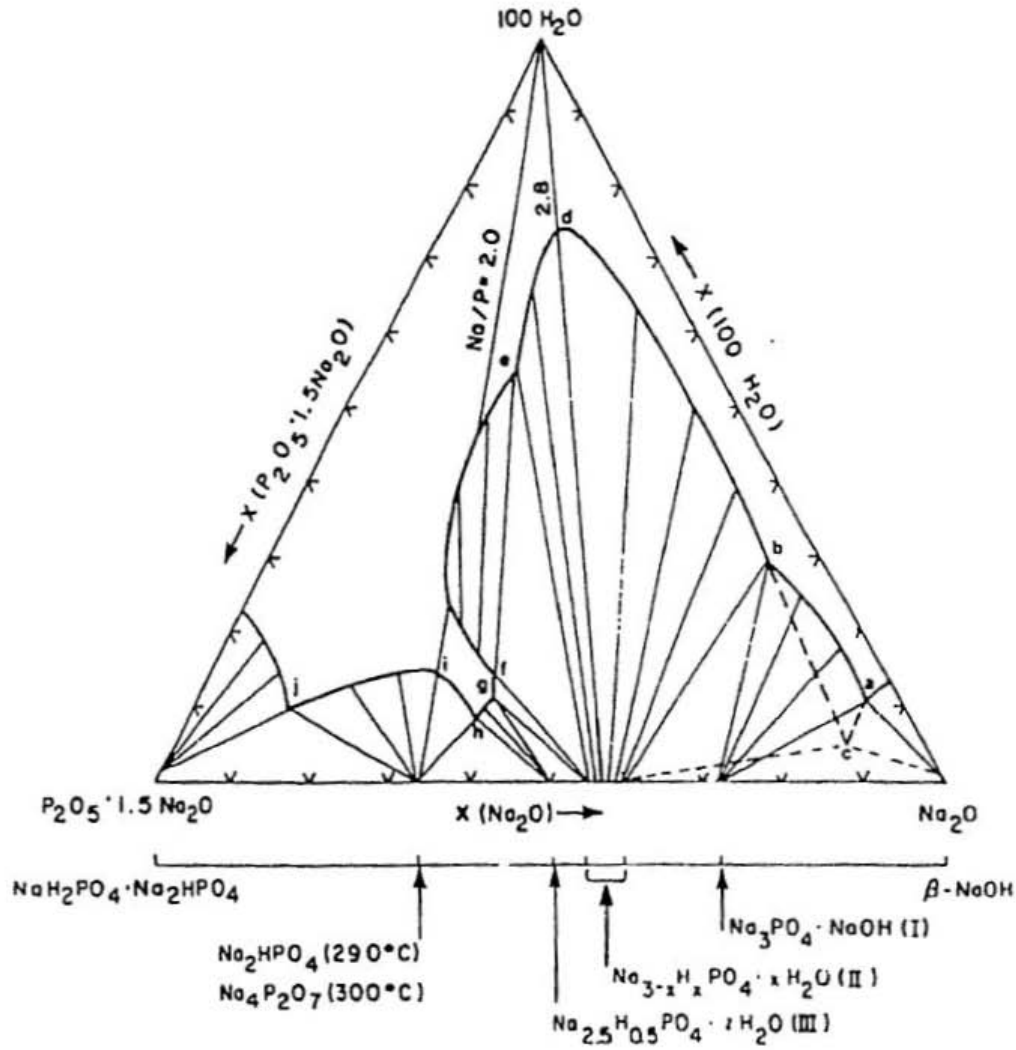


Figure 1.6 Sodium-phosphate-water phase behavior at 300°C (Taylor et al., 1979).

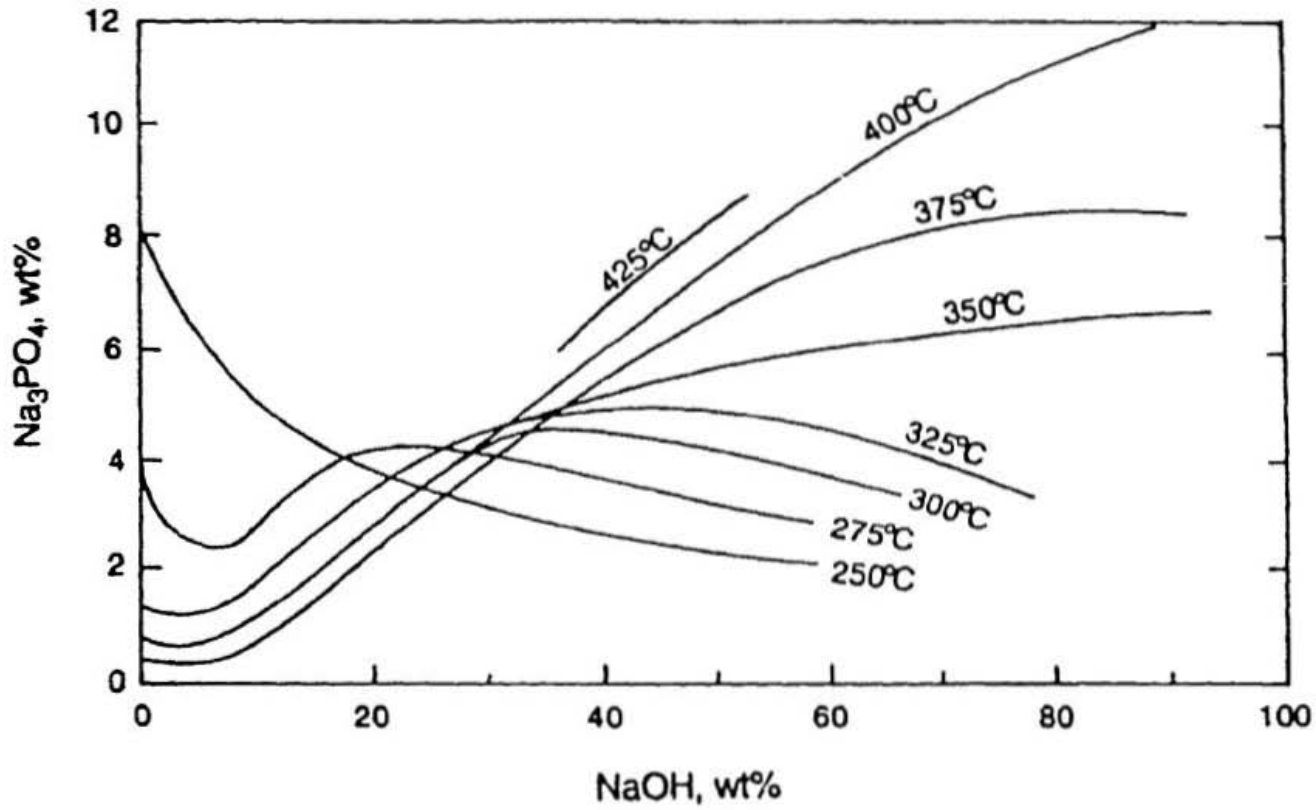


Figure 1.7 Solubility of trisodium phosphate in sodium hydroxide solutions (Borovaya and Ravich, 1968).

1.5 Magnetite-Phosphate Interactions

1.5.1 Hideout Reaction Simulations

The first reports of phosphate interactions with magnetite in high-temperature water were made by Economy et al (1975) and Connor et al (1983), who conducted detailed flow experiments at temperatures up to 316°C. Their experiments showed that the sodium phosphate sorption is reversible, and that the temperature must exceed 177°C before significant uptake occurs. Economy and his coworkers also reported that the sodium phosphate concentration must exceed a threshold value before reactivity with magnetite is observed, and that the reaction is a bulk, rather than surface, phenomenon. The amount that can be sorbed is many times in excess of the monolayer coverage. At 316°C, the threshold concentrations lie within 10 to 20 percent of the solubility limit of the pure sodium phosphate $Na_{2.8}(H_2O)_{0.2}PO_4$ (Wetton, 1981). However, the increase in the sodium-phosphate ratio of the effluent solution is not consistent with the precipitation of this salt, because the sodium/phosphate ratio in the aqueous phase increases, rather than decreasing as would be the case when $Na_{2.8}(H_2O)_{0.2}PO_4$ precipitated from aqueous solutions at a lower sodium/phosphate ratio. Similar changes in Na/PO_4 ratio and pH have been observed by Broadbent et al. (1978) and Balakrishnan (1977) through experiments in which magnetite-containing corrosion products were allowed to react with aqueous phosphate in batch vessels. These observations, and the reversible nature of the uptake reaction, suggested that sorption is due to the precipitation of a new phase, and that the new phase contains iron.

Three major studies have been undertaken to extend the work on phosphate-iron interactions. The Central Electricity Generating Board (CEGB) (Broadbent et al., 1978; Wetton, 1980 and in prep.), the Knolls Atomic Power Laboratory (Ziemniak et al., 1992, 1993), and the Canadian Electrical Association (Tremaine at al , 1992, 1994) have reported studies to identify the phase relations and solid reaction products associated with sodium phosphate/magnetite hideout reactions. Recent batch experiments by Ziemniak et al (1992, 1993) up to 300°C, and flow studies up to 360°C (Tremaine at al , 1992, 1994) have determined the molalities of aqueous sodium and phosphate in equilibrium with magnetite and the hideout reaction product mixtures at ratios typical of operating conditions. The redox conditions needed to derive thermodynamic data were not well defined in these experiments.

1.5.2 Magnetite Reaction Products

In their studies on corroding steel systems, Broadbent et al. (1978) identified several Fe(II) phases that appeared as major reaction products. These include $NaFe^{II}PO_4$ (maricite), $Na_{3-2x}Fe^{II}_xPO_4$, $Na_3Fe^{II}(OH)(HPO_4)_2$ and two unidentified Fe(II) containing compounds. Subsequent work (Wetton, 1980; Pollard and Edwards, 1963) showed that $Na_3Fe^{II}(OH)(HPO_4)_2$ is not a stable phase, and that $Na_{3-2x}Fe^{II}_xPO_4$ is a major reaction product in reduced environments along with maricite. $Na_{3-2x}Fe^{II}_xPO_4$ is apparently a solution of Fe(II) in cubic γ Na_3PO_4. Broadbent's results suggest that a 4.9 to 9.8 weight percent iron ($x = 0.2 - 0.3$) corresponds to a unit cell dimension of 7.392 Å, while

γ Na_3PO_4 has a unit cell of 7.410 Å (Mair, 1976). At low temperatures, pure γ Na_3PO_4 transforms to orthorhombic α Na_3PO_4. In the absence of sodium, both $Fe^{II}HPO_4$ and $Fe^{II}_2P_2O_7$ have been observed at 300°C (Pollard and Edwards, 1963) while at higher temperature, $Fe^{II}_2P_2O_7$ is probably the stable phase

Recently published research at the Knolls Atomic Power Laboratory (Galonian et al., 1982; Ziemniak et al., 1989) has shown that a ferric compound, $Na_4Fe^{III}OH(PO_4)_2 \cdot \frac{1}{3}NaOH$ (designated sodium iron (III) hydroxy phosphate, or "SHIP"), forms as a major reaction product at 300°C. The X-ray diffraction pattern of this compound has been confirmed (Ziemniak et al., 1981, 1992) to be the same as that observed for reaction products in our work and in the studies reported by Connor and Panson (1983) and Broadbent et al. (1978).

The results for the batch solids characterization experiments carried out by Tremaine et al. (1992, 1994) are summarized below. At Na/PO_4 ratios of 1.0, magnetite reacts to form maricite along with a second unidentified product which must contain Fe(III). This product is probably a phosphate or pyrophosphate with a Na/PO_4 ratio of 1.0 and for convenience, we designate it "$Na_2Fe^{III}(HPO_4)PO_4$".

$$Fe_3O_4 + 5Na^+(aq) + 5HPO_4^{2-}(aq) + H_2O \rightarrow NaFe^{II}PO_4 + 2Na_2Fe^{III}(HPO_4)PO_4 + 5OH^-(aq) \qquad (1.27)$$

Reaction at higher sodium/phosphate ratios (Na/PO_4 = 1.5 and 2.0) yields maricite and

sodium ferric hydroxyphosphate, the reaction product observed by Connor and Panson (1983)

$$Fe_3O_4 + 5\,HPO_4^{2-}(aq) + 9\tfrac{2}{3}Na^+(aq) \rightarrow$$
$$NaFe^{II}PO_4(s) + 2Na_4Fe^{III}OH(PO_4)_2.\tfrac{1}{3}NaOH(s) + \tfrac{1}{3}OH^-(aq) + H_2O(l) \quad (1.28)$$

Still higher Na/PO_4 ratios apparently favour the formation of a solid solution in which Fe^{2+} replaces some sodium ions in the lattice of γNa_3PO_4, according to the reaction.

$$Fe_3O_4 + \left(4 + \frac{1}{x}\right)HPO_4^{2-} + \left(\frac{20}{3} + \frac{3}{x}\right)Na^+ \rightarrow$$
$$2Na_4Fe^{III}OH(PO_4)_2.\frac{1}{3}\,NaOH + \frac{1}{x}\,Na_{3-2x}Fe^{II}_xPO_4 + \quad (1.29)$$
$$\left(\frac{4}{3} - \frac{1}{x}\right)OH + \frac{1}{x}\,H_2O$$

From XRD data, solid solutions formed from the reactant mixture with $Na/PO_4 = 3.0$ are consistent with values of $x = 0.2$. Those from reagents with $Na/PO_4 = 3.5$ are consistent with lower Fe(II) content ($x < 0.1$).

Orthorhombic α Na_3PO_4 is the stable low temperature form of pure Na_3PO_4. Its presence as the major product from the run at $Na/PO_4 = 4.0$ indicates that no reaction between phosphate and magnetite took place.

The reaction products observed at 350°C are similar to those observed at 320°C, except that the cubic solid solution, $Na_{3-2x}Fe^{II}_xPO_4$ was only a minor product relative to the

iron (III) hydroxyphosphate, $Na_3Fe^{III}OH(PO_4)_2 \cdot \frac{1}{3}NaOH$. This is an important difference because it indicates that, at 350°C, the ferrous iron in the magnetite is oxidized according to the reaction.

$$Fe_3O_4 + 13Na^+(aq) + 6HPO_4^{2-}(aq) \rightarrow$$
$$3Na_3Fe^{III}OH(PO_4)_2 \cdot \frac{1}{3}NaOH + H^+(aq) + \frac{1}{2}H_2(aq) \qquad (1.30)$$

The sodium phosphate ratio required to avoid the formation of maricite and SHP according to Reaction 1.28 rises from Na/P>2.3 at 315°C to Na/P >2.7 at 360°C. Sodium phosphate ratios Na/P>3.5 appear to form only sodium phosphate phases without undergoing iron reactions.

The solubilities of all the iron products except maricite appear to increase with decreasing temperatures.

1.5.3 Phosphate Hideout in Magnetite Corrosion Product Deposits

Magnetite is the major protective corrosion product on carbon steel surfaces under steam-generator conditions. Typically, the oxide has a two-layer structure (Bornak, 1987; Potter and Mann, 1965), with a relatively thick continuous inner layer and a loose, porous outer layer of more well-developed magnetite crystals. Hideout reactions may replace the protective magnetite film with phosphate reaction products. Corrosion studies near 300°C (Broadbent et al., 1978) suggest that these products may not be protective

The increase in local pH that accompanies the hideout process is also of concern if dryout conditions are present.

The flow experiments reported by Tremaine et al. (1992, 1994) confirmed the results of Conner and Panson (1983) at 315°C, and showed for the first time that similar sodium-iron-phosphate reactions also take place at 360°C. The major iron reaction products that cause hideout at Na/PO_4 ratios near 2.5 have been identified from the batch experiments as $NaFe^{II}PO_4$ (maricite) and $Na_4Fe^{III}(OH)(PO_4)_2 \cdot \frac{1}{3}NaOH$. At higher Na/PO_4 feed ratios, $Na_{1-2x}Fe^{II}_xPO_4$ (a solid solution with cubic trisodium phosphate, Na_3PO_4) replaces maricite as the stable reaction product. At 360°C, hideout behaviour is similar except that there appear to be no significant amounts of iron(II)-containing reaction products that form from boiler water with Na/PO_4 ratios of 2.5 or higher. If the sodium phosphate ratio is sufficiently large ($Na/PO_4 > 3.5$) no hideout reactions involving magnetite appear to take place. A schematic diagram of the hideout mechanisms is presented in Figure 1.8.

The reaction product mixtures, noted above, all have an inverse solubility gradient. Since phosphate hideout only occurs in boilers when the local concentration exceeds the saturation threshold of the reaction products, it is favoured by the high temperatures associated with high-load operations where strong concentration mechanisms take place within deposits. The preferential deposition of phosphate in the reaction products increases the relative concentration of sodium in the under-deposit fluids and in the bulk boiler water, thereby creating more caustic solutions. Under dryout conditions these

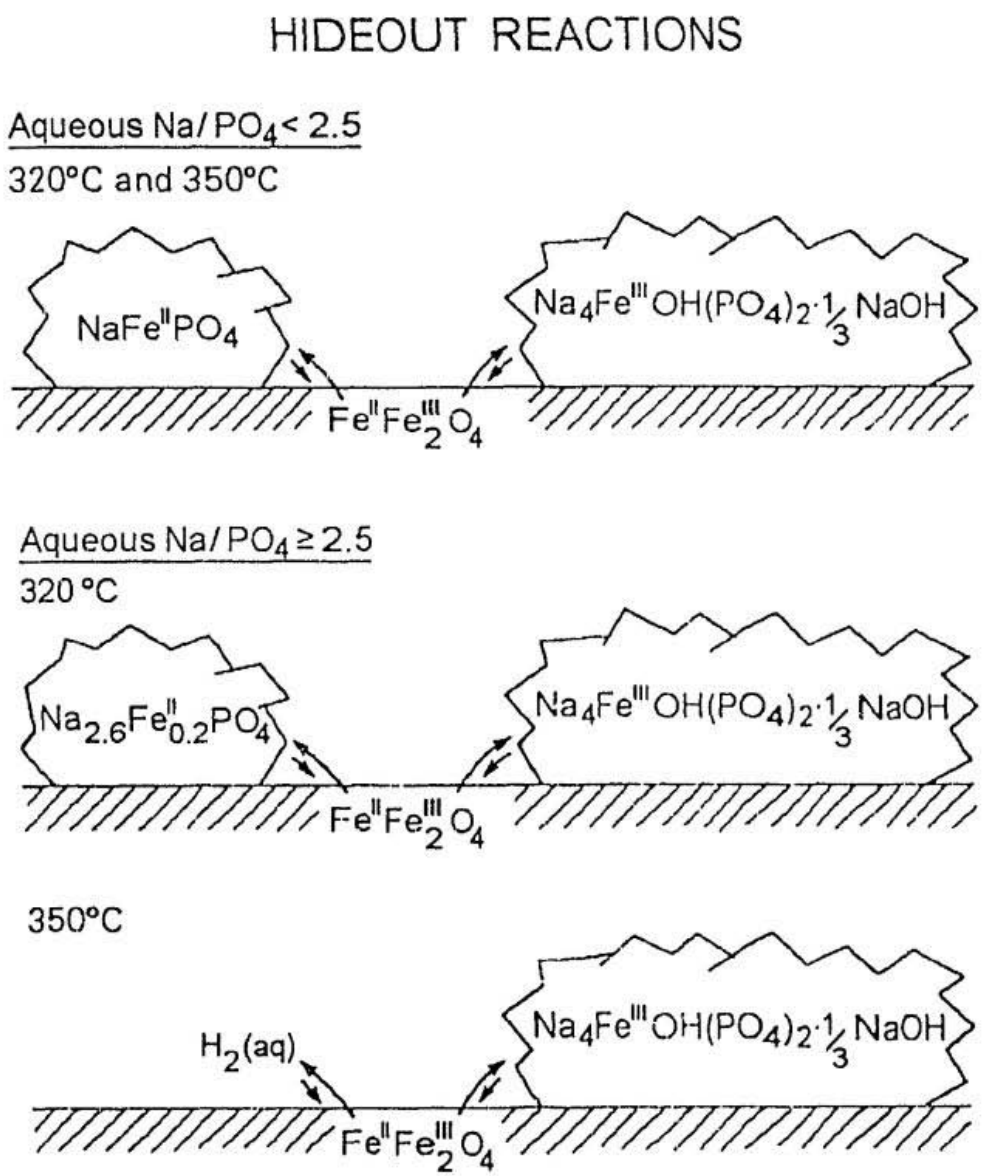


Figure 1.8 Summary of phosphate hideout reactions with magnetite at 320 and 350°C

processes may create the high local concentrations typically associated with caustic gouging and cracking. When the load (and the temperature) are reduced, the reaction products redissolve.

The mechanism of redissolution of the iron-phosphate reaction products has not been studied in depth. Experiments at 360°C indicate that the dissolution reactions do regenerate magnetite, when hydrogen is present. Hematite was regularly observed by Conner and Panson (1983), in flow experiments with deaerated water, and has been found with maricite on corroding steel surfaces in power station boilers (Dooley, 1994).

2.0 EXPERIMENTAL

2.1 Chemicals and Materials

Sodium phosphate solutions were prepared from reagent grade $Na_3PO_4 \cdot 12H_2O$ (Fisher Scientific, ACS Reagent Grade, assay 98.9%), Na_2HPO_4 (Aldrich, ACS Reagent Grade, 99+%), $NaH_2PO_4 \cdot 2H_2O$ (BDH, assay 99.0-101.0%), and NaOH (BDH, ACS Reagent Grade), used as received, with Nanopure water (resistivity ~18MΩcm). The stoichiometry of waters of hydration in the reagent grade materials was confirmed by measuring the weight loss on drying overnight at 150°C. Otherwise, the solids were used without purification. Solutions were prepared in units of molality to simplify high temperature solution calculations.

Several solids were used as sources of iron in this study, including Fe_2O_3 (Aldrich, 99+%, BDH, ~97%), Fe_3O_4 (Aldrich, 98%), $FePO_4$ (Johnson-Matthey, $FePO_4 \cdot xH_2O$, 17% H_2O), $NH_4Fe(SO_4)_2$ (BDH, ACS Reagent Grade), and Fe powder (BDH).

The two supplies of hematite and the magnetite were analyzed by SEM and the particle sizes were found to be 0.2 μm and 0.6 - 1.0 μm respectively for the Aldrich and BDH hematite, and 0.2 - 1.0 μm for magnetite.

Other chemicals used in these experiments were $N(CH_2CO_2H)_3$, nitrilotriacetic acid (Aldrich, 99%), CuO (BDH), and $NaNO_3$ (BDH).

2.2 Apparatus

2.2.1 Teflon-Lined Filtration Cells

In order to synthesize the desired compounds, *in situ* filtration was required to prevent hydration or redissolution of reaction products. Steam could not simply be blown off without possible dehydration of the products.

Modified Parr 4744 General Purpose Bombs were used to synthesize the solids at high temperature. These are 45 mL 316 stainless steel pressure vessels with Teflon liners. The liners were bored out to allow the insertion of an inner Teflon liner with a removable cap for holding a stainless steel filter. Filters for use at high temperatures were fabricated from 316 stainless steel mesh (100, 200, 325-mesh) obtained from Small Parts Inc., Miami Lakes, Florida

A schematic diagram of this vessel is shown in Figure 2.1. This design allows *in situ* isolation of the solid reaction products by simply inverting the cell while in a high temperature oven, to permit the liquid to drain through the stainless steel filter. Three small grooves on the outside of the inner liner allowed vapour to escape from the bottom compartment while filtration took place.

To avoid refluxing the filtrate, the cell was cooled to room temperature by placing it on an aluminum plate in cold flowing water so that the lower compartment of the cell was colder than the top during the cooling process.

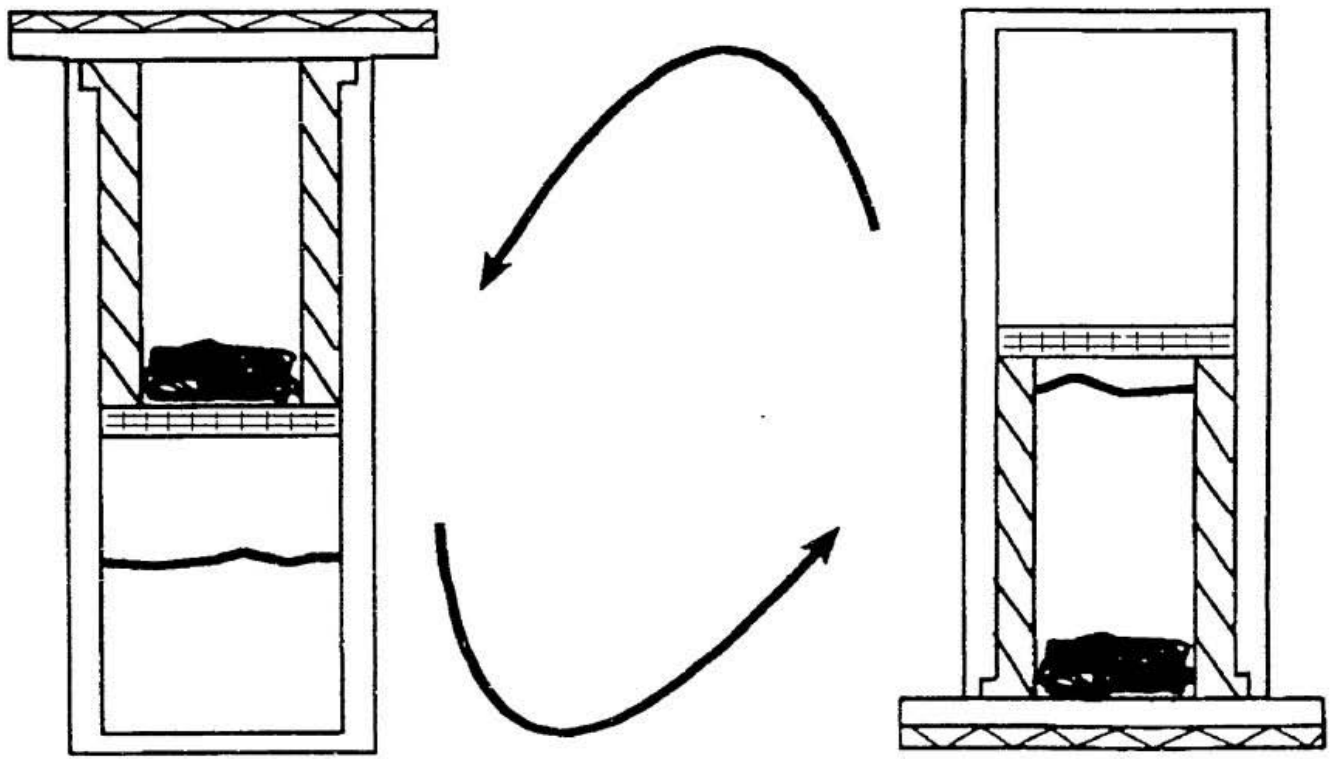


Figure 2.1 45 mL Teflon lined cells. At left, vessels before reaction and after filtration. At right, vessel during reaction.

2.2.2 Stirred Reaction Vessel

A 450 mL Parr Stirred Mini-Reactor (Model 4562) with a proportional-integral-derivative (PID) temperature controller (Model 4842) was used to study the solubility of the SHIP phase. This reactor is rated for a maximum pressure of 207 bars and temperatures up to 350°C. A schematic diagram of this reactor can be found in Figure 2.2.

Temperature was controlled to ±1°C with a PID controller. The Parr 4842 temperature controller is a full feature, microprocessor based, digital temperature control system with adjustable PID control A variable speed control is provided for the stirrer motor, along with a digital tachometer, and a high temperature cutoff is provided to prevent temperature excursions. The pressure display module with a second high pressure cutoff, provides an additional safety mechanism to protect against an unexpected pressure buildup

Several modifications were made to the standard reactor to increase its suitability for this project. The head, cylinder, and all inner parts were constructed of Hastelloy C for corrosion resistance. A wider and lower impeller was also designed to provide increased agitation, reducing deposition of solids. The reactor head was equipped with a rupture disk lined with gold, to prevent corrosion and premature rupture. Despite the precautions, severe pitting corrosion was encountered above 300°C under solids deposited on the bottom of the vessel. This led to the purchase of an additional cylinder fabricated from zirconium for use in experiments with sodium-phosphate ratios of 3.0.

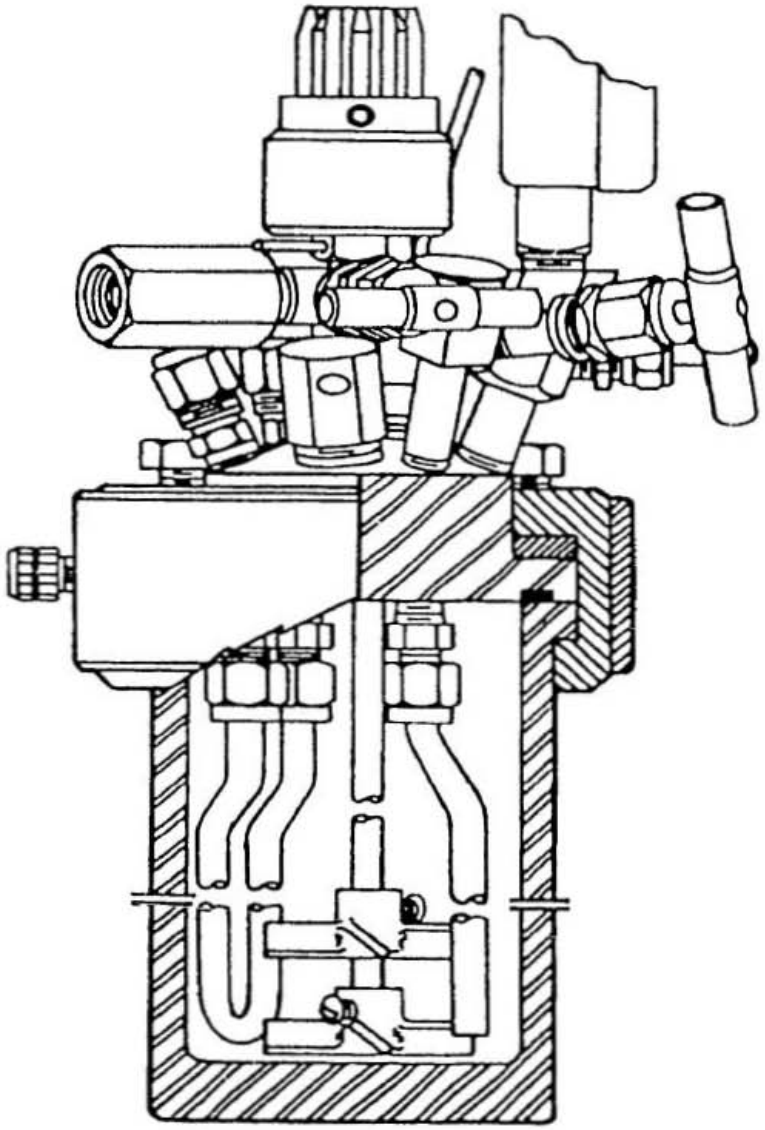


Figure 2.2 Schematic diagram of Parr 450 mL stirred reaction vessel.

Unfortunately, in the experiments with a Na/P ratio of 3 0 and temperatures above 300°C, the zirconium vessel also had major problems with severe corrosion accompanied by removal of the protective oxide layer and considerable hydrogen evolution

Aside from corrosion problems, modifications were required to permit liquid sampling at elevated temperatures A condenser, consisting of a valve attached to a length of 0 125 in Hastelloy C tube inside a 0.25 in copper tube and cooled by cold flowing water, was inserted in the system just before the liquid sampling valve to allow sampling at high temperature A filter, consisting of a modified 0.25 in Swagelok union containing a frit or several layers of stainless steel mesh, was connected to the inlet end of the liquid sampling tube inside the vessel. Due to the small particle size of the hematite, it was difficult to filter the samples. Several frit materials were used, including 316 stainless steel, Inconel 600, and zirconium oxide. All of these frits clogged before finishing even a single run An alternative design that employed several layers of 325 mesh 316 stainless steel filters was found to be suitable, although some carry-over of particulate material was frequently encountered.

2.3 Analytical Methods

2.3.1 Powder X-Ray Diffraction

Solid products were analyzed using a Rigaku RU-200 X-ray diffractometer (XRD) with a 12 kW rotating anode Cu Kα X-ray source and a diffracted beam monochromator. The diffractometer was operated at 40 kV, and 100 mA and a scan rate of 10° (2θ) per

minute, except where otherwise noted. Samples were prepared by grinding to a fine powder with a mortar and pestle. Methanol was added, and the resulting mixture was transferred to a slide and placed under a lamp to dry. The JCPDS file was used for a search-match database, using the software package MDI Jade+ for its search-match algorithm.

The XRD was also used for semi-quantitative analysis of unreacted hematite in one solid product, by a method of standard additions. The product was analyzed using the XRD, recovered, and then re-analyzed with known mass fractions of hematite added. This was done at 0.01, 0.05, and 0.10 mass fraction hematite. The intensity of the hematite peak at 2.53Å was measured relative to the main peak of the reaction product at 2.67Å. The relative peak height was plotted against the mass fraction of hematite to obtain the original amount of unreacted starting material in the product.

2.3.2 Single Crystal X-Ray Diffraction

The structure of single crystals isolated in this study were analyzed by Dr. John Bridson and David Miller with a Rigaku AFC6S diffractometer with low temperature capability and a VAX3100 workstation with a laser printer, tape drive, and the TEXSAN TEXRAY Structure Analysis Package (Molecular Structure Corporation Inc.). A complete report of the methods and results of this work can be found in Appendix II.

2.3.3 ICP Emission Spectroscopy

Liquid samples taken from the stirred reactor were diluted by mass to approximately 50-250 ppm in sodium and phosphorus and analyzed using an ARL 3520 DES ICP spectrometer at the Department of Mines and Energy, operated by Chris Finch and Peter Haring. The spectrometer was controlled by Plasma Vision 60 software, and samples were handled by a Gilson Model 222 sample changer

In all, nine batches of solutions were analyzed for sodium and phosphorus concentrations by ICP emission spectroscopy. Before each batch of samples was analyzed, three standard solutions were run - at concentrations of 0, 100, and 200 ppm sodium and phosphorus. The 3-point calibration curve was fitted by a simple quadratic equation. Two samples of deionized water were measured in order to establish a baseline signal, followed by another 100 ppm standard solution. The 100 ppm standard was also analyzed after every ten unknown samples to detect any drift in the response of the equipment during the analysis. Before a measurement was made on each sample, the solution was flushed through the system for approximately one minute to eliminate contamination error. Once the solutions were placed in the sample changer, the entire analysis was automated

When each run was completed, the raw data was imported into a standard Lotus 1-2-3 spreadsheet where it was converted to concentrations of molality. These concentrations were then used to calculate the original sodium and phosphate concentrations before the solutions were diluted.

Aside from the previously mentioned standardization procedure, up to nine known standard solutions were included in each batch of unknown solutions as a second check A summary of the accuracy of the analyses is given in Table A III 1 in Appendix III Due to an oversight, no standards were analysed for the Na/P 3 runs The results show the ICP ES measurements to be within 0.03-3 percent of the expected concentrations of phosphorus, and 0.07-7 percent of the expected sodium concentrations For the majority of the samples, the results for identical samples agreed to within 3 percent For the first several batches, each sample was diluted to give three replicate aliquots, but this was found to be redundant, and the practice was discontinued

The ICP spectrometer was also used to obtain an elemental analysis of several solid products. Approximately 0.1 g of each sample and 0 5 g of $LiBO_2$ were accurately weighed in graphite crucibles. The contents were mixed with a glass rod, and fused in a furnace at 1000°C for one hour. The fusion beads were poured into plastic digestion bottles containing 25 mL of 4 percent hydrochloric acid by volume and 5 mL of concentrated hydrofluoric acid. The mixtures were digested in a bath at 90°C for one hour. The samples were removed to cool. Once the samples cooled to room temperature, 50 mL of boric acid (50g/L) was added, and the samples were returned to the bath for an additional one and a half hours. The samples were removed, and once cool, were transferred to 100 mL polypropylene volumetric flasks, and made up to the mark with deionized water. The samples were then transferred to plastic storage bottles, and analyzed by ICP ES as other samples described above.

2.3.4 Electron Microscopy

Solid products from the iron phosphate, hematite, magnetite, and iron nitrilotriacetate reactions were analyzed by scanning electron microscopy (SEM). Samples were mounted on aluminum stubs with double sided tape and sputter coated with gold in an Edwards S150A sputter coater. The gold coated samples were examined in a Hitachi S570 scanning electron microscope at an accelerating voltage of 20 kV. A Tracor Northern 5500 energy dispersive X-ray analyzer equipped with a Microtrace silicon X-ray spectrometer, Model 70152, with a spectral resolution of 145 eV was used to perform X-ray analysis in the beam spot mode. Detector/sample positioning gave an effective take-off angle of 30°. Secondary electron images were recorded on Polaroid Type 655 Positive/Negative film.

2.4 Synthesis and Characterization of Hideout Reaction Products

2.4.1 Experimental Design

Problems associated with recovering the equilibrium phosphate phases are formidable (Taylor et al., 1977; Tremaine et al., 1993) because the expected iron (III) phase, SIHP, redissolves in the presence of liquid water below 177°C, and because hydrates may form with other reaction products. Removal of water by evaporation to dryness may precipitate non-equilibrium phases or cause pyrophosphate condensation reactions.

The experiments were therefore designed to synthesize the equilibrium sodium iron

phosphate phase of interest in an aqueous reaction medium, then to isolate and recover the solid while avoiding dehydration or contact with liquid water using the modified Parr 4744 reaction vessel.

Initially in all synthesis experiments, the solid starting materials were placed in the Teflon insert on top of the filter. The solution was placed in the Teflon liner, below the filter. Care was taken to ensure that the liquid level would be below the filter when cooling, allowing for the thermal expansion effect. The vessel was then assembled and inverted in an oven at 250°C. By inverting the vessels, the solution was allowed to drain through the filter and react with the solid starting material. The vessels were shaken daily for 1-4 weeks, depending on the reaction, then set upright in the oven for 1-5 hours to filter the reaction product. This filtration before cooling is necessary to prevent contact with liquid water to avoid hydration of solid products during the cooling cycle.

The vessels were then removed from the oven and placed on an aluminum plate in cold running water. By cooling the bombs from the bottom, a temperature gradient formed such that the top of the vessels was hotter than the bottom. This prevented condensation from forming on the reaction product and causing redissolution. Moreover, the presence of unsaturated water vapour in the upper chamber of the vessel during cooling also prevents dehydration of the reaction products. The vessels could not be directly quenched in water because the pressure seal would break. Once the bombs were cooled to room temperature over a period of 2-3 hours, they were immediately opened and the resulting solids and solutions were collected. The isolated solids were analyzed by

X-ray diffraction and electron microscopy.

The risk of contamination by solids dropping through the screen made solution analysis unreliable.

2.4.2 Syntheses of Sodium Iron Hydroxy Phosphate ("SIHP")

2.4.2.1 Iron Phosphate Experiments

SIHP was synthesized according to the following reaction with iron phosphate as the iron source:

$$3FePO_4(s) + 13Na^+(aq) + 3HPO_4^{2-}(aq) + 7OH^-(aq) \rightleftharpoons 3Na_4FeOH(PO_4)_2 \cdot \tfrac{1}{3}NaOH(s) + 3H_2O(l) \qquad (2.1)$$

Fourteen runs using iron phosphate as a starting material were carried out during the study, with varying reaction times (5 days to 4 weeks), sodium-phosphate ratios (2.15 to 2.8), and both with and without frequent agitation. The initial mass of iron phosphate in the vessels ranged from 0.8 to 2.1 g. The concentration of the initial phosphate solution was from 0.5-1.5 mol kg^{-1}. The temperature was 250°C throughout every run. On the basis of these runs, it was determined that frequent agitation and a reaction time of three weeks was required to drive the reaction to completion. Typically under these conditions, the product was a deep red solid.

When the vessels were removed before three weeks, or if there was not sufficient

agitation, the solids were usually yellow-green, or red and yellow mixtures. Powder patterns of the yellow-green mixtures did not match previously reported patterns for SIHP, but did match that of iron phosphate. The red and yellow mixtures matched the XRD powder patterns previously reported for SIHP, with some iron phosphate detected. These results suggest the reaction simply had not gone to completion, and the yellow-green solid was unreacted iron (III) phosphate.

2.4.2.2 Hematite Experiments

Hematite was used as a starting material for the synthesis of SIHP according to the following reaction:

$$3Fe_2O_3(s) + 26Na^+ + 12HPO_4^{2-}(aq) + 2OH^-(aq) \cdots$$
$$6Na_4FeOH(PO_4)_2 \cdot \tfrac{1}{3}NaOH(s) + 3H_2O(l) \qquad (2.2)$$

Hematite was used as a starting material in 19 runs with sodium-phosphate ratio from 2.15 to 2.5. The initial mass of hematite was from 0.05 to 2.2 g, and the initial concentration of phosphate was 0.5 - 1.5 mol kg^{-1}. Syntheses with hematite were maintained at 250°C for 3 to 4 weeks with frequent shaking. Three runs were done to determine optimal reaction conditions and a further 16 runs were carried out to obtain more reaction product.

In one set of runs, designed to produce crystals large enough for single crystal XRD analysis, a very small amount of hematite was used with a 0.6mol kg^{-1} $Na_{2.15}H_{0.85}PO_4$

solution. The temperature was set at 200°C for one week, then raised gradually over a week to 250°C and left for another week. The theory behind this experiment was that the small amount of SIHP produced would be soluble at 200°C, then as the temperature was raised, precipitation would occur. Since there was no solid left in the vessel, there would be fewer nucleation sites, and larger crystals could grow.

2.4.2.3 Magnetite Experiments

The following reaction was used for the synthesis of SIHP from magnetite:

$$2Fe_3O_4(s) + 26Na^+(aq) + 12HPO_4^{2-}(aq) \leftrightarrow$$

$$6Na_4FeOH(PO_4)_2 \cdot \tfrac{1}{2}NaOH(s) + 2H^+(aq) + H_2(aq) \qquad (2.3)$$

Magnetite was used as a starting material in 4 runs, with sodium-phosphate ratios of 2.15 to 2.5. The initial mass of magnetite was 0.2 to 0.4 g and the phosphate concentrations were 0.5 to 1.8 mol kg^{-1}. All runs were allowed to react for 3 to 4 weeks at 250°C with frequent agitation.

In one experiment, parallel runs with iron phosphate, hematite, and magnetite in separate vessels were carried out under identical "optimum" reaction conditions so that the relative yield of reaction product could be analyzed by XRD and an elemental analysis could be done by ICP emission spectroscopy to compare the different syntheses of SIHP.

2.4.3 Syntheses of Maricite

2.4.3.1 Iron Powder Experiments

The hydrothermal synthesis of maricite requires reducing conditions or the use of reagents containing a low oxidation state of iron. Since magnetite is known to produce maricite in addition to iron (III) products, it was thought that the use of iron powder might produce maricite alone, according to the following reaction

$$Na^+(aq) + Fe(s) + H_2PO_4^-(aq) \rightarrow NaFePO_4(s) + H_2(g) \qquad (2.4)$$

Three identical runs were carried out in which 0.5 g Fe was added to 10 mL of 0.9 m NaH_2PO_4 solution in the 45 mL Teflon-lined vessels and allowed to react at 250°C for three weeks with frequent agitation. The amount of reagent was calculated to ensure the vessels could contain the extra pressure resulting from the hydrogen gas produced by the reaction. After three weeks at 250°C, the vessels were removed from the oven. The vessels were opened under nitrogen and stored in a vacuum desiccator to avoid air oxidation.

2.4.3.2 Iron Nitriloacetate (FeNTA) Experiments

Booy and Swaddle (1978) have reported a procedure for the homogeneous precipitation of monodisperse crystallites of magnetite, by thermally decomposing FeNTA(aq) in pressure vessels at 220°C for one week. It was thought that the reducing

conditions created by the decomposition of the $NTA^{3-}(aq)$ would create suitable conditions for the formation of maricite if the reaction was carried out in the presence of sodium phosphate.

FeNTA was prepared by boiling 20 g of ammonium ferric sulfate, $NH_4Fe(SO_4)_2 \cdot 12H_2O$ with 8 g of nitrilotriacetic acid, H_3NTA in 400 mL of deionized water for one hour according to the following reaction

$$Fe^{3+}(aq) + H_3NTA(aq) \rightleftharpoons FeNTA(s) + 3H^+(aq) \qquad (2.5)$$

The resulting yellow-green solid was suction filtered, washed with cold deionized water and dried in air overnight.

Twelve experiments were done with FeNTA as a starting material according to the following reaction:

$$FeNTA(aq) + HPO_4^{2-}(aq) + Na^+(aq) \rightleftharpoons$$
$$NaFePO_4(s) + \text{decomposition products of } HNTA^{2-}(aq) \qquad (2.6)$$

The first two used 0.6 g FeNTA with 10 mL of 0.6 mol kg^{-1} $Na_{2.15}H_{0.85}PO_4$ solution at 250°C. Two more runs were carried out at the same conditions to synthesize more of the reaction product for heat capacity measurements. In an attempt to grow crystals more slowly, four more runs were done at 205°C.

An attempt was also made to use FeNTA decomposition for the synthesis of single crystals of SIHP. To create a more oxidizing environment suitable for synthesizing the iron (III) product, two runs were done with 6 mL of 1 mol kg^{-1} $NaNO_3$ solution, 6 mL of 0.6 m $Na_{2.15}H_{0.85}PO_4$ solution and 0.6 g FeNTA. In a second attempt, 0.4 g CuO was added to the reaction mixture for two runs. All runs were done at 250°C for 3-7 days

2.5 Solubility Measurements in the Stirred Reaction Vessel

2.5.1 Kinetics

In order to determine the time required to reach equilibrium, and to confirm that the reaction was reversible, several kinetic studies were done using runs that lasted for periods of up to two weeks. The kinetics study consisted of three parts. The first step was the determination of the rate of approach to equilibrium at 250°C from supersaturated conditions. The temperature was then lowered to 225°C, and the kinetics were determined approaching equilibrium from unsaturated conditions. The third step, an independent experiment to measure the kinetics at 225°C while approaching equilibrium from supersaturated conditions was conducted to ensure the reaction was reversible. It was thought the excessive solid deposition would make redissolution slow

The experiments to determine the kinetics of SIHP formation at 225 and 250°C were done in the following way. Approximately 25-30 g of hematite was placed in the zirconium cylinder with 220-270 mL of 0.5 mol kg^{-1} $Na_{2.5}H_{0.5}PO_4$ solution. This is a large excess of hematite to ensure that all aqueous iron species were in equilibrium with the iron

(III) oxide. The maximum allowable mass of water in the vessel was determined by calculating the volume after thermal expansion from the steam tables of Haar et al. (1984). The vessel was then assembled and brought up to a temperature sufficient to exceed the saturation index of the reaction product. The reaction was allowed to proceed under isothermal conditions until equilibrium was reached. Samples of 4-5 mL were withdrawn at regular intervals. The first 3-5 mL of solution withdrawn were discarded to ensure the sample line was flushed adequately. At the end of every run, the solutions were diluted for ICP ES analysis. The experiments were stopped when sample flow became erratic, suggesting the liquid level had dropped below the sample tube.

The rate of the reverse reaction was determined immediately after the kinetic experiment at 250°C. The redissolution reaction was initiated by quickly lowering the temperature to 225°C so that the solutions were unsaturated relative to the SIHP reaction product, and again allowing the reaction to proceed to equilibrium at constant temperature.

Fourteen such experiments were conducted. All but five ended prematurely due to power failures, leaks, or clogging of the filter. The first three experiments were to determine the kinetics of SIHP formation at 250°C. Samples were taken regularly over a period of up to 200 hours to determine the kinetics for the formation of the SIHP reaction product. At this point, the temperature was lowered to 225°C, and samples were withdrawn for an additional 200 hours to determine the kinetics of the reverse reaction. In this phase of the experiment, equilibrium was approached from unsaturated conditions.

Three of these experiments were required to obtain enough data points for analysis

In the other two experiments, the kinetics of the SHP formation reaction were determined at 225°C. As in the previous experiments, the vessel was loaded with 25-30g of hematite and 220-270 mL of 0.5mol kg^{-1} sodium phosphate solution with a Na/P ratio of 2.5. Samples were withdrawn for up to 300 hours to ensure equilibrium was achieved.

2.5.2 Solubility

Due to time constraints and corrosion problems, it was impossible to determine the equilibration time at each temperature or to allow equilibration for more than two to four days. In subsequent solubility studies, the reaction was maintained at a temperature for approximately two days before withdrawing samples. The results of the kinetics study were used to estimate the equilibrium concentration

The temperature was raised in a stepwise manner to keep the reaction conditions supersaturated with respect to the iron-phosphate reaction product, but unsaturated with respect to the nickel-phosphate reaction product. Hastily C is largely composed of nickel, and as such can be very reactive with phosphate under suitable conditions Figure 2.3 is a schematic plot of equilibrium phosphate concentration versus temperature for the nickel oxide-aqueous phosphate (Ziemniak and Opalka, 1986) and hematite-aqueous phosphate reactions from this work. The iron reaction is more favourable, but large increases in temperature could supersaturate the solution enough to cause the formation of the nickel-phosphate reaction product, and thus corrode the vessel. As long as the

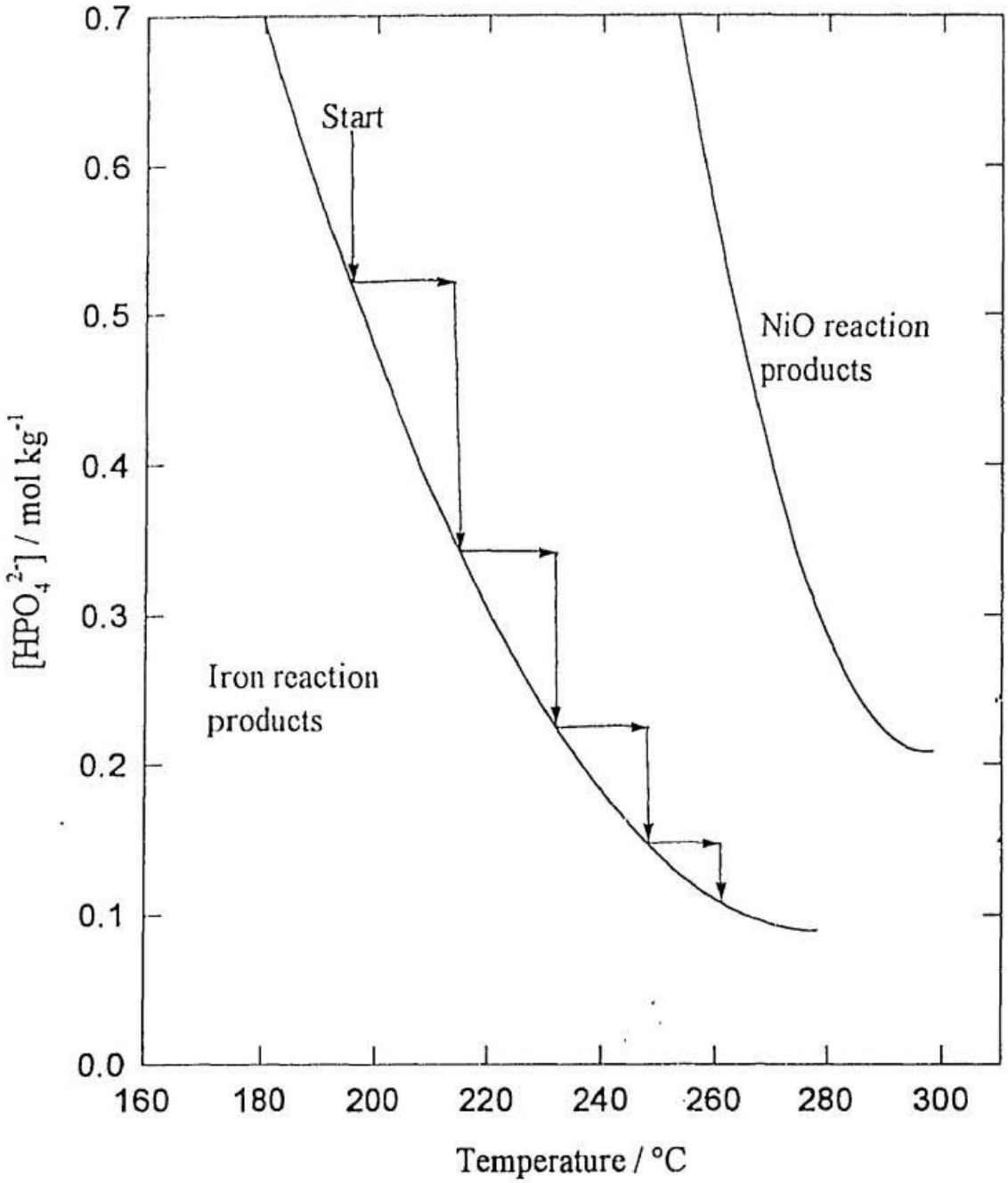


Figure 2.3 Experimental design for Hastelloy C stirred reaction vessel experiments: Solubility of nickel oxide reaction products, and iron oxide reaction products under uncontrolled redox conditions.

temperature was raised in small increments, this problem could be essentially avoided

The vessel was loaded with 25-30 g of hematite and approximately 250 mL of 0.5 mol kg^{-1} sodium phosphate solution. As in the kinetic runs, a large excess of hematite was used to ensure equilibrium between aqueous iron and the iron (III) oxide. The vessel was heated from room temperature to 200°C and allowed to react for up to four days with constant stirring. Approximately 5 mL of solution was collected to flush the sample line before two 5 mL samples were withdrawn, and the temperature was raised 10-25°C and left for two days before this procedure was repeated. This continued until the solution level dropped below the sampling tube or until the temperature reached 325°C. Solubility runs typically lasted up to three weeks.

Seven of these experiments were done at two initial sodium-phosphate ratios: five at Na/P= 2.5 and two at Na/P= 3.0. As the temperature was raised, the precipitation of SHP removed sodium and phosphate from the solution incongruently, causing the Na/P ratio to rise. The Na/P=2.5 solubility runs were done in the Hastelloy C cylinder. Unfortunately there was substantial corrosion on the bottom of the vessel under solid deposits at some temperature above 300°C, where the large heat flux from the heater jacket apparently caused the solution under the thin layer of unstirred hematite and SHP reaction product to be supersaturated with respect to the nickel-phosphate reaction. The zirconium cylinder was used in subsequent runs at Na/P=3.0. At temperatures above 300°C, there were also corrosion problems with this vessel due to reaction of the

zirconium to form zirconium oxide, a zirconium-phosphate reaction product, and excessive amounts of hydrogen gas.

2.5.3 Recovery of the Equilibrium Solid Reaction Product

In order to confirm that the correct phase was being synthesized in the stirred reaction vessel, it was necessary to recover some of the solid reaction product for analysis. It was not possible to obtain this solid from the bottom of the vessel because SIHP is not stable in water below 177°C (Conner and Panson, 1983). Fortunately, in one of the early Na/P = 2.5 runs at a maximum temperature of 275°C, some solid was recovered from an area of the sampling tube above the level of the residual solution left in the vessel after measurements were complete, so that the reaction product was isolated from the liquid at high temperature, preventing redissolution. This solid was analyzed by powder XRD and found to be a mixture of SIHP and hematite. Normally, powder patterns of the solids obtained from the bottom of the vessel showed little or no SIHP. This confirmed that the correct phase was produced in the solubility studies and that it reconverted to hematite and aqueous phosphate on cooling, as observed by Conner and Panson (1983). The powder pattern for this solid can be found in Appendix I.

3.0 SYNTHESIS OF HIDEOUT REACTION PRODUCTS

3.1 The Iron (III) Product: "$Na_3FeOH(PO_4)_2 \cdot \frac{1}{3}NaOH$"

A summary of the sodium iron hydroxy phosphate reaction products recovered from the experiments described in Sections 2.4.2 and 2.4.3 is found in Table 3.1. The most well-formed, homogeneous crystals were obtained with a reaction time of 3-4 weeks with frequent shaking. Typically under these conditions, the product was a deep red solid. Solid samples from all synthetic routes were analyzed by powder X-ray diffraction and scanning electron microscopy. The energy-dispersive X-ray, (EDX) elemental analyses in the SEM studies were qualitative, but the photographs were revealing. The results of the XRD study are listed in Appendix 1.

The solids produced from the iron phosphate runs were typically a flaky light red cake on the outside, with a hard, deep red center. The inner red solid consisted of hard packed microcrystals, while the outer layer was much more lightly packed. The XRD powder patterns for both inner and outer layer were identical, and matched that of the SIHP reported by Tremaine et al. (1992), Ziemniak et al. (1992), Conner and Panson (1983), and Broadbent et al. (1978). Unfortunately, the microcrystals were too small for a single crystal X-ray diffraction analysis.

The powder patterns for the iron phosphate products and the EDX analysis of random crystallites in the SEM studies show no trace of iron phosphate, hematite or magnetite. XRD studies of SIHP with standard additions of hematite suggest that the

Table 3 1 Summary of synthetic runs in Teflon-lined filtration cells. All temperatures 250°C unless noted.

Starting material	mass of iron source	Na/P	m(P_{Total})	Time	comments
$FePO_4$	1.35 g	2.8	0.7m	5 days	red/yellow solid mixture
	1.35 g	2.8	0.7m	2 weeks	red solid cake
	1.35 g	2.8	0.7m	2 weeks	red solid cake
	1.35 g	2.8	0.7m	3 weeks	red solid cake
	1.35 g	2.8	0.7m	3 weeks	red solid cake
$FePO_4$	1.35 g	2.8	0.7m	1 week	red solid cake
	1.35 g	2.8	0.7m	1 week	red solid cake
$FePO_4$	2.12 g	2.15	1.5m	10 days	yellow/green solid
	2.12 g	2.15	1.5m	3 weeks	red/yellow solid mixture
	2.12 g	2.15	1.5m	3 weeks	red/yellow solid mixture
$FePO_4$	2.14 g	2.15	1.5m	3 weeks	red/yellow solid Na/P sol'n ppt'd below filter.
	2.14 g	2.15	1.5m	3 weeks	"
Fe_2O_3	2.14 g	2.15	1.5m	3 weeks	red solid. Na/P sol'n ppt'd below filter
	2.14 g	2.15	1.5m	3 weeks	"
Fe_3O_4	0.37 g	2.15	1.5m	3 weeks	red/brown solid
	0.38 g	2.15	1.5m	3 weeks	"
Fe_2O_3	0.38 g	2.15	1.5m	3 weeks	red solid
$FePO_4$	1.63 g	2.15	1.5m	3 weeks	red solid
Fe_2O_3	0.21 g	2.5	0.5m	1 week	asbestos and HC tube in good shape, red solid
	0.22 g	2.5	0.5m	1 week	red solid

Starting material	mass of iron source	Na/P	m(P_{Total})	Time	comments
Fe_3O_4	0.19 g	2.5	0.5m	1 week	red brown solid
	0.19 g	2.5	0.5m	1 week	asbestos turned black, black solid, HC tube good
$FePO_4$	0.80 g	2.5	0.5m	1 week	yellow/green solid
Fe_2O_3	0.44 g	2.5	1.0m	4 weeks	red solids. Power outage caused
	0.44 g	2.5	1.0m	4 weeks	stoppage of run.
	0.44 g	2.5	1.0m	4 weeks	Solids recovered
	0.44 g	2.5	1.0m	4 weeks	before decomposition
	0.44 g	2.5	1.0m	4 weeks	occurred.
Fe_2O_3	0.44 g	2.5	1.0m	3 weeks	red solid
	0.44 g	2.5	1.0m	3 weeks	"
	0.44 g	2.5	1.0m	3 weeks	"
	0.44 g	2.5	1.0m	3 weeks	"
	0.44 g	2.5	1.0m	3 weeks	"
Fe	0.51 g	1.0	0.9m	3 weeks	green solid (turned blue)
	0.50 g	1.0	0.9m	3 weeks	"
	0.48 g	2.5	0.9m	3 weeks	vessel leaked. NR
Fe_2O_3	0.13 g	2.15	0.6m	3 weeks	200-250°C gradually, red microcrystalline powder
	0.14 g	2.15	0.6m	3 weeks	"
	0.06 g	2.15	0.6m	3 weeks	"
	0.05 g	2.15	0.6m	3 weeks	"

Starting material	mass of iron source	Na/P	m(P_{Total})	Time	comments
FeNTA	0.65 g	2.15	0.6m	3 days	creamy off-white solid
	0.58 g	2.15	0.6m	2 weeks	"
FeNTA	0.51 g	2.15	0.6m	6 days	6mL 1m NaNO3 added.
	0.71 g	2.15	0.6m	6 days	black/blue solid
FeNTA	0.68 g	2.15	0.6m	4 days	0.4g CuO added.
	0.64 g	2.15	0.6m	5 days	red/brown solid
FeNTA	0.65 g	2.15	0.6m	4 days	creamy off-white solid
	0.57 g	2.15	0.6m	4 days	"
FeNTA	0.67 g	2.15	0.6m	8 days	205°C
	0.71 g	2.15	0.6m	8 days	"
	0.83 g	2.15	0.6m	8 days	"
	0.84 g	2.15	0.6m	8 days	"

concentration of hematite, and presumably other impurities is less than 5 mass percent The detection limit is less than 3 percent under the scan conditions used.

A sample of the iron phosphate reaction product, shown in Figure 3 1a, b, and c, consisted of thin, needle-like crystals that were stacked in an organized fashion Each layer had crystals lying perpendicular to the crystals in the layer above and below It appeared that the crystals had grown on a surface that subsequently dissolved. No unreacted starting material could be found visually or by elemental analysis using the SEM. This suggests the crystals grew out of the solid iron phosphate starting material, rather than from the solution. The crystals were approximately 2-3 μm thick and up to 100 μm long, and all roughly the same size. The elemental analysis confirmed the presence of iron, sodium, and phosphorus. While some of these crystals were long enough for single crystal XRD, they were not thick enough.

The sodium-phosphate ratio did not have any noticeable effect on the product when varied between 2 15 and 2.8.

The hematite experiments also worked best when the vessels were left in the oven for 3-4 weeks with frequent shaking. The solids produced were dark red microcrystalline clumps. These solids were more homogenous than the iron phosphate products, but the crystals were smaller.

In one set of experiments designed to obtain larger crystals, a very small amount of hematite was used at 200°C for one week, then raised to 250°C gradually over a week, and left at 250°C for a week. It was thought that by having less solid present, there would



Figure 3.1 a, b, and c: Scanning electron micrographs of solid reaction products obtained from iron phosphate and aqueous sodium phosphate (Na/P=2.15) at 250°C for three weeks.

be fewer nucleation sites, leading to larger crystals. The temperature was adjusted in this manner to take advantage of the inverse solubility gradient of the SIHP. The crystals produced by this reaction were larger than normally obtained from hematite, but still not large enough for single crystal X-ray diffraction.

The powder patterns for these solids matched those previously reported for SIHP equally well as specimens prepared from iron phosphate. There were, however, traces of hematite in the solids. One batch of solids was analyzed by XRD with standard additions of hematite of 0, 1, 5, and 10 percent. The peak heights for the 2.53Å hematite peak were measured and plotted versus mass percent hematite and the results suggested the product contained approximately 5 percent hematite. The powder patterns for this analysis are described in Appendix I, the plot can be found in Figure 3.2, and the data in Table 3.2.

The crystals from the hematite reaction, as shown in Figure 3.3a and b were slightly smaller, but were seen to be growing radially, as if from a common center. Elsewhere on the specimen, round clumps were found with crystals growing from them in a radial pattern. One of these clumps is shown in the upper right corner of Figure 3.3b, and another is magnified in Figure 3.3c. The crystals were of the same composition as the others in the sample, but the clump had sodium and phosphorus, with little or no iron. This suggests the SIHP crystals grew out of precipitated sodium phosphate, as opposed to the mound of hematite.

There was a second type of crystal which was much larger than the others. Figure 3.3a shows one which was approximately 18-20 μm thick and 60-80 μm long. Both types

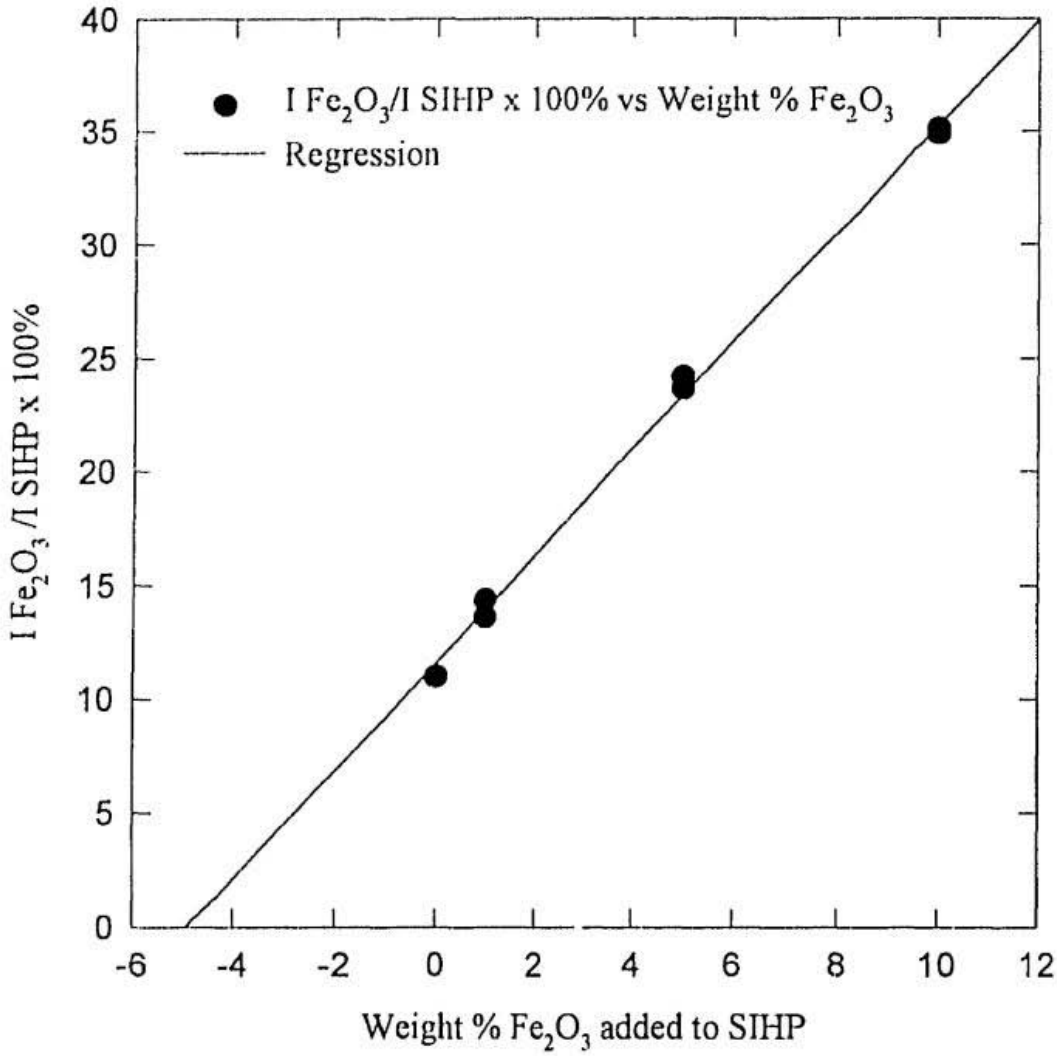


Figure 3.2 Determination of Weight % Fe_2O_3 in SIHP

Table 3.2 Summary of data from XRD quantiative analysis.

Weight % SIHP	# of counts 2.53Å peak	# of counts	% Fe_2O_3
0	4655	491	11.0
1	5267	718	13.6
1	5174	746	14.4
5	4710	1116	23.7
5	4640	1124	24.2
10	4558	1598	35.1
10	4655	1576	34.9



Figure 3.3 a, b, and c: Scanning electron micrographs of solid reaction products obtained from hematite and aqueous sodium phosphate (Na/P=2.5) at 250°C for three weeks.

of crystals, however, had similar ratios of Na, Fe, and P consistent with SIHP.

Again, as in the iron phosphate runs, the Na/P ratio had no obvious effect on the size or morphology of the crystals.

The runs done with magnetite produced solids very similar in appearance to those from the hematite experiments, except the solids were slightly darker than the hematite reaction products. It was thought this was due to the presence of unreacted magnetite, although there were no traces of magnetite in the powder patterns.

The reaction product from the magnetite reaction (Figure 3.4a and b) contained crystals of similar size to the iron phosphate and hematite reaction products, but the crystals grew in clumps of parallel crystals. The crystals were not as uniform and there appeared to be many crystal fragments. The EDX elemental analysis suggested these crystals were of similar composition to the iron phosphate and hematite reaction products

In one set of experiments, all three of the above starting materials were used in separate vessels under identical reaction conditions and reacted for three weeks with frequent agitation. The products were all analyzed by XRD and found to be virtually identical. Elemental analyses of these solids were done by ICP ES A sample of $FePO_4$ was included in the unknown samples as a standard; the ratio of iron to phosphate was found to be 1.02, as expected. The ratios of Fe:P:Na are within experimental error of the previously reported stoichiometry of SIHP except for the hematite product However, if the mole percent of unreacted hematite is included, the analysis is as predicted. The results of these analyses can be found in Table 3.3





Figure 3.4 a and b : Scanning electron micrographs of solid reaction products obtained from magnetite and aqueous sodium phosphate (Na/P=2.15) at 250°C for three weeks.

Table 3.3 ICP ES elemental analysis of SIHP from different synthetic routes.

Sample	Description	% P_2O_5	% Fe_2O_3	% Na_2O	mol P/mol Fe	mol Na/mol P
SQ30E1	dark red $FePO_4$ reaction product	37.92±0.26	21.09±0.29	37.32±0.40	2.023±0.015	2.254±0 017
SQ30E2	light red $FePO_4$ reaction product	37.55±0.10	22.40±0.06	36.75±0.17	1.886±0.004	2.241±0.005
SQ36A	dark red Fe_2O_3 reaction product	35.09±0.15	21.98±0.14	35.15±0.29	1.796±0.008	2.294±0.010
SQ30A	dark red Fe_3O_4 reaction product	39.66±0.13	23.01±0.05	37 02±0.27	1.939±0 004	2.138±0.008
SQ30A2	dark red Fe_3O_4 reaction product	37 71±0 23	23 60±0 13	36 94±0.26	1.798±0 008	2.243±0 009
SIHP	theoretical	38.56	21.69	36.48	2.000	2 167
SQ40A	$FePO_4$ (standard)	44 02±0.20	48 51±0 12	0 48±0 03	1 021±0 005	0 024±0 06
$FePO_4$	theoretical	47 06	52.94	0 000	1 000	0 000

As previously mentioned, the EDX elemental analyses of these solids were qualitative, but the relative abundances of the main elements could be observed. The presence of the gold coating interfered with the phosphorus analysis since the peaks overlapped, but its presence could be detected. The analyses showed that all crystalline products contained iron, sodium, and phosphorus in similar ratios

In all the iron (III) reaction products examined by SEM, there appeared to be no unreacted starting material, or other deposited material Even in the hematite reaction product, which had 5 percent hematite as determined by XRD, no hematite could be found The crystals were apparently pure and the reactions presumably went to completion. Figure 3.5 shows reaction products reported by Tremaine et al. (1992). These products have considerable deposition of materials other than SIHP, including maricite and sodium phosphate.

Figures 3.6a, b, and c are electron micrographs of the two hematite supplies and the magnetite used in these experiments These samples required a much higher magnification than others examined, however, nothing resembling these particles was found in any of the micrographs of the reaction products.

3.2 The Iron (II) Product: $NaFePO_4$

3.2.1 The Iron Powder Synthesis

In an effort to produce maricite, $NaFePO_4$, iron powder was added to a 1 mol kg^{-1} NaH_2PO_4 solution in the 45 mL vessels at 250°C and maintained at that temperature for

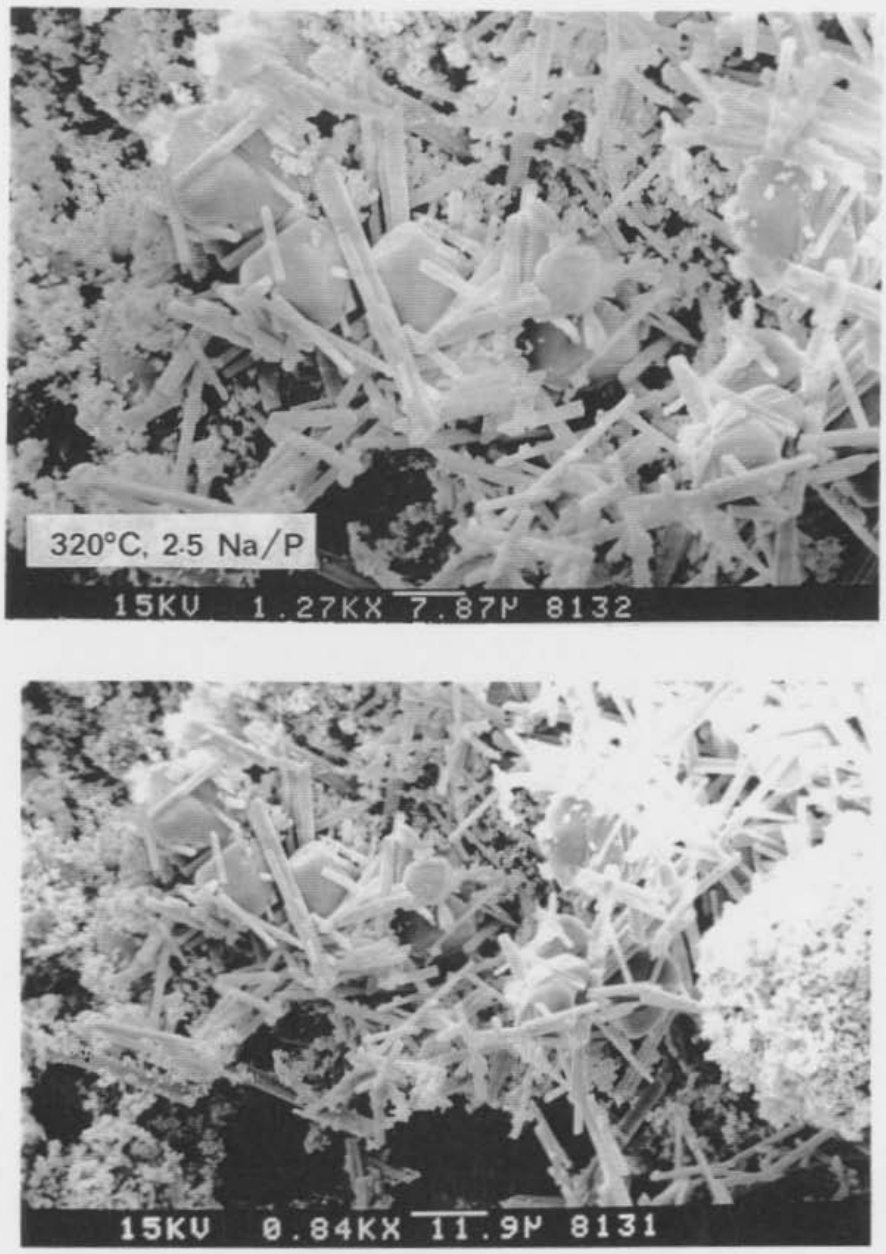
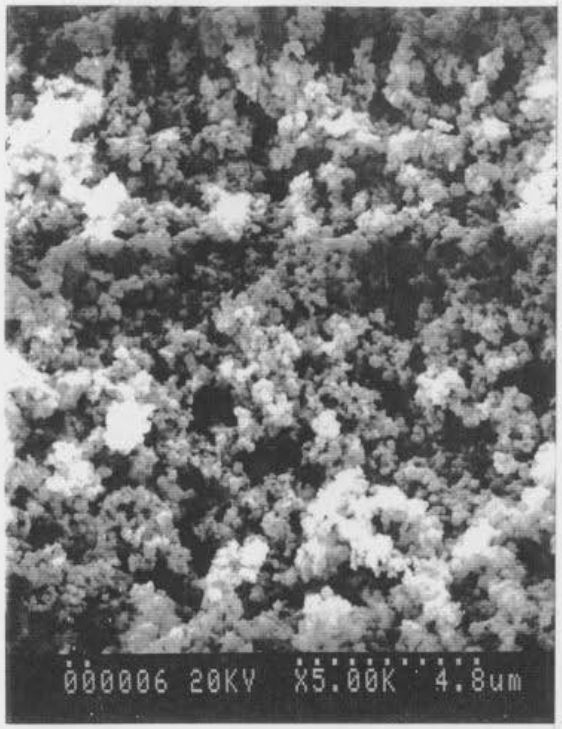
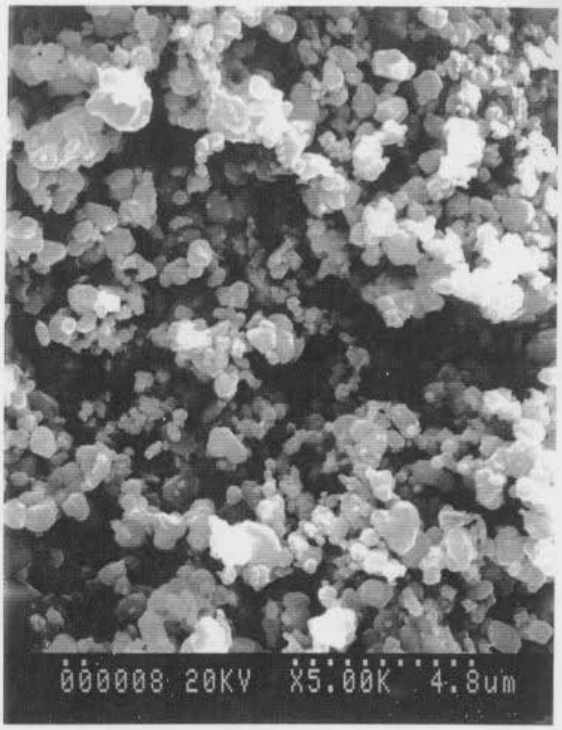


Figure 3.5 a and b : Scanning electron micrographs of solid reaction products obtained from magnetite and aqueous sodium phosphate (Na/P=2.5) at 320°C for two weeks (Tremaine et al., 1992).





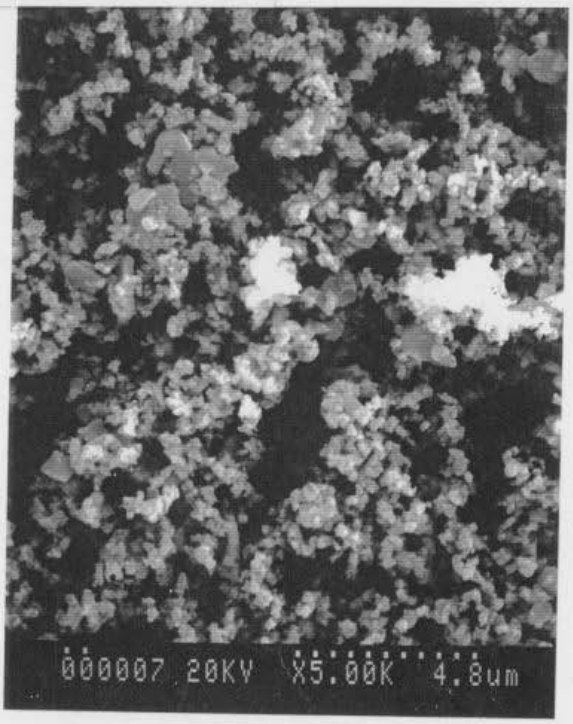


Figure 3.6 a, b, and c: Scanning electron micrographs of solid starting materials. Figures 3.6 a and b are the two hematite sources, and Figure 3.6 c is the magnetite source.

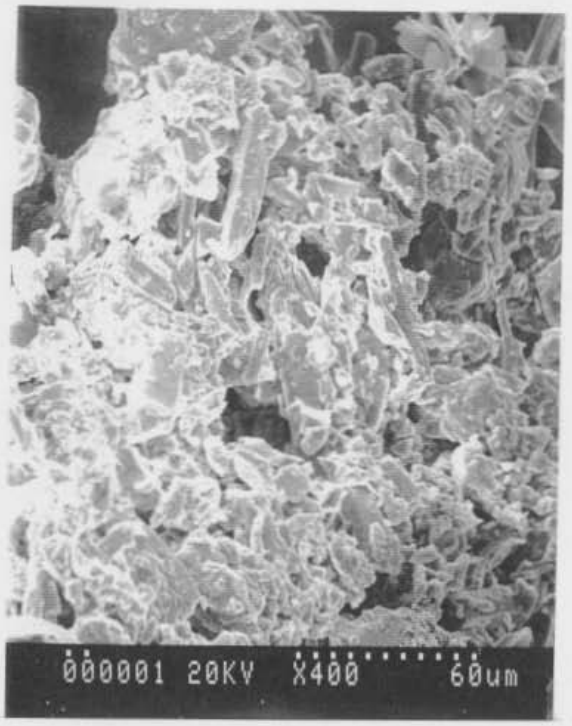
three weeks. The solid products recovered from the cooled vessel were originally a green powder, but over a few weeks, turned dark blue despite being opened in a nitrogen atmosphere and stored in a vacuum desiccator.

The powder patterns of the resulting solids matched that of maricite. These powder patterns are described in Appendix I.

Figures 3.7a and b show electron micrographs of the solid produced in these experiments. The solid consisted of crystals approximately 60 μm long and 10 μm thick. A broad maximum in the XRD pattern, and the visual appearance of specimens suggested that the sample contained amorphous material of unknown composition. The EDX elemental analysis of the whole mixture was consistent with what would be expected from maricite, that is, approximately equal amounts of iron, phosphorus, and sodium.

3.2.2 The FeNTA Synthesis

Booy and Swaddle (1978) have reported a hydrothermal synthesis of magnetite that produced crystals large enough to use in single crystal XRD. The key to producing relatively large magnetite crystals was to use a soluble iron complex, FeNTA, as a source of iron. The NTA^{3-} ligand decomposed slowly over 2-3 days, releasing the iron into a reducing environment created by the NTA^{3-} decomposition products. This reducing environment was responsible for the production of magnetite instead of the iron (III) oxide, hematite. It was thought that this reaction could be used to produce maricite, if it was carried out in the presence of an excess of aqueous sodium phosphate. Several runs



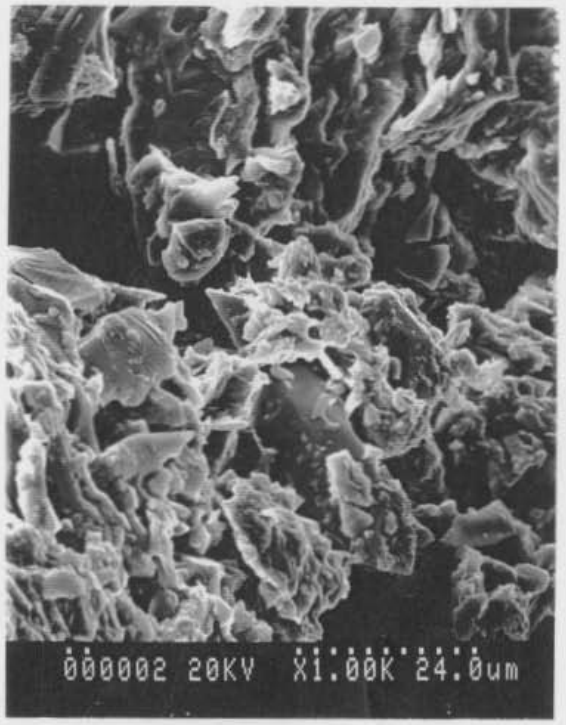


Figure 3.7 a and b: Scanning electron micrographs of solid reaction products obtained from iron powder and aqueous sodium phosphate (Na/P=1.0) at 250°C for three weeks.

were done using FeNTA with $NaHPO_4$(aq) in the Teflon-lined pressure vessels at 205 and 250°C. When the vessels were opened, the product was found to be creamy white. This solid was analyzed by XRD and was identified as maricite.

The reaction product from the FeNTA reaction was analyzed using the scanning electron microscope. Secondary electron images of these products can be found in Figure 3.8a and b. The ratios of iron, sodium, and phosphorus were much different from those of the iron phosphate, hematite, and magnetite reaction products. The ratio of iron to sodium and phosphorus was much higher for the maricite sample than for the other reaction products, as expected.

The crystals from the FeNTA reaction were much different from those of the other reaction products as well. From the blossom-like growth, it appears the crystals grew out of solution by homogeneous nucleation, as opposed to nucleation or epitaxial reactions on the mound of solid at the bottom of the vessel, as was the case for the iron phosphate reaction product. These products are much larger than the iron (III) solids and appear to be longer versions of the block-like crystals reported by Tremaine et al. (1992), shown in Figure 3.9.

In an attempt to make individual crystals suitable for single crystal XRD, the temperature was lowered to slow down the reaction. This proved to be successful since large single crystals were obtained from these runs. Figure 3.10 a and b show single crystals similar to the one used to obtain the structure. These samples were much larger and separable, unlike those previously grown.



Figure 3.8 a and b: Scanning electron micrographs of solid reaction products obtained from FeNTA and aqueous sodium phosphate (Na/P=2.15) at 250°C for one week.

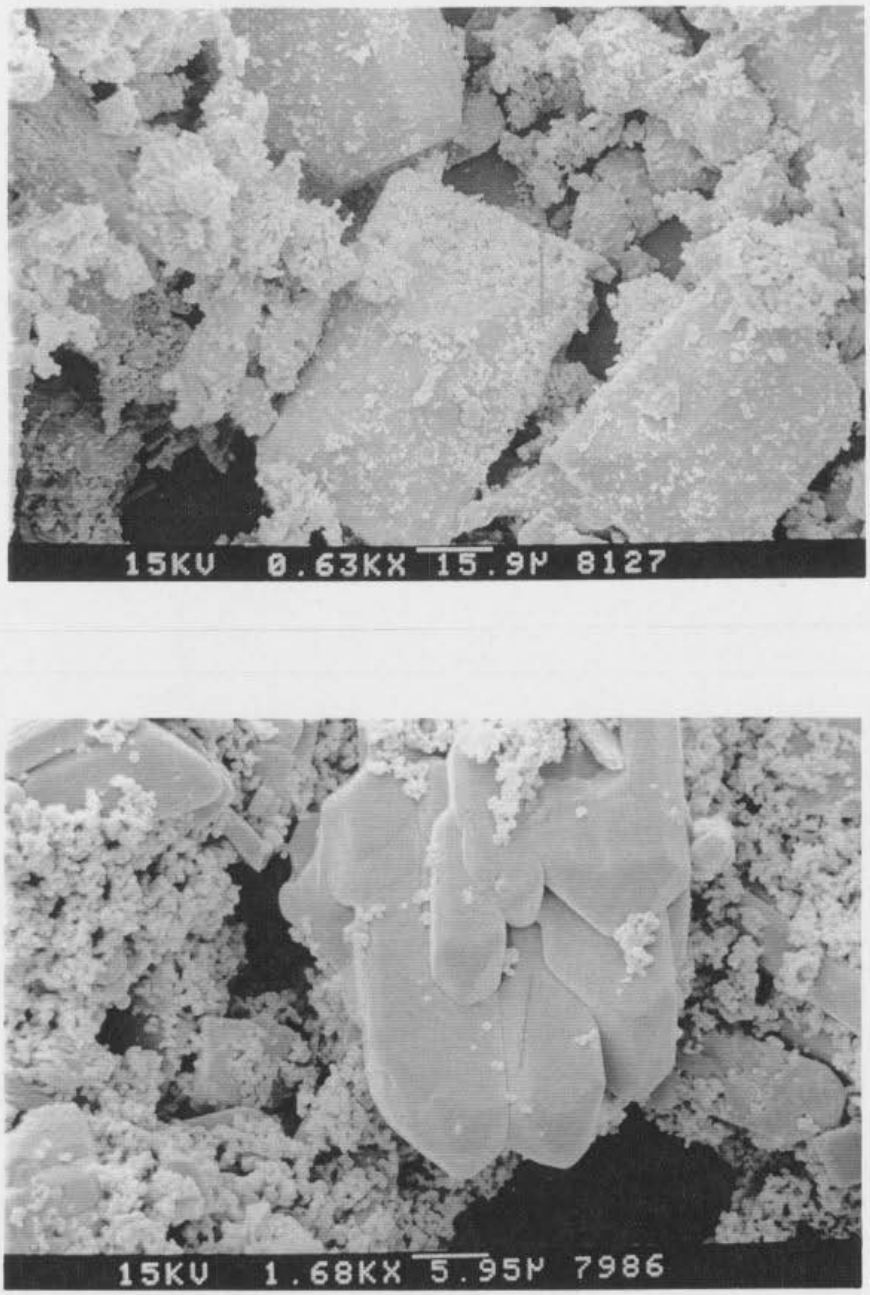


Figure 3.9 a and b : Scanning electron micrographs of solid reaction products obtained from magnetite and aqueous sodium phosphate (Na/P=1.0 and 1.5) at 320°C for three weeks (Tremaine et al., 1992).

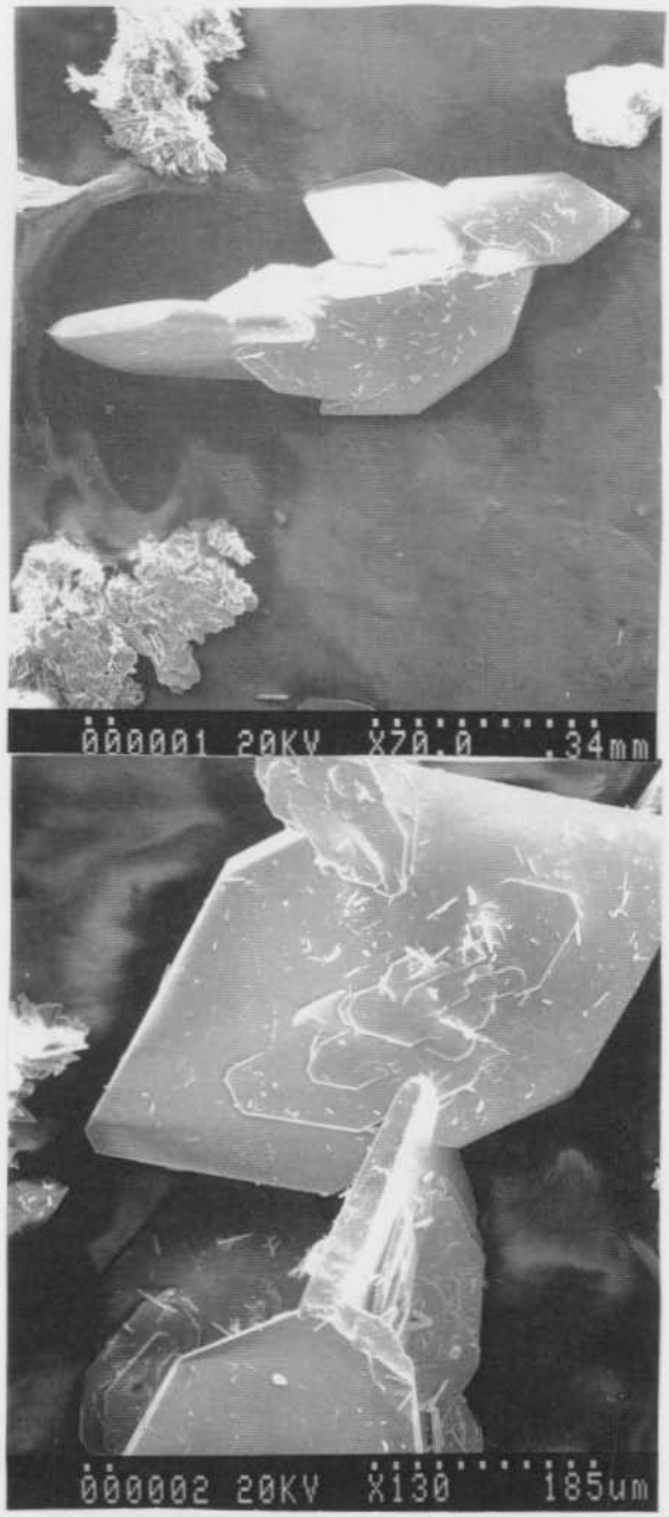


Figure 3.10 a and b: Scanning electron micrographs of solid reaction products obtained from FeNTA and aqueous sodium phosphate (Na/P=2.15) at 205°C for three weeks.

Efforts were made to synthesize SHIP from FeNTA by carrying out the hydrothermal decomposition in the presence of an oxidizing agent. It was thought that CuO might be used to prevent the formation of an iron (III) phase since Cu^{2+} does not react with phosphate. The experiment was repeated with 0.4 g of CuO. The solid product was brown and the XRD powder pattern matched copper(I) oxide, Cu_2O, from the JCPDS database. Traces of copper, Cu, copper (II) oxide, CuO, maricite and magnetite were also found. No evidence of SHIP could be found in the sample. This suggests that the reaction proceeded as before, and that the presence of the CuO caused the environment to be sufficiently oxidizing to form a mixture of magnetite and maricite, but that CuO was not a strong enough oxidizing agent to produce SHIP.

Another oxidizing agent that was tried was $NaNO_3$. The initial experiment was repeated with 6 mL of 1 mol kg^{-1} $NaNO_3$ solution. The product was deep blue (almost black) solid. Initially, this solid was thought to be magnetite, but while preparing the solid for XRD analysis, the color was found to be dark blue. The XRD analysis was inconclusive, but there were traces of maricite, magnetite, and possibly hematite in these solids. The powder patterns of these solids are described in Appendix 1.

3.3 The Crystal Structures of the Iron (III) and Iron (II) Products

Sodium iron(III) hydroxy phosphate, $Na_4Fe(OH)(PO_4)_2 \cdot \frac{1}{3}NaOH$, is believed to be the major iron(III) reaction product causing sodium phosphate hideout. The compound was first reported in the early 1980's, from pressure vessel studies on hideout (Conner and

Panson, 1983, Ziemniak and Opalka, 1992), and its stoichiometry was inferred from elemental analyses on solid reaction products and hydrothermal solutions during hideout experiments. It is important to determine its structure, both to confirm the stoichiometry and to gain insights into the mechanisms of its formation.

As discussed in previous sections, several attempts to synthesize large crystals were made in the low-pressure Teflon cells using Fe_3O_4, Fe_2O_3 and $FePO_4$ as sources of iron(III). Attempts were made to mount the largest crystals (0.05 x 0.02 x 0.1 mm) obtained from our synthesis for single crystal X-ray diffraction but these proved to be unsuccessful. In the laboratory of a collaborator, crystals of SIHP were formed fortuitously during the preconditioning of a new stainless steel (Type 347) autoclave. A concentrated alkaline sodium phosphate solution (26000 ppm, Na/P = 2.4) containing a lesser amount of an inorganic oxidizing agent was heated beyond the expected threshold of reaction with magnetite. Upon opening the autoclave after continuous operation at 288°C in a refreshed mode for 400 hours, profuse growths of these reddish colored crystals were observed on the walls of the vessel. The crystals ranged in size from 0.2 to 0.4 mm in length. A crystal structure was successfully determined using one of these crystals. Scanning electron micrographs of samples of these crystals are found in Figure 3.11 a and b. The crystals are very similar to the one shown in Figure 3.3 a.

The coordinates of the atoms are given in Table 3.4, and the structure is shown in Figure 3.12. A detailed analysis of the crystal structure of SIHP can be found in Appendix II. The X-ray diffraction pattern is consistent with an orthorhombic unit cell containing 8





Figure 3.11 a and b: Scanning electron micrographs of solid reaction products obtained from flow experiment involving a stainless steel vessel and aqueous sodium phosphate at 288°C for 17 days.

Table 3.4 Positional parameters for SIHP.

atom	x	y	z	occupancy
Fe(1)	1/4	1/4	1/4	1/2
P(1)	0.3811(1)	0.3780	1/2	1/2
P(2)	0.1209(1)	0.3833(1)	0	1/2
Na(1)	0 2701(2)	1/2	1/4	1/2
Na(2)	1/2	0.4721(3)	3/4	1/4
Na(3)	0	0.2628(2)	1/4	1/2
Na(4)	.01384(2)	0.3814(2)	1/2	1/2
Na(5)	0	1/2	1/4	1/4
Na(6)	0.3806(4)	0.3777	0	0.274
O(1)	0.3260(2)	0.3546(2)	0.3223(5)	
O(2)	0.4732(3)	0.3347(3)	0.5000	1/2
O(3)	0.3914(3)	0.4767(3)	1/2	1/2
O(4)	0.1482(2)	0.3329(2)	0.1790(5)	
O(5)	0.0168(3)	0.3914(3)	0	1/2
O(6)	0.1656(4)	0.4720(3)	0	1/2
O(7)	0.3064(3)	0.2551(3)	0	1/2
H(1)	0.3296	0.3052	0	0.226

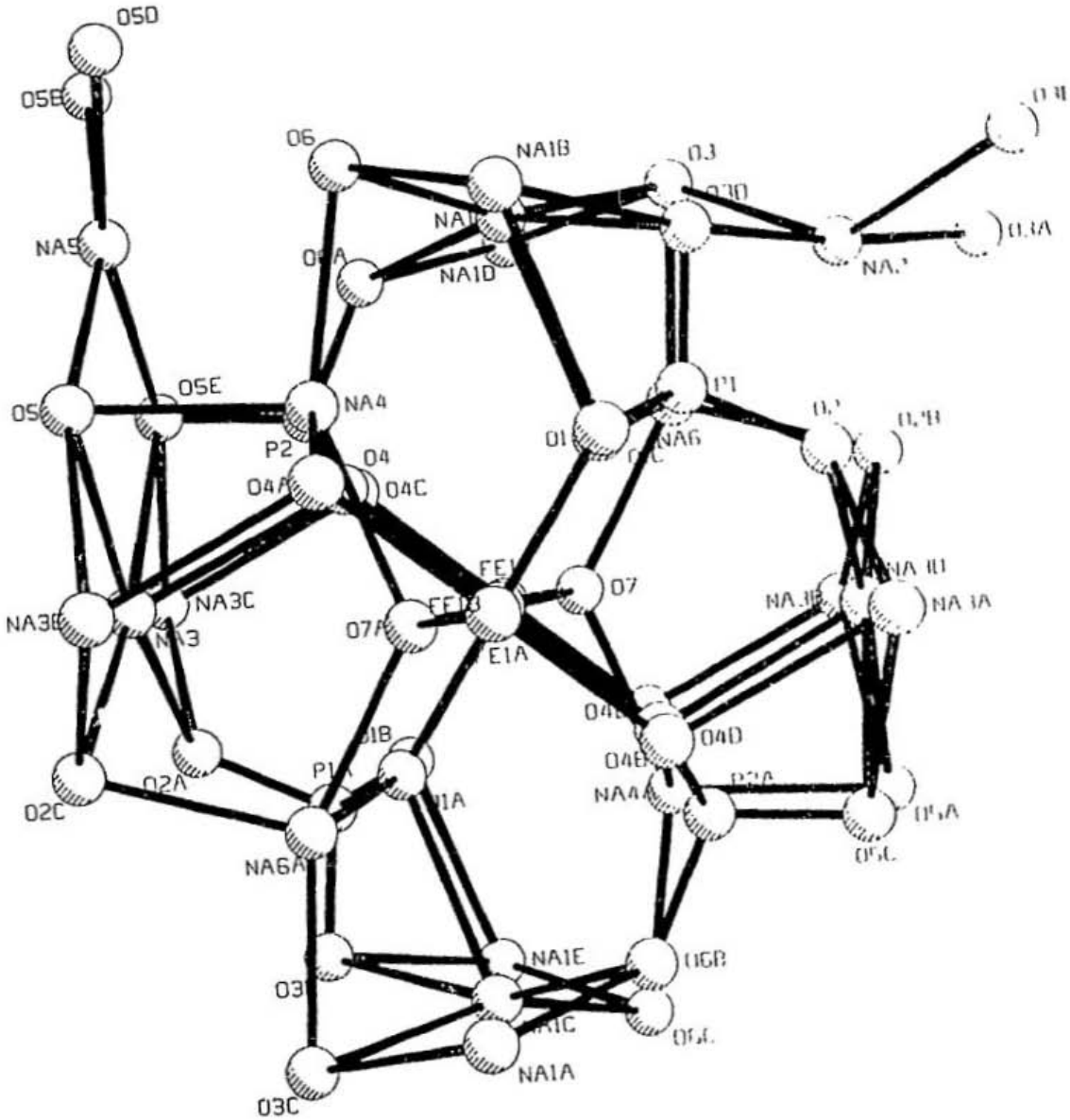


Figure 3.12 Crystal structure of SHP.

molecules with the formula $Na_3Fe(PO_4)_2(Na_{2(1-x)}H_{2x}O)$, with $x \approx 0.22$. This is similar, but not identical, to the formula $Na_3Fe(OH)(PO_4)_2 \cdot \frac{1}{3}NaOH$ proposed by Ziemniak and Opalka (1992). The main structural feature is a chain of Fe(III) ions linked by bridging oxygens and phosphate bridges. The crystal structure analysis in Appendix II indicates that alternating iron and oxygen atoms with Fe-O-Fe and O-Fe-O angles of 129.8° and 180° respectively form zig-zag chains parallel to the c axis. Iron lies at the centre of symmetry and the Fe-Fe distances are 3.58 Å. Completing the metal coordination sphere are two phosphate ions linking adjacent iron atoms. The phosphorus and ligating oxygen atoms lie on the mirror plane, *m*. The structure can thus be visualised as a core of iron surrounded by an inner layer of coordinating oxygen atoms, one of which bridges irons directly, the remainder belonging to phosphate ions. The outer layer of oxygen atoms carrying the balance of phosphate negative charge includes sodium ions in 5 distinct sites. The analysis also indicates that the bridging oxygens of the central core are associated with either a proton or a sixth sodium non-stoichiometrically, and in a disordered fashion. However, a report of a double cell observed in powder analysis of another sample of this compound (Tremaine et al., 1993) suggests the presence of a superlattice which could reasonably exhibit regular alternation of sodium ions and protons and hence a 50:50 ratio. From a bonding point of view, a more realistic interpretation would have the iron chains including both oxide and hydroxide bridges distributed in a random fashion along the chain in the sample, or alternating in samples which display the superlattice. It is reasonable to speculate that the completely disordered non-stoichiometric structure on one hand, and a

stoichiometric superlattice on the other are extremes in a range of structures dependent upon the exact conditions of crystallization. A structural feature which may well be associated with this phenomenon is the disordered distribution of one of the sodium ions close to *222*. Although the hypothesis has not been tested, it is certainly possible that this sodium ion corresponds to two related but non-equivalent sites in the superlattice.

The structure is significant in that it explains the variable stoichiometry observed in powder diffraction patterns in this and other work (Tremaine et al., 1993), and it supports the possibility of a superlattice in the structure. Also of importance is the identification of the stoichiometry of hydrogen and oxygen, which cannot be determined from solubility studies or routine methods for inorganic elemental analysis. The fact that there is no water in the lattice helps to explain why SIHP is stable only at high temperatures - where the activity of liquid water is small. At lower temperatures, SIHP is unstable relative to hydrated aqueous phosphate species.

Structural information for SIHP had been limited. In a previous study (Ziemniak and Opalka 1993), SIHP was analyzed by Mössbauer and infrared spectroscopy. Results from the Mossbauer analysis showed that iron was distributed nearly equally between two distinct lattice sites, and that the iron ions in the crystal were solely in the Fe(III) oxidation state. Absorption peaks at 3550 cm^{-1} (major) and 3580 cm^{-1} (minor) in the infrared spectrum suggested the presence of hydroxyl ions. These results were confirmed by the crystal structure of SIHP.

One of the crystals from the maricite prepared from FeNTA at 205°C was also successfully mounted. The crystal structure and interatomic spacings were identical to those reported by LePage and Dornay (1977) for a natural crystal with 10 percent of the Fe(II) sites substituted with Mn, Mg, and Ca. The crystal structure is presented in Appendix II.

4.0 SOLUBILITY AND REACTION KINETICS

4.1 Kinetics of Phosphate-Hematite Reaction

The central premise of this work is that aqueous sodium phosphate solutions undergo reversible reactions with hematite to form sodium iron(III) hydroxy phosphate according to the reaction

$$\tfrac{1}{2}\ Fe_2O_3(s) + 13/3\ Na^+(aq) + 2\ HPO_4^{2-}(aq) + \tfrac{1}{3}\ OH^-(aq) \rightleftharpoons Na_3Fe(PO_4)_2\cdot(Na_{1.3}H_{2.3}O)(s) + 5/6\ H_2O \qquad (4.1)$$

Kinetic experiments to determine the rate of SIHP formation were carried out in the zirconium 450 mL stirred reaction vessel at 225 and 250°C, according to the methods described in Section 2.5.1. The rate of SIHP redissolution to form aqueous phosphate and hematite was determined at 225°C only. The results are plotted in Figures 4.1 and 4.2.

The hydrodynamic conditions and the available surface areas for hematite and SIHP could not be controlled well in these experiments, although the conditions used in the solubility measurements are duplicated. As a result, we chose to describe the data with a simple rate equation commonly used in mineral dissolution studies (Stumm and Morgan, 1970; Blesa et al., 1993):

$$d\ m(PO_4,t) / dt = k\ a\ [m(PO_4, sat) - m(PO_4, t)]^n \qquad (4.2)$$

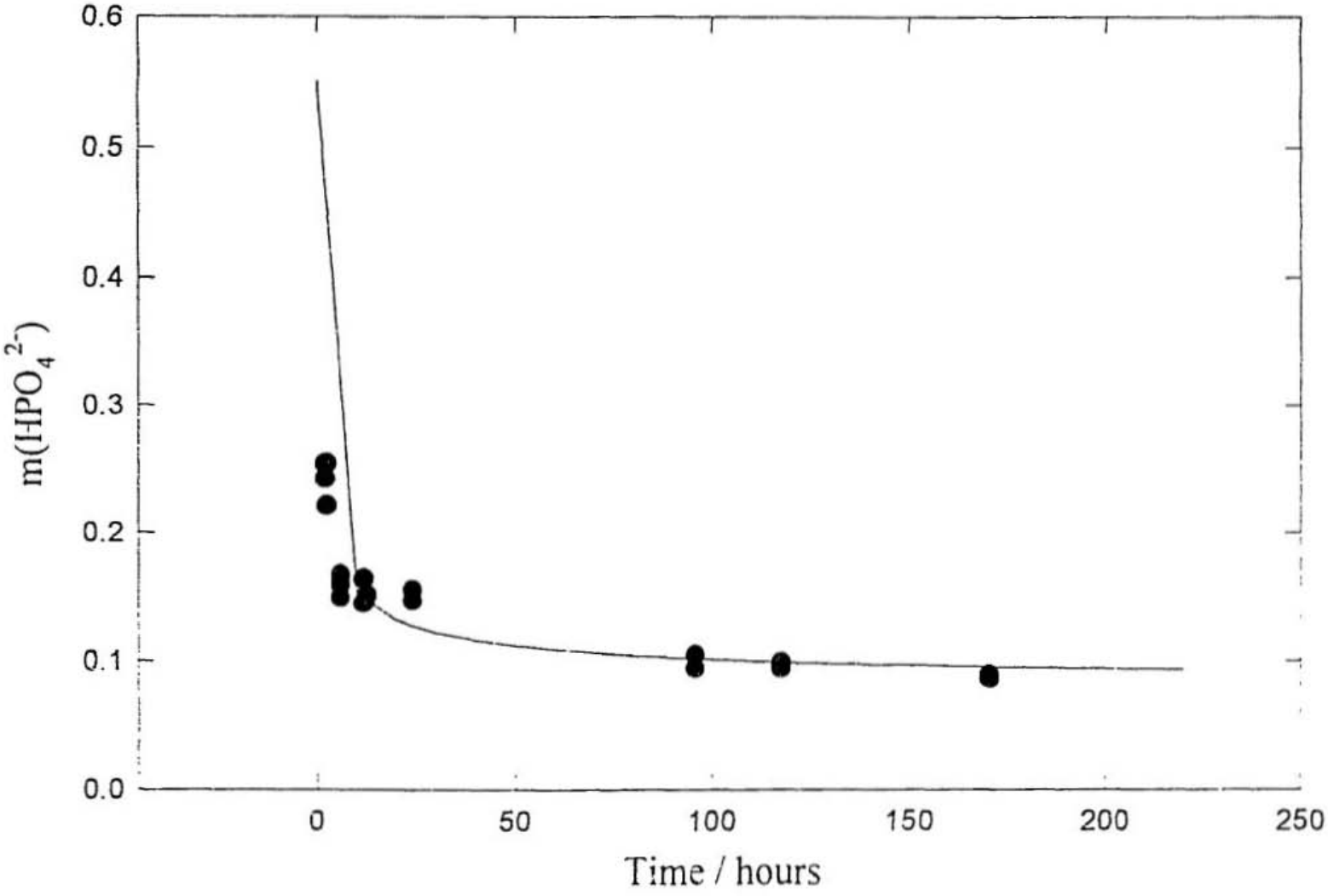


Figure 4.1 Kinetics of precipitation of SIHP at 250°C.

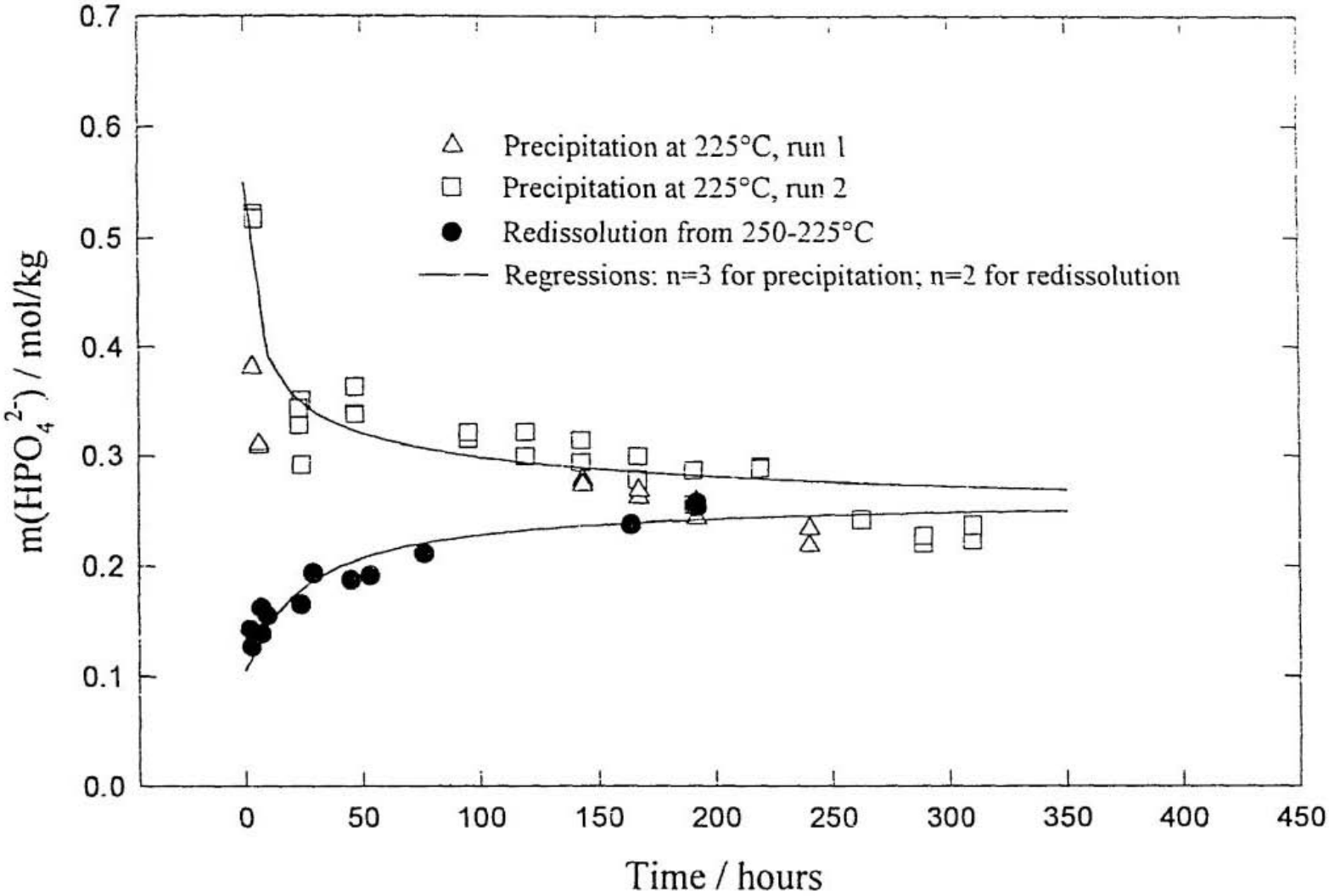


Figure 4.2 Kinetics of precipitation and redissolution at 225°C.

where k is the rate constant, and a_{ox} is the oxide surface area. Here, $m(PO_4,t)$ and $m(PO_4, sat)$ are the total molalities of phosphate species at time t and equilibrium, respectively. The value n = 1 corresponds to diffusion controlled kinetics, while values in the range 3 > n > 1 are typical of surface activation control. Integration yields the expression

$$m(PO_4,t) = m(PO_4,sat) + [(n - 1)\, k\, a\, t + \{ m(PO_4,t = 0) - m(PO_4,sat)\}^{(1-n)}]^{1/(1-n)} \qquad (4.3)$$

The kinetic data in Figures 4.1 and 4.2 were represented well by least squares fits to Equation 4.3 with n = 3 for precipitation and n = 2 for redissolution. The results are shown by the solid curves in the figures. The rate constant for the redissolution reaction at 225°C was 0.251 $mol^{-1}\, kg\, hr^{-1}\, m^{-2}$. The rate constants for the precipitation reactions at 225 and 250°C were 1.81, and 8.10 $mol^{-2}\, kg^2\, hr^{-1}\, m^{-2}$ respectively. The temperature dependence of the rate constant for the formation reaction was used to define an activation energy, according to the simple Arrhenius equation. The equation for the rate constant, k, for the precipitation reaction is given below.

$$k = A e^{-E_a/RT} \qquad (4.4)$$

where E_a is 129.7 kJ mol^{-1} and A is 7.27 x 10^{13} $mol^{-2} kg^2 hr^{-1} m^{-2}$

The Arrhenius activation energy, E_a, from Equation 4.4 is consistent with surface activation control mechanisms (Stumm and Morgan, 1970). While the experimental conditions in the measurements discussed above are too complex to allow us to identify the rates with one kinetic process, we can speculate about some of the factors controlling the rate of formation of SHP.

Blesa and coworkers (1994) have reviewed recent work on the dissolution mechanisms of iron oxides in considerable detail. While much is known about magnetite, much less work has been done on hematite. Almost no work has been reported on studies in high temperature water.

As discussed in Section 4.3.1, $HPO_4^{2-}(aq)$ is the predominant phosphate species in aqueous solutions with sodium phosphate ratios in the range $2.5 \leq Na/PO_4 \leq 3.0$ at temperatures above 250°C. $HPO_4^{2-}(aq)$, which is isoelectronic with $SO_4^{2-}(aq)$, is known to form strong complexes with Fe^{3+} (aq) (Ziemniak et al., 1992, 1993, 1994). The morphology of the SHP formed in our experiments suggests that it was formed by precipitation from aqueous solution, rather than by epitaxial growth. The reaction must have been preceded by the dissolution of hematite, probably through the formation of a surface phosphate complex. We speculate that the following reactions may be involved:

$$HPO_4^{2-}(aq) \rightarrow HPO_4^{2-}(ads) \qquad (4.5)$$

$$\tfrac{1}{2}\, Fe_2O_3(s) + HPO_4^{2-}(ads) + 3/2\, H_2O(l) \rightarrow FeHPO_4^{+}(aq) + 3\, OH^{-}(aq) \qquad (4.6)$$

$$FeHPO_4^+(aq) + 13/3\ Na^+(aq) + HPO_4^{2-}(aq) + 10/3\ OH^-(aq) \rightarrow$$

$$Na_3Fe(PO_4)_2\cdot(Na_{1.4}H_{1.4}O)(s) + 7/3\ H_2O(l) \qquad (4.7)$$

Diffusion of $HPO_4^{2-}(aq)$ to form the adsorbed complex is fast at these temperatures in a stirred vessel, and the rate-determining step is undoubtedly Reaction 4.6, 4.7 or some other surface controlled process. Despite the high surface area of finely divided hematite in these experiments, access to the hematite surface may be impeded by a surrounding layer of reaction product during latter stages of the reaction.

The data in Figure 4.2 are extremely significant because they confirm that the same solubility value is obtained for SIHP in the presence of hematite from conditions of both supersaturation and undersaturation, i.e. the results prove that Reaction 4.1 is reversible.

4.2 Solubility of the Iron (III) Product

The solubility of SIHP was determined from several runs with sodium-phosphate ratios of 2.5 and 3.0 using stepwise temperature increments from 200-325°C. The equilibration time used in these measurements was limited by experimental considerations to 24-48 hours. At the lower temperatures, this time was not sufficient to achieve equilibrium. As a result, the rate constant expressions from Section 4.1 were used to correct the solubility data obtained in this study by extrapolating the initial and final phosphate concentrations to their equilibrium values, according to Equation 4.3. The

equilibrium sodium concentrations were calculated from the change in phosphate concentration, assuming all phosphate precipitated as SIHP. Table A.III.3 contains the experimental and corrected concentrations from the Na/P = 2.5 and Na/P = 3.0 runs. All concentrations are expressed as molalities. The sodium and phosphate concentrations were measured by ICP-ES, and the hydroxide concentrations were determined from the charge balance of the sodium and phosphate concentrations. Figure 4.3 shows a plot of the phosphate concentrations obtained in this study and those observed by Ziemniak (1986, 1992) with NiO and Fe_3O_4. From these results it can be seen that the concentrations were below those necessary for significant nickel-phosphate interactions to occur.

The data from the Na/P = 3.0 runs above 280°C may be suspect due to serious corrosion problems encountered in the zirconium vessel. The vessel reacted excessively with the phosphate solution above 280°C, producing large amounts of hydrogen (a hydrogen partial pressure in excess of 50 bars at 313°C when the vessel was shut down). The extent of reaction below 280°C is not known, but deviations in the equilibrium constants calculations (Section 4.3.3) from the Na/P = 2.5 and 3.0 data become noticeable above 240°C suggesting the corrosion may have started earlier than previously thought. The lower temperature data for this run also deviates from the Na/P = 2.5 data. This may be due to incomplete precipitation of SIHP. The reaction was allowed to proceed for four days before samples were taken, but this may not have been sufficient for the Na/P = 3.0 runs.

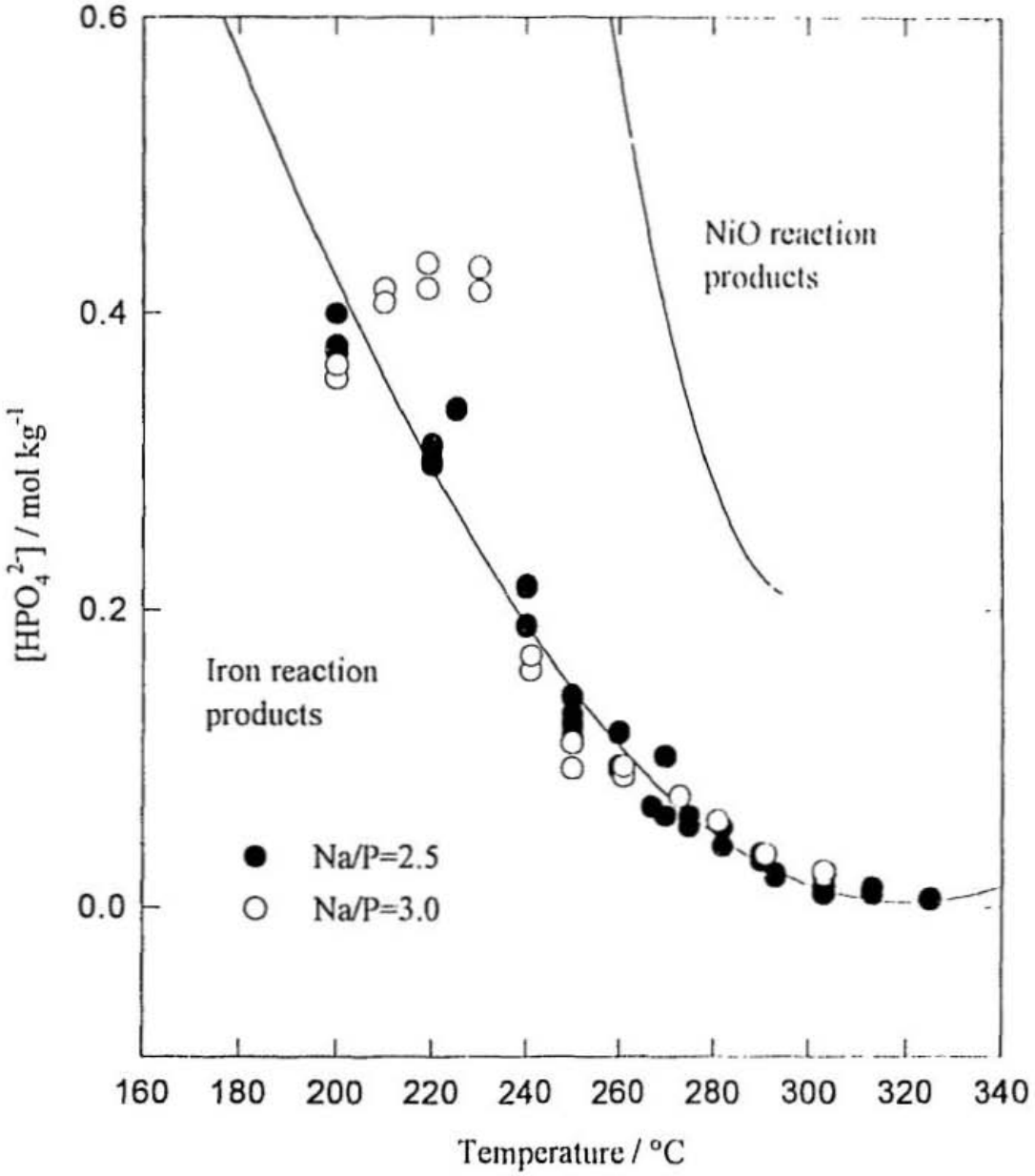


Figure 4.3 Solubility of known hideout reaction products The top solid line is a fit of the data for NiO reaction products from Ziemniak et al. (1989). The solid line through the data points is a fit to the data obtained in this study.

4.3 A Thermodynamic Model

4.3.1 Phosphate Ionization Equilibria

Supcrt'92 is a software package for calculating standard partial molal thermodynamic properties of minerals, gases, and aqueous species at elevated temperatures and pressures from the HKF model presented in Section 1.2. The program was used to calculate the thermodynamic properties for the three ionization equilibria of phosphoric acid from 25 to 350°C along the liquid side of the H_2O vaporization boundary using data from Shock and Helgeson (1988).

The following are the reactions and equilibrium constants used in these calculations:

$$H_3PO_4(aq) + OH^-(aq) \rightleftharpoons H_2PO_4^-(aq) + H_2O(l) \tag{4.8}$$

$$K_1 = \frac{a(H_2PO_4^-)}{a(H_3PO_4)a(OH^-)} \tag{4.9}$$

$$H_2PO_4^-(aq) + OH^-(aq) \rightleftharpoons HPO_4^{2-}(aq) + H_2O(l) \tag{4.10}$$

$$K_2 = \frac{a(HPO_4^{2-})}{a(H_2PO_4^-)a(OH^-)} \tag{4.11}$$

$$HPO_4^{2-}(aq) + OH^-(aq) \rightleftharpoons PO_4^{3-}(aq) + H_2O(l) \tag{4.12}$$

$$K_3 = \frac{a(PO_4^{3-})}{a(HPO_4^{2-})a(OH^-)} \qquad (4.13)$$

The standard state properties of relevant species are found in Table 4.1. The HKF equation-of-state coefficients for relevant species are found in Table 4.2. The Maier-Kelley coefficients for hematite, magnetite, and SHP are listed in Table 4.3. The data obtained from calculations of the first, second, and third ionizations of phosphoric acid are tabulated in Tables 4.4, 4.5, and 4.6 respectively. Figure 4.4 is a plot of log K for these reactions versus temperature with Mesmer's (1973) data for the first two ionizations of phosphoric acid. The agreement between the calculated values and Mesmer's data is excellent. The phosphate anion, PO_4^{3-}, hydrolyses at elevated temperatures and no experimental values for the third ionization constant above 150°C have been reported. The values in Table 4.6 do agree well with extrapolations based on solvent density functions and 25°C heat capacity data (Anderson et al. 1991).

4.3.2 Activity Coefficient Model

The model discussed in Section 1.3 was used to estimate the activity coefficients of aqueous sodium, phosphate, and hydroxide species in the solubility study. Figure 4.5 shows the predicted and experimental (Mesmer and Baes, 1973) Q_f which is given by the following equation

Table 4.1 Standard state properties at 25°C and 1 bar[a]

	$\Delta_f G^\circ$ cal mol^{-1}	$\Delta_f H^\circ$ cal mol^{-1}	S° cal mol^{-1} K^{-1}	V° cm^3 mol^{-1}	C_p° cal mol^{-1} K^{-1}
H_4PO_4 (aq)	-273100	-307920	38.000	48.2	23.6
$H_2PO_4^-$ (aq)	-270140	-309820	21.600	30.9	-6.9
HPO_4^{2-} (aq)	-260310	-308815	-8.000	4.4	-58.0
PO_4^{3-} (aq)	-243500	-305300	-53.000	-32.3	-114.3
Na^+ (aq)	-62591	-57433	13.96	-1.2	9.1
H^+ (aq)	0	0	0	0	0
OH^- (aq)	-37595	-54977	-2.560	-4.7	-32.6
H_2 (aq)	4236	-1000	13.800	25.3	39.9
H_2 (g)	0	0	31.234	0	6.9
O_2 (g)	0	0	49.029	0	7.0
O_2 (aq)	3954	-2900	26.040	30.5	56.0
H_2O (l)	-56688	-68317	16.712	18.1	18.0
Fe_3O_4 (s)	-242574	-267250	34.830	44.524	36.3
Fe_2O_3 (s)	-178155	-197720	20.940	30.274	25.0
SHIP (s)[b]	-831916	-880150	148.3	122.2	54.1
$NaFePO_4$	-333006[c]	-353355[c]	(40.39)[d]	46.87[e]	(35.92)[d]

[a] Data from Shock and Helgeson (1988) unless noted.

[b] This work

[c] Values calculated using data from flow experiments at 320°C (Tremaine et al., 1993).

[d] Data for $NaZnPO_4$ (Ziemniak et al., 1990).

[e] Calculated from crystal structure.

Table 4.2 HKF equation of state coefficients for aqueous species [a,b]

	$a_1 \times 10^1$	$a_2 \times 10^{-2}$	a_3	$a_4 \times 10^{-4}$	c_1	$c_2 \times 10^{-4}$	$\omega \times 10^{-5}$
H_3PO_4(aq)	8.2727	12.4182	0.8691	-3.2924	17.9708	1.7727	-0.2200
$H_2PO_4^-$ (aq)	6.4875	8.0594	2.5823	-3.1122	14.0435	-4.4605	1.3003
HPO_4^{2-} (aq)	3.6315	1.0857	5.3233	-2.8239	2.7357	-14.9103	3.3363
PO_4^{3-} (aq)	-0.5259	-9.0654	9.3131	-2.4042	-9.4750	-26.4397	5.6114
H_2(aq)	5.1427	4.7758	3.8729	-2.9764	27.6251	5.0930	-0.2090
Na^+ (aq)	1.8390	-2.285	3.2560	-2.7260	18.1800	2.9810	0.3306
H^+ (aq)	0	0	0	0	0	0	0
OH^- (aq)	1.2527	0.0738	1.8423	-2.7821	-4.1500	-10.3460	1.7246
O_2 (aq)	5.7889	6.3536	3.2528	-3.0417	35.3530	8.3726	-0.3943

[a] Units. a_1, cal mol^{-1} bar^{-1}; a_2, cal mol^{-1}, a_3, cal K mol^{-1} bar^{-1}, a_4, cal K mol^{-1}, c_1, cal mol^{-1} K^{-1} ; c_2, cal K mol^{-1}, ω, cal mol^{-1}

[b] Shock and Helgeson (1988).

Table 4.3 Maier-Kelley coefficients for heat capacities of solids

	a cal $mol^{-1} K^{-1}$	b x 10^3 cal $mol^{-1} K^{-2}$	c x 10^{-5} cal $mol^{-1} K$
Fe_2O_4 (s)[a]	23.49	18.60	-3.55
Fe_3O_4 (s)[a]	21.88	48.20	0.0
SHP (s)[b]	54.1	0.0	0.0

[a] Shock and Helgeson (1988).
[b] This work

Table 4.4 Standard state properties of the following reaction calculated from data in Tables 4.1 to 4.3

$$H_3PO_4(aq) + OH^-(aq) \rightleftharpoons H_2PO_4^-(aq) + H_2O(l)$$

T °C	p bar	d_{H_2O} g cm^{-3}	log K	$\Delta_r G^\circ$ cal mol^{-1}	$\Delta_r H^\circ$ cal mol^{-1}	$\Delta_r S^\circ$ cal mol^{-1} K^{-1}	$\Delta_r V^\circ$ cm^3 mol^{-1}	$\Delta_r C_p^\circ$ cal mol^{-1} K^{-1}
25.00	1.000	0.997	11.825	-16133	-15240	2.9	5.5	20.2
50.00	1.000	0.988	10.972	-16224	-14789	4.3	4.0	16.5
75.00	1.000	0.975	10.261	-16347	-14395	5.5	3.3	15.2
100.00	1.013	0.958	9.662	-16498	-14019	6.5	3.2	14.9
125.00	2.320	0.939	9.152	-16673	-13645	7.5	3.3	15.1
150.00	4.757	0.917	8.714	-16873	-13265	8.4	3.8	15.3
175.00	8.918	0.892	8.336	-17094	-12882	9.3	4.5	15.3
200.00	15.536	0.865	8.008	-17337	-12499	10.1	5.3	15.5
225.00	25.479	0.834	7.721	-17599	-12108	10.9	6.2	15.9
250.00	39.736	0.799	7.469	-17880	-11726	11.7	7.2	14.2
275.00	59.431	0.759	7.247	-18176	-11484	12.1	7.5	1.6
300.00	85.838	0.712	7.043	-18471	-11870	11.5	2.6	-52.6
325.00	120.458	0.655	6.841	-18722	-14583	6.9	-30.3	-301.7
350.00	165.211	0.575	6.591	-18795	-30745	-19.2	-275.6	-3027.1

Table 4.5 Standard state properties of the following reaction calculated from data in Tables 4.1 to 4.3

$$H_2PO_4^-(aq) + OH^-(aq) \rightarrow HPO_4^{2-}(aq) + H_2O(l)$$

T °C	p bar	d_{H2O} g cm^{-3}	log K	$\Delta_r G°$ cal mol^{-1}	$\Delta_r H°$ cal mol^{-1}	$\Delta_r S°$ cal mol^{-1} K^{-1}	$\Delta_r V°$ cm^3 mol^{-1}	$\Delta_r C_p°$ cal mol^{-1} K^{-1}
25.00	1.000	0.997	6.790	-9263	-12335	-10.3	-3.7	-0.5
50.00	1.000	0.988	6.089	-9004	-12349	-10.4	-5.7	-0.7
75.00	1.000	0.975	5.489	-8744	-12372	-10.4	-6.8	-1.2
100.00	1.013	0.958	4.967	-8482	-12408	-10.5	-7.5	-1.8
125.00	2.320	0.939	4.510	-8217	-12461	-10.7	-8.1	-2.5
150.00	4.757	0.917	4.105	-7948	-12534	-10.9	-8.6	-3.3
175.00	8.918	0.892	3.743	-7675	-12627	-11.1	-9.1	-4.2
200.00	15.536	0.865	3.417	-7397	-12747	-11.3	-9.6	-5.6
225.00	25.479	0.834	3.120	-7112	-12915	-11.7	-10.4	-8.2
250.00	39.736	0.799	2.849	-6819	-13154	-12.1	-11.6	-11.5
275.00	59.431	0.759	2.597	-6515	-13456	-12.7	-13.5	-13.0
300.00	85.838	0.712	2.365	-6201	-13695	-13.1	-15.1	-3.9
325.00	120.458	0.655	2.151	-5887	-13445	-12.6	-9.4	57.7
350.00	165.211	0.575	1.965	-5602	-9558	-6.4	69.3	958.7

Table 4.6 Standard state properties of the following reaction calculated from data in Tables 4.1 to 4.3.

$$HPO_4^{2-}(aq) + OH^-(aq) \rightleftharpoons PO_4^{3-}(aq) + H_2O(l)$$

T °C	p bar	d_{H_2O} g cm^{-3}	log K	$\Delta_r G^\circ$ cal mol^{-1}	$\Delta_r H^\circ$ cal mol^{-1}	$\Delta_r S^\circ$ cal mol^{-1} K^{-1}	$\Delta_r V^\circ$ cm^3 mol^{-1}	$\Delta_r C_p^\circ$ cal mol^{-1} K^{-1}
25.00	1.000	0.997	1.673	-2283	-9825	-25.7	-13.9	-5.8
50.00	1.000	0.988	1.105	-1634	-9959	-26.2	-16.2	-5.2
75.00	1.000	0.975	0.612	-975	-1009	-26.6	-17.7	-5.6
100.00	1.013	0.958	0.179	-306	-1024	-27.0	-18.7	-6.5
125.00	2.320	0.939	-0.205	374	-1042	-27.4	-19.7	-7.8
150.00	4.757	0.917	-0.550	1065	-1063	-28.0	-20.6	-9.1
175.00	8.918	0.892	-0.862	1768	-10875	-28.5	-21.6	-10.1
200.00	15.536	0.865	-1.148	2485	-11146	-29.1	-22.7	-11.9
225.00	25.479	0.834	-1.410	3214	-11479	-29.8	-24.1	-15.1
250.00	39.736	0.799	-1.654	3959	-11887	-30.5	-26.0	-17.4
275.00	59.431	0.759	-1.881	4719	-12247	-31.2	-27.9	-8.3
300.00	85.838	0.712	-2.089	5480	-12002	-30.7	-25.1	48.4
325.00	120.458	0.655	-2.263	6194	-9214	-26.0	10.1	332.3
350.00	165.211	0.575	-2.355	6714	9409	4.1	313.4	3749.6

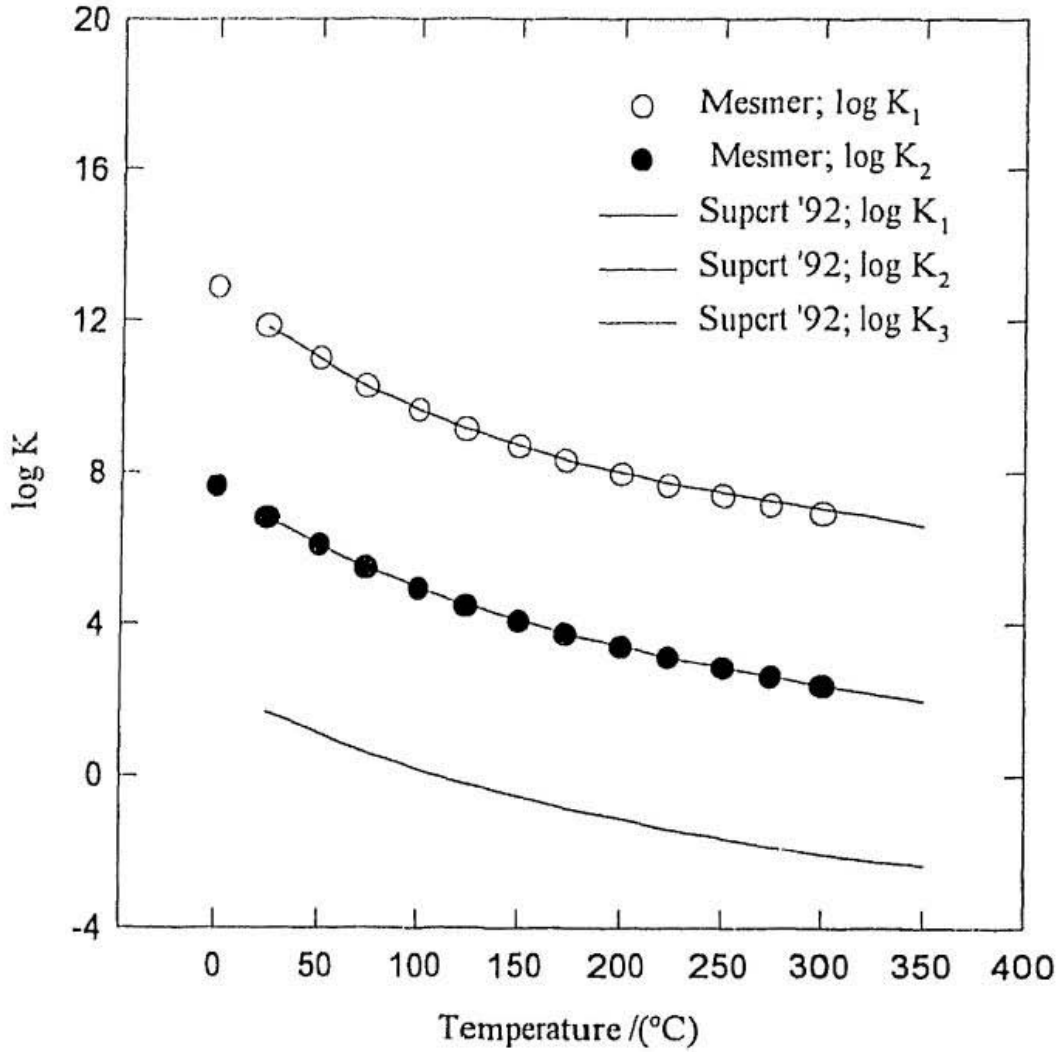


Figure 4.4 Phosphate ionization equilibria.

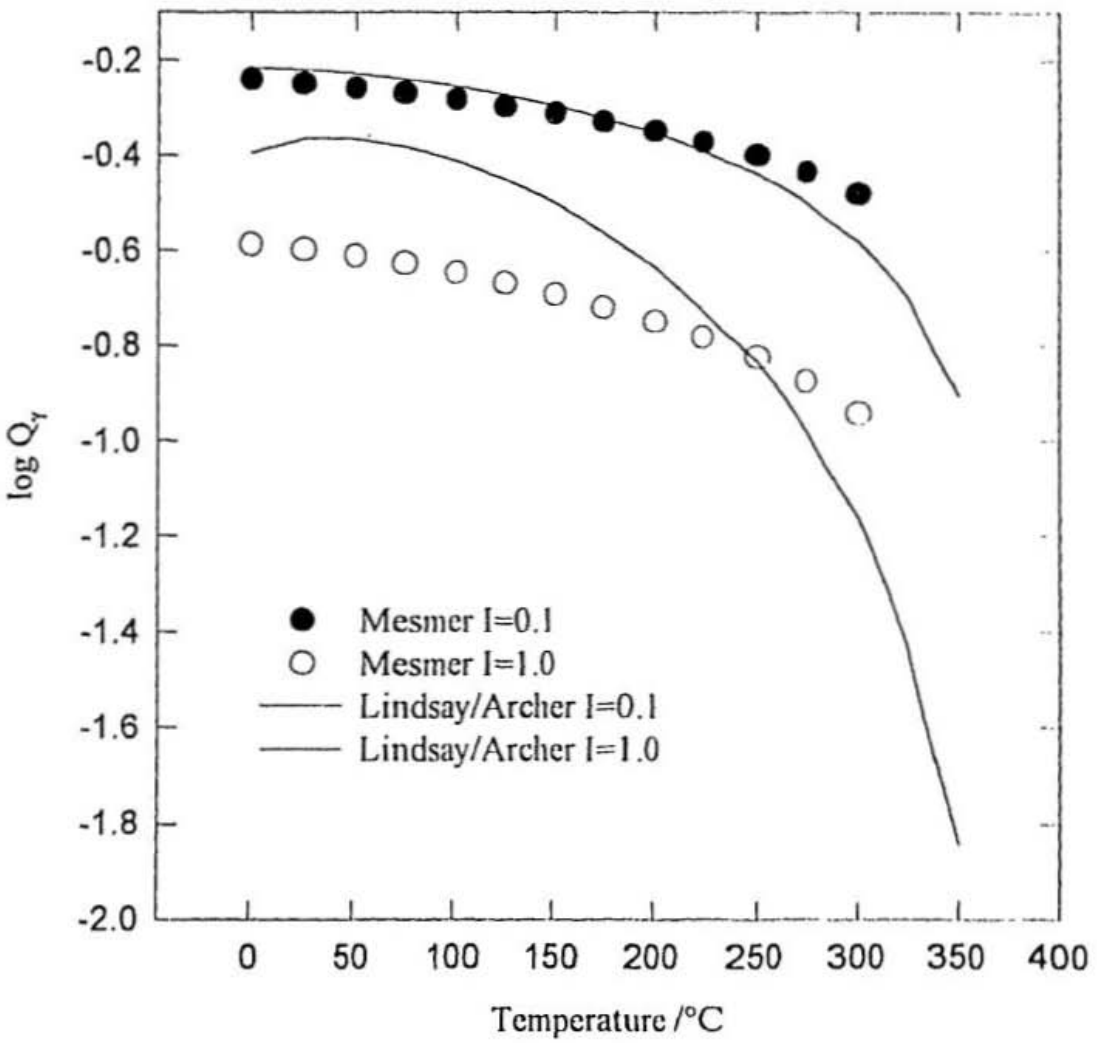


Figure 4.5 Comparison of Experimental and Predicted Q_γ

$$Q_\gamma = \frac{\gamma(HPO_4^{2-})}{\gamma(H_2PO_4^-)\cdot\gamma(OH^-)} \qquad 4.14$$

where γ is the activity coefficient of the given species. Agreement is quite acceptable for dilute solutions (I=0.1), but at higher ionic strength (I=1.0), the model is not as good. Mesmer made measurements to only 250°C, and these were extrapolated to 300°C. For the purposes of this study, activity coefficients were required to 325°C, and although this model is not ideal, it is the best available.

4.3.3 Equilibrium Constants for SIHP

The following is the equilibrium constant for the formation of SIHP from hematite and aqueous sodium phosphate according to Reaction 4.1:

$$K = \frac{a(H_2O)^{\frac{5}{6}}}{a(Na^+)^{\frac{13}{3}}\, a(HPO_4^{2-})^2\, a(OH^-)^{\frac{1}{3}}} \qquad (4.15)$$

The ionization constants in Tables 4.4 to 4.6 and the rate equations for SIHP formation (Equation 4.4) were used to calculate equilibrium values for m(HPO_4^{2-}, aq), m(OH^-,aq), and m(Na^+, aq) from the experimental results for m(Na, aq, total) and m(PO_4, aq, total). These are tabulated in Table A.III.3 along with the corresponding values of Q calculated from them. Values for the activity coefficients from the Lindsay model, a(H_2O), and the

resulting experimental values of ln K for Reaction 4.1 are listed in Table A.III.4. These are plotted as $\Delta_r G°_T$ (Reaction 4.1) in Figure 4.6.

Experimental values for the apparent Gibbs energies of formation of SIHP were calculated from the expression

$$\Delta_a G_T^o(SIHP) = \Delta_r G_T^o + \sum \Delta_a G_T^o(reactants) \quad 5/6\,\Delta_a G_T^o(H_2O,l) \qquad (4.16)$$

The results which are plotted in Figure 4.7, were used with a non-linear least squares algorithm to fit parameters in the equation

$$\Delta_a G_T^o(SIHP) = \Delta_f G_{T_r}^o - S_{T_r}^o(T - T_r) + C_{p_r}^o(T - T_r - T\ln T/T_r) \qquad (4.17)$$

Here $C_p°$ is the mean value from 25-325°C. Values for the fitted parameters are included in Tables 4.2 and 4.3. Equilibrium constants for the reaction of hematite with aqueous sodium phosphate to give SIHP which were calculated from these parameters are listed in Table 4.7. The value for the mean heat capacity, $C_p°(SIHP) = 54.1$ cal $K^{-1}mol^{-1}$, is consistent with values for most solids, which typically lie in the range 20-100 cal $K^{-1}mol^{-1}$. The value undoubtedly includes artifacts of uncertainties in the heat capacity functions for $Na^+(aq)$ and $HPO_4^{2-}(aq)$ which are very large at temperatures above 250°C (Table 4.6). It should be regarded as a fitting parameter that reproduces the experimental values for log K in the range 225-325°C.

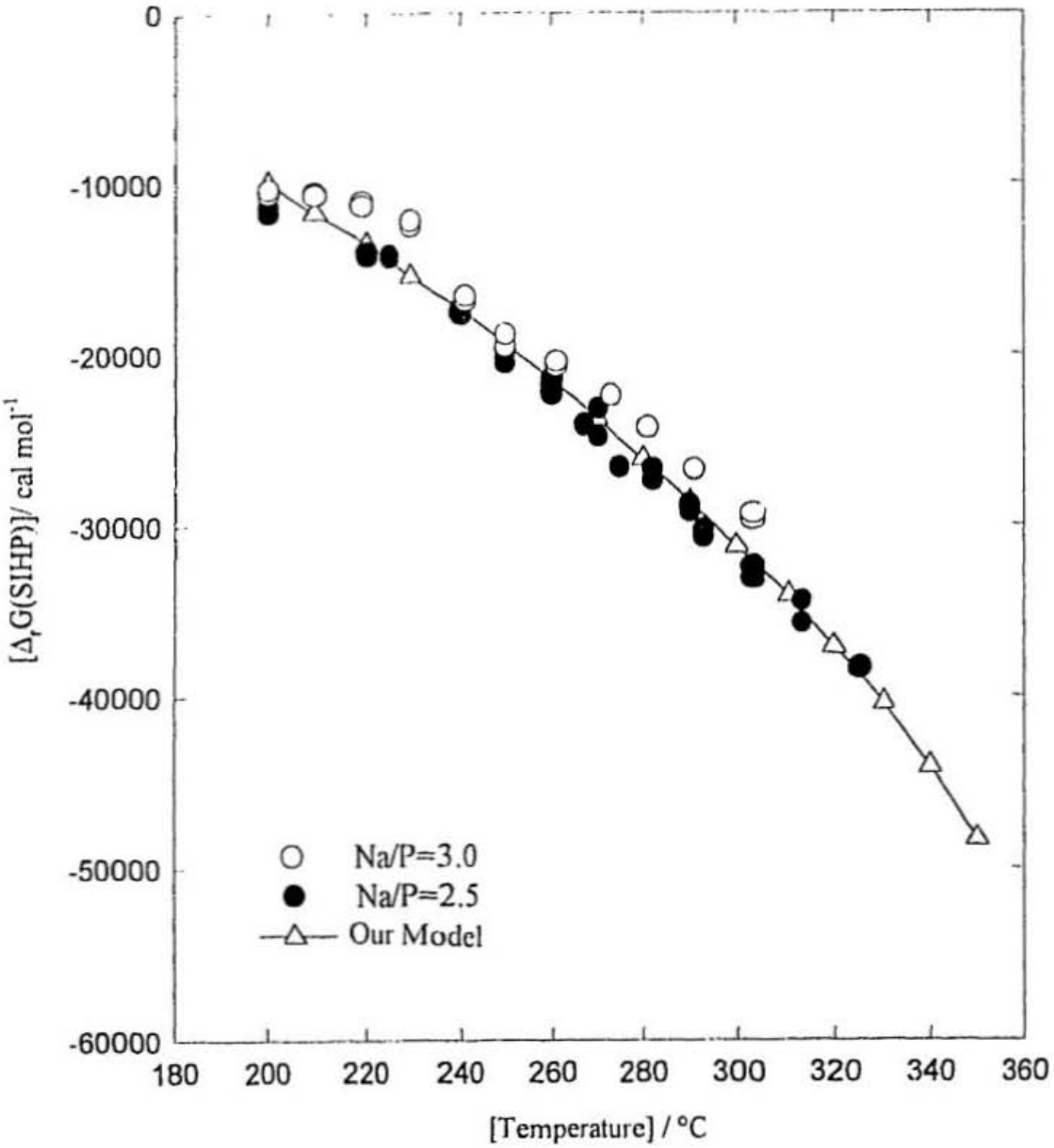


Figure 4.6 $\Delta_r G°$ (SIHP) versus Temperature.

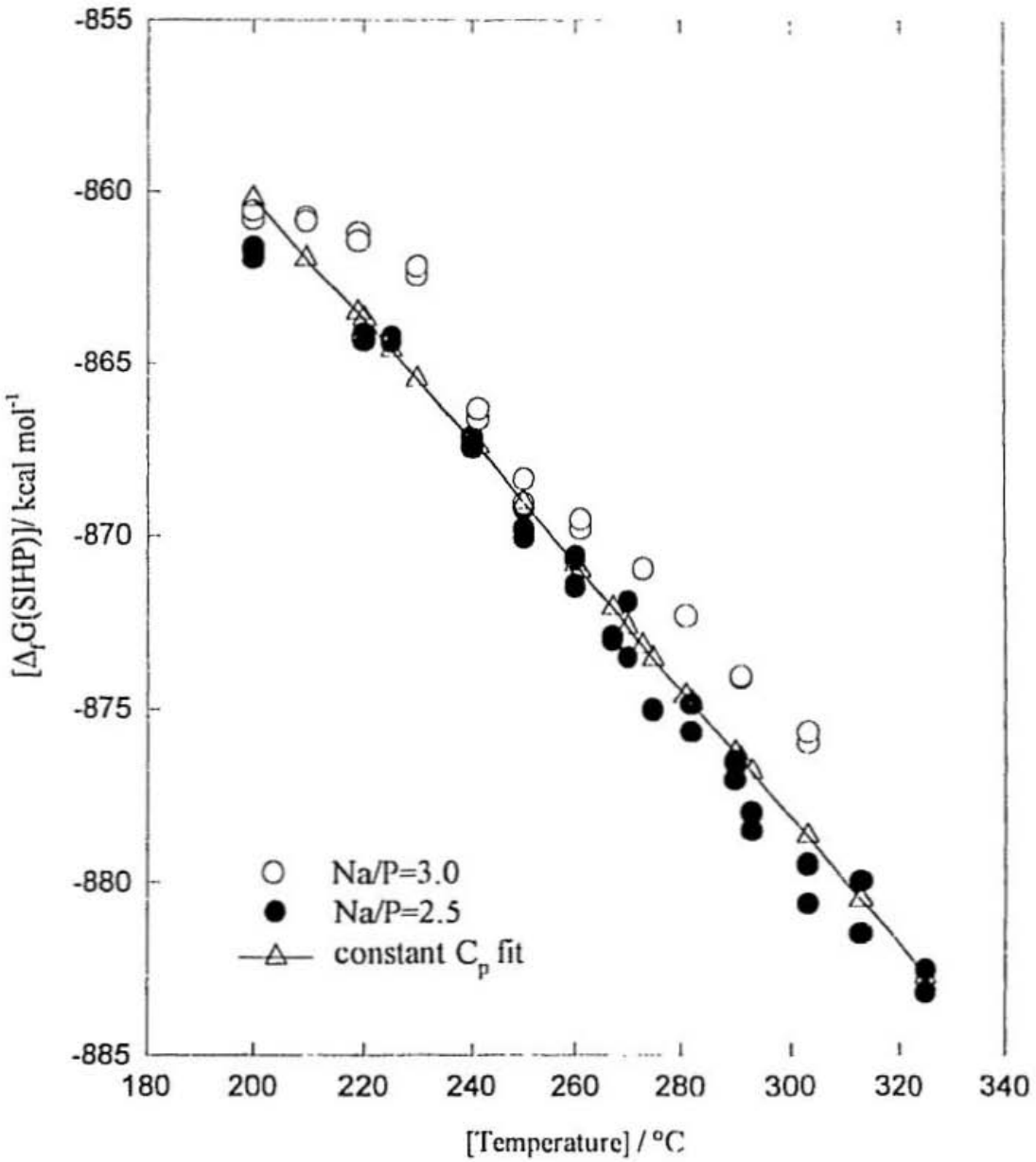


Figure 4.7 $\Delta_f G°$ (SIHP) versus Temperature.

Table 4.7 Standard state properties of the following reaction calculated from data in Tables 4.1 to 4.6.

$$3Fe_2O_3(s) + 26Na^+(aq) + 12HPO_4^{2-}(aq) + 2OH^-(aq) \rightleftharpoons 6Na_3Fe(PO_4)_2 \cdot (Na_{4.3}H_{2.3}O)(s) + 5H_2O(l)$$

T °C	p bar	d_{H2O} g cm^{-3}	log K	$\Delta_r G°$ cal mol^{-1}	$\Delta_r H°$ cal mol^{-1}	$\Delta_r S°$ cal mol^{-1} K^{-1}	$\Delta_r V°$ cm^3 mol^{-1}	$\Delta_r C_p°$ cal mol^{-1} K^{-1}
25.00	1.000	0.997	-30.668	41838	17900	-81.6	5.5	2369.5
50.00	1.000	0.988	-28.104	41556	73929	99.0	4.0	2160.3
75.00	1.000	0.975	-23.264	37061	127366	258.3	3.3	2133.3
100.00	1.013	0.958	-16.821	28720	181304	407.9	3.2	2193.4
125.00	2.320	0.939	-9.166	16698	237540	553.7	3.3	2318.0
150.00	4.757	0.917	-0.537	1039	297592	699.9	3.8	2502.4
175.00	8.918	0.892	8.924	-18299	362914	849.8	4.5	2757.4
200.00	15.536	0.865	19.142	-41442	436168	1008.6	5.3	3181.8
225.00	25.479	0.834	30.133	-68684	522823	1186.6	6.2	3909.8
250.00	39.736	0.799	42.017	-100578	631356	1398.4	7.2	5107.9
275.00	59.431	0.759	55.009	-137972	773795	1662.7	7.5	7055.8
300.00	85.838	0.712	69.409	-182029	970582	2010.4	2.6	10681.7
325.00	120.458	0.655	85.749	-234692	1286725	2542.9	-30.3	20928.8
350.00	165.211	0.575	105.956	-302116	2045369	3766.5	-275.6	70242.5

The experimental design used in this work caused the Na/P ratio to rise at progressively higher temperatures. Thus as SHHP was produced, the Na/P ratio went from 2.5 to values as high as 9.9 at 325°C, and from 3.0 to values as high as 6.6 at 260°C. To confirm that HPO_4^{2-} was the main species even at these extreme sodium-phosphate ratios, the degree of dissociation to give PO_4^{3-} was calculated and found to be less than 0.3 percent at 250°C and less than 0.02 percent at 325°C.

4.4 Comparison With Data From Other Workers

4.4.1 Background

A principal objective of this work was to obtain unambiguous Gibbs energy data for $Na_3Fe(PO_4)_2{\cdot}(Na_{4.3}H_{2.3}O)(s)$ by carrying out solubility experiments in equilibrium with Fe_2O_3 rather than Fe_3O_4, so that the measurements did not require a knowledge of the reduction potential of the system. With the thermodynamic data in Tables 4.1-4.3, it is possible to reanalyze previous measurements in systems containing Fe_3O_4.

Some of the most unambiguous experiments are the flow experiments done in Alberta (Tremaine et al., 1992). The experiments measured the uptake from sodium phosphate solutions purged with hydrogen at 25°C flowing through a magnetite bed at 196 bar (saturation pressure 186.6 bar). The sodium phosphate reactions with magnetite were reversible, and since an excess of magnetite was present, the molalities of sodium and phosphate in the outlet solutions can be used to calculate equilibrium quotients. The stoichiometry of the reaction product was calculated from mass balance from the

difference in composition between the inlet and outlet solutions. These yield equilibrium solubilities for SHP and maricite in equilibrium with Fe_3O_4 at 325 and 360°C and, at higher sodium/phosphate ratios, SHP in equilibrium with Fe_3O_4 and H_2(aq) at 360°C.

Ziemniak et al. (1981, 1992, 1993) have reported solubility data for SHP in equilibrium with Fe_3O_4 up to 300°C. The hydrogen concentration was not fixed and was assumed to be that of the Fe_3O_4/Fe_2O_3 redox buffer. Experiments were carried out in a platinum lined stirred vessel. With the exception of the uncertainty with reduction potential, the results are of very high quality and are also suitable for solubility product determinations.

Equilibrium constants for the reaction of magnetite with aqueous sodium phosphate to give SHP were calculated from the model and are presented in Table 4.8. These values are not directly comparable to those obtained by Ziemniak and Opalka (1992) due to the fact that the reaction was written with H^+ and H_2(g) instead of OH^- and H_2(aq) as in this work. The data from Ziemniak and Opalka's (1992) paper (Table I) was taken and values for log K were calculated with the second version of the reaction and assuming that the amount of hydrogen present was solely due to the oxidation of the Fe^{2+} in magnetite. The results of this comparison are shown in Figure 4.8. The fact that the data are in good agreement suggests that the model developed in this work will prove to be of use in future studies.

Table 4.8 Standard state properties of the following reaction calculated from data in Tables 4.1 to 4.6.

$$2Fe_3O_4(s) + 26Na^+(aq) + 12HPO_4^{2-}(aq) + 2OH^-(aq) \rightleftharpoons 6Na_3Fe(PO_4)_2\cdot(Na_{1.4}H_{1.6}O)(s) + 4H_2O(l) + H_2(aq)$$

T °C	p bar	d_{H2O} g cm^{-3}	log K	$\Delta_r G^\circ$ cal mol^{-1}	$\Delta_r H^\circ$ cal mol^{-1}	$\Delta_r S^\circ$ cal mol^{-1} K^{-1}	$\Delta_r V^\circ$ cm^3 mol^{-1}	$\Delta_r C_p^\circ$ cal mol^{-1} K^{-1}
25.00	1.000	0.997	-71.404	97413	288325	639.2	730.0	887.9
50.00	1.000	0.988	-54.526	80624	307258	700.3	710.4	674.9
75.00	1.000	0.975	-39.233	62499	323542	748.8	720.8	646.6
100.00	1.013	0.958	-25.301	43199	340302	795.3	754.9	706.1
125.00	2.320	0.939	-12.479	22734	359375	844.7	813.7	830.4
150.00	4.757	0.917	-0.510	988	382281	900.3	903.1	1014.9
175.00	8.918	0.892	10.830	-22208	410495	964.8	1032.2	1270.4
200.00	15.536	0.865	21.750	-47089	446705	1042.9	1217.5	1696.0
225.00	25.479	0.834	32.486	-74048	496420	1144.5	1496.6	2426.8
250.00	39.736	0.799	43.329	-103720	568180	1283.7	1946.8	3630.4
275.00	59.431	0.759	54.632	-137026	674138	1479.2	2706.7	5591.4
300.00	85.838	0.712	66.806	-175201	835028	1762.0	4022.4	9252.9
325.00	120.458	0.655	80.476	-220259	1116793	2234.8	6456.2	19635.7
350.00	165.211	0.575	97.661	-278466	1848041	3412.0	12352.5	70119.6

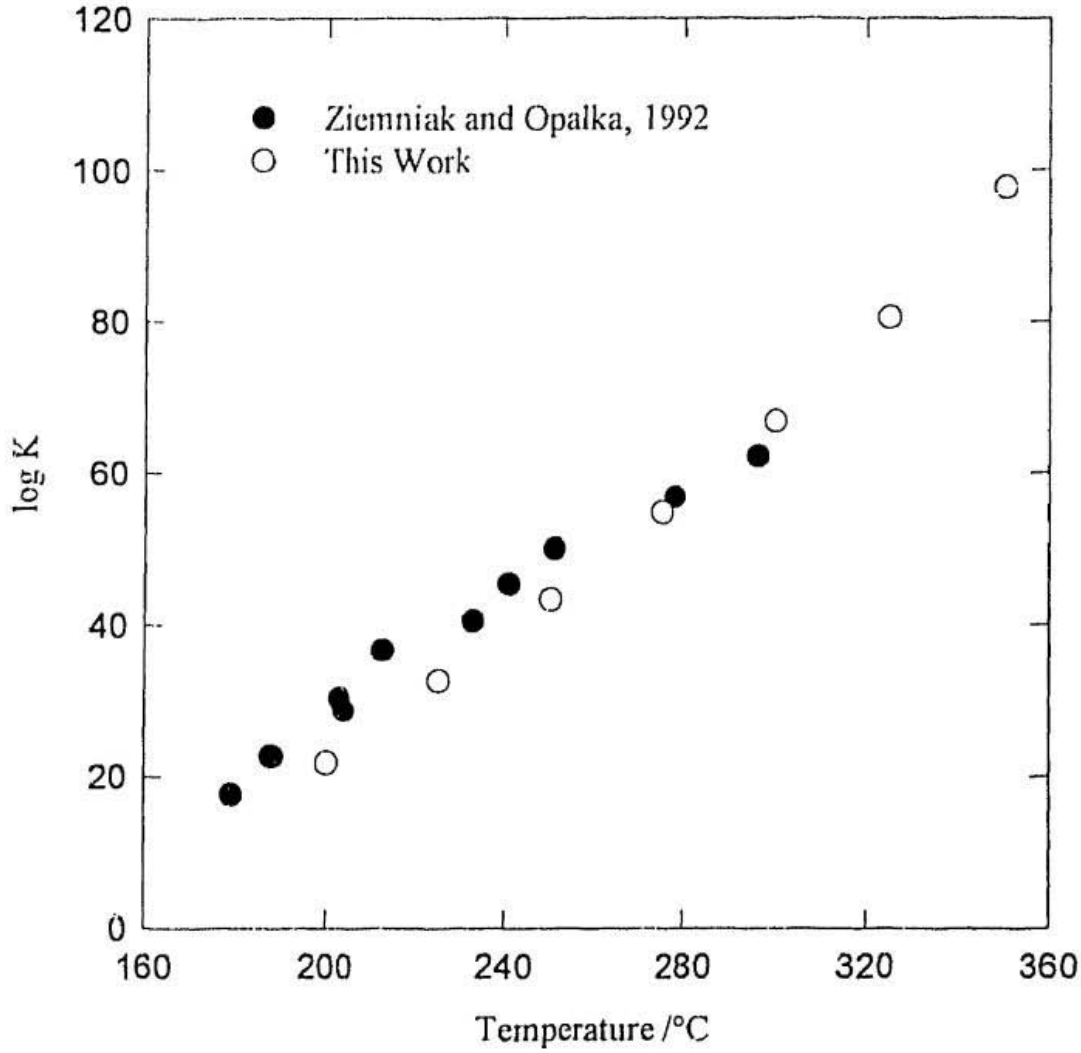


Figure 4.8 Comparison of log K from previous studies and calculated values using the model developed in this work

4.4.2 Sodium Iron Hydroxy Phosphate (SIHP) at 360°C

Data were obtained by Tremaine et al. (1992) for the reaction

$$2Fe_3O_4(s) + 26Na^+(aq) + 12HPO_4^{2-}(aq) + 2OH^-(aq) \cdots$$

$$6Na_3Fe(PO_4)_2\cdot(Na_{4.3}H_{2.3}O)(s) + H_2(aq) + 4H_2O(l) \qquad (4.18)$$

The molality of $H_2(aq)$ in the feed solutions is nominally 7.8×10^{-4} mol kg^{-1}, but we estimate losses by reaction with oxides in the sealed pumps reduced $m(H_2)$ to 4.3×10^{-4} mol kg^{-1}. Activity coefficients for the phosphate species under these conditions are very uncertain both because the data is limited and because of the fundamental problems in the definition of activity coefficients according to the model presented above (Pitzer, 1991)

4.4.3 Maricite at 320 and 360°C

At Na/PO_4 ratios below 3.0, Fe_3O_4 was observed to form both SIHP and maricite at 320 and 360°C according to the reaction

$$3Fe_3O_4(s) + 15HPO_4^{2-} + 29Na^+(aq) \cdots$$

$$6Na_3Fe(PO_4)_2\cdot(Na_{4.3}H_{2.3}O)(s) + 3NaFePO_4(s) + OH^-(aq) + 5H_2O(l) \quad (4.19)$$

The Gibbs phase rule requires that magnetite, SIHP, and maricite can coexist at equilibrium at only one defined value of $m(H_2)$. To be consistent with the equation above, we must assume that the excess of magnetite in the flow experiments ensures that Reaction 4.19 is at equilibrium, and that the system must act as a redox buffer, independent of the concentration of H_2 originally added to the system

Uncertainties in the near-critical activity coefficients and data for SIHP make the

calculation from the 360°C data impractical However an assessment of the data at 320°C to obtain $\Delta_f G^\circ$ for maricite was completed

Using the data listed in Table 4.9, the equilibrium constant for Reaction 4.19 was calculated according to the following equation

$$K = \frac{a(H_2O)^5 a(OH^-)}{a(Na^+)^{2y} a(HPO_4^{2-})^{1-y}} \qquad (4.20)$$

The Gibbs free energy of reaction, $\Delta_r G_1^\circ$ was calculated at 320°C from Equation 1.10. The HKF model was then used to calculate the free energies of the species other than maricite in Reaction 4.19, so that the apparent free energy of maricite, $\Delta_f G^\circ_{593K}$ could be obtained.

The temperature dependence of the Gibbs energies, $\Delta_f G_1^\circ$, of maricite can be calculated from the entropy and heat capacity, according to Equation 4.17. This data is not available for maricite, but data has been reported for an analogous zinc compound, $NaZnPO_4$ (Ziemniak et al , 1990). This data was used with the apparent free energy of maricite at 320°C in Equation 4.17 to estimate the standard state properties of maricite at 298.15K The values are listed in Table 4.1.

These results include large uncertainties, but they provide the only means available to estimate the temperature dependence of maricite equilibrium constants at this time, and should be valid over a narrow range near 320°C and steam saturation. Experimental data for S° and C_p° of both maricite and SIHP are needed to refine the results from this work.

Table 4.9 Solubility data from flow experiments at Alberta Research Council at 320°C

	$m(Na^+)$ mol kg^{-1}	$m(PO_4$, total) mol kg^{-1}
initial	0.236	0.095
final	0.200	0.080

4.5 Discussion

The thermodynamic data for SIHP obtained in this study and the provisional data for maricite from the analysis of the flow experiments data from the Alberta Research Council can be used to examine the key parameters governing hideout equilibria. As an example, a plot of the log of activity of hydrogen versus temperature from 200-330°C for the various equilibria is presented in Figure 4.9. The following reactions were considered:

$$2Fe_3O_4(s) + 26Na^+(aq) + 12HPO_4^{2-}(aq) + 2OH^-(aq) \rightleftharpoons 6Na_3Fe(PO_4)_2\cdot(Na_{4.3}H_{2.3}O)(s) + H_2(aq) + 4H_2O(l) \quad (4.21)$$

$$Fe_3O_4(s) + 3Na^+(aq) + 3HPO_4^{2-}(aq) + H_2(aq) \rightleftharpoons 3NaFePO_4 + 3OH^-(aq) + H_2O(l) \quad (4.22)$$

$$2Na_3Fe(PO_4)_2\cdot(Na_{4.3}H_{2.3}O)(s) + H_2(aq) + \tfrac{2}{3}H_2O(l) \rightleftharpoons 2NaFePO_4 + 20/3Na^+(aq) + 2HPO_4^{2-}(aq) + 8/3OH^-(aq) \quad (4.23)$$

$$2Fe_3O_4(s) + H_2O(l) \rightleftharpoons 3Fe_2O_3(s) + H_2(aq) \quad (4.24)$$

Reaction 4.21 controls the oxidation of magnetite to form SIHP. It is extremely sensitive to the molality of $Na^+(aq)$ and $HPO_4^{2-}(aq)$.

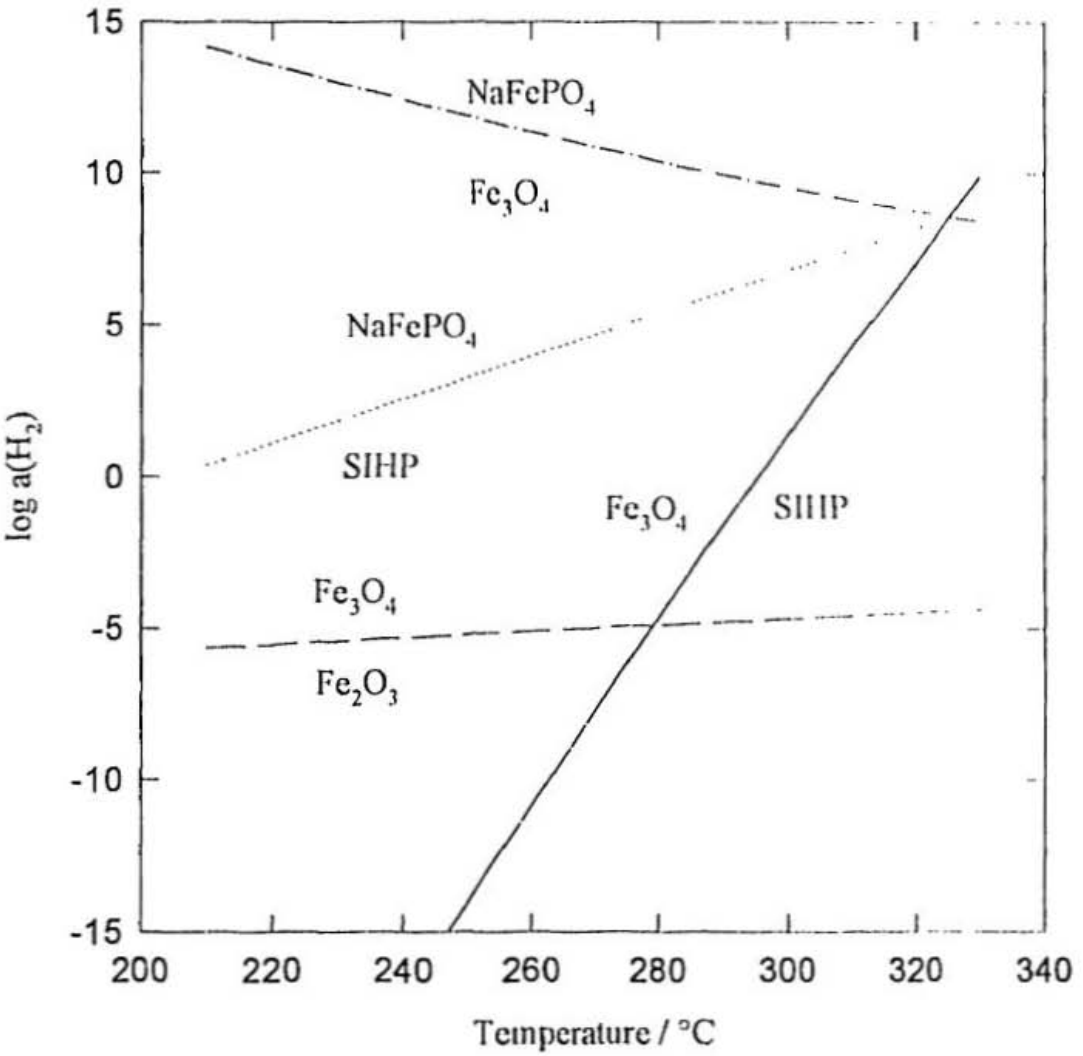


Figure 4.9 Equilibrium activities of aqueous hydrogen, $a(H_2)$, for magnetite and various phosphate hideout products for a 0.08m solution at $Na/PO_4 = 2.5$

$$a(H_2, aq) \sim m(Na^+, aq)^{26} \cdot m(HPO_4^{2-}, aq)^{12} \cdot a(OH^-, aq)^2 \qquad (4.25)$$

This has practical implications for phosphate hideout and corrosion reactions in industrial boilers in that dissolved sodium and phosphate may play a much larger role than dissolved oxygen or hydrogen in controlling the redox chemistry of iron oxides. Because the reduction potential is so sensitive to the molality of sodium and phosphate, values of log $a(H_2)$ are very sensitive to small errors in the activity coefficient model. The unrealistic values of log $a(H_2)$ in Figure 4.9 ($\sim 10^8$ at 320°C) undoubtedly arise from magnification of small uncertainties. Refinements to the database for redox calculations are needed. However, the plot gives a good qualitative description of the system over the temperature range. It shows that the magnetite/SIHP equilibrium dominates except under highly reducing conditions, and that a high partial pressure of hydrogen was necessary to produce maricite from magnetite.

The lines representing the equilibria in Equations 4.21, 4.22, and 4.23 intersect at 320°C, as must be the case, since the calculation of the free energy of maricite was done assuming all species were in equilibrium at 320°C.

4.6 Future Work

The work presented in this thesis has been successful in developing a thermodynamic database for describing the role of SIHP in sodium phosphate hideout under boiler conditions. Further experiments are needed to extend the thermodynamic

model to maricite, and to describe redox equilibria with acceptable accuracy. For example, more solubility data at lower Na/P ratios, and independent measurements of $C_p°$ and $\Delta_f H°$ for the solids would allow activity coefficients of the ionic species to be calculated directly, without using the activity coefficient model described in Section 1.3, which has limitations. Accurate values for the solubility of maricite over a similar temperature range would complete the model.

5.0 CONCLUSIONS

The work reported here has successfully identified the structure and stoichiometry of the major iron (III) reaction product associated with phosphate hideout. Synthetic routes have been developed to produce SIHP in bulk with a high degree of purity from three starting materials - hematite, magnetite, and iron phosphate. Maricite has been produced by two routes. The first synthesis yielded maricite from iron powder with acceptable purity, but the second synthesis, the thermal decomposition of FeNTA in the presence of aqueous sodium phosphate, gave much better results - large, well-formed crystals, with no detectable impurities. This synthesis also has the potential to yield SIHP if the right redox conditions can be found.

The crystal structure of SIHP has been determined and has removed much of the ambiguity associated with the previously accepted stoichiometry. The structure of maricite has been confirmed.

Equilibrium solubility data and kinetic data have been obtained at steam saturation pressures from 200 to 325°C. The thermodynamic model successfully reproduces the experimental solubility data over the experimental temperature range. The model is consistent with the MULTEQ, except that Archer and Wang's (1990) database was used instead of the Meissner equation (Meissner, 1980, and Lindsay, 1989) to obtain values of $\gamma_{\pm}$(NaCl). It has the potential to be an important tool in modelling hideout reactions. An improved activity coefficient model and independent heat capacity and enthalpy of solution

data for SIHP are needed to extend the model over the full temperature range from 180-360°C.

The experimental techniques developed here can be extended to the maricite system with proper modifications to control $m(H_2)$. Maricite is the major iron (II) phase identified with phosphate hideout reactions. A compatible thermodynamic model for maricite interactions with magnetite will yield a comprehensive treatment for iron-phosphate hideout reactions.

6.0 BIBLIOGRAPHY

Abraham M., and Marcus Y. (1986) The thermodynamics of solvation of ions. Part 1.- The heat capacity of hydration at 298.15 K. *J. Chem. Soc. Faraday Trans. I* **82,** 3255-3274.

Abraham M., Matteoli E., and Liszi J. (1983) Calculation of the thermodynamics of solvation of gaseous univalent ions in water from 273-573K. *J. Chem. Soc. Faraday Trans. I* **79,** 2781-2800.

Adams W.A., Preston C.M., and Chew H.A.M. (1979) A high-pressure conductivity and laser raman spectroscopic study of aqueous orthophosphate solutions at 25°C. *J. Chem. Phys.* **70,** 2074-2080.

Alexander J.H., and Luu L. (1989) MULTEQ: Equilibrium of an electrolyte solution with vapor-liquid partitioning and precipitation, Vol I. Users Manual. *EPRI Report NP-5561-CCM.*

Allmon W.E., Mravich N.J., Saia R.J., and Passell, T.O. (1980) Deposition of salts from steam. *Proc. 41st Int. Water Conf.* (Pittsburgh, PA.) pp. 127-138.

Anderson G.M., and Crerar D.A. (1993) *Thermodynamics in Geochemistry - The Equilibrium Model.* Oxford University Press, New York, NY.

Anderson G.M., Castet S., Schott J., and Mesmer R.H. (1991) The density model for estimation of thermodynamic parameters of reactions at high temperatures and pressures. *Geochim. Cosmochim. Acta.* **55,** 1769-1779.

Archer D.G., and Wang P. (1990) The dielectric constant of water and Debye-Hückel limiting law slopes. *J. Phys. Chem. Ref. Data* **19,** 371-411.

Ashoff A.F., Lee Y.H., Sopocy D.M., and Jonas O. (1986) Interim consensus guidelines on fossil plant cycle chemistry. *EPRI Report CS-4629.*

Atkinson R.J., Posner A.M., and Quirk J.P. (1972) Kinetics of isotopic exchange of phosphate at the alpha FeOOH-aqueous solution interface. *J. Inorg. Chem.* **34,** 2201-2211

Atlas E., Culberson C., and Pytkowicz R.M. (1976) Phosphate association with Na^+, Ca^{2+}, and Mg^{2+} in seawater. *Marine Chemistry* **4,** 243-254.

Babcock and Wilcox (1987) Boiler water phosphate chemistry. *B&W Plant Service Bull.* PSB 25-2M-P7/87.

Balakrishnan P.V. (1977) A study of phosphate hide-out from boiling water. *Can. J. Chem. Eng.* **55,** 592-596.

Baldwin W.G., and Sillen L.G. (1969) Phosphate equilibria. I. Dissociation of phosphoric acid in 3 M sodium perchlorate. *Ark. Kemi* **31,** 391.

Bashkinskii E.V., Degtyarev V.A., and Ignotov Yu. I. (1988) The question of the

advisability of using phosphates for correcting water conditions of high-pressure boilers. *Thermal Eng.* **35,** 707-708.

Becker Jr. L.F., and Esposito J.N. (1981) Steam generator sludge pile model boiler testing - sludge characterization. *EPRI Report NP-2041.*

Benson S.W. (1968) *Thermochemical Kinetics.* Wiley, New York, NY.

Berl E., and van Taack F. (1933) Ober die einwirkung von laugen und salzen auf flusseisen (The impact of caustic and salts on mild steel). *Forsch. Arb. Geb. Ingenieurwesen* **330,** 1-31.

Berl E., Staudinger H., and Plagge K. (1927) Untersuchungen über die einwirkung von laugen und verschiedenen salzen auf eisen (Investigations of the impact of caustic and various salts on iron). *Forschungsarbeiten auf dem Gebiete des Ingenieurwesens* **295,** 7 17.

Bignold G.J., Garnsey R., and Mann G.M.W. (1972) High temperature aqueous corrosion of iron: Development of theories of equilibrium solution phase transport through a porous oxide. *Corrosion Sci.* **12,** 325-330.

Blesa M.A., Morando P.J., and Regazzoni A.E. (1994) *Chemical Dissolution of Metal Oxides.* CRC Press, Boca Raton, FL.

Bohnsack G. (1976a) Significance of phosphate in the iron/water system. *VGB Kraftwerkstechnik* **56,** 523 - 534.

Bohnsack G. (1976b) The importance of phosphate in the iron/water system. Part 2. The chemistry of the system. *VGB Kraftwerkstechnik* **56,** No. 10, 638-644.

Bohnsack G. (in preparation) Chemical interaction of iron, iron oxide and phosphate.

Booy M., and Swaddle T.W. (1978) Hydrothermal preparation of magnetite from iron chelates. *Can. J. Chem.* **56,** 402-403.

Bornak W.E. (1987) Chemistry of iron and its corrosion products in boiler systems. *Corrosion* **44,** 154-158.

Borovaya F.E., and Ravich M.I. (1968) Solubility of sodium carbonate and orthophosphate in aqueous solutions of sodium hydroxide at elevated temperatures. *Russ. J. Inorg. Chem.* **13,** 1720-1723.

Boudart M. (1991) *Kinetics of Chemical Processes.* Butterworth-Heinemann, Boston, MA.

Bourcier W. L., and Barnes H.L. (1987) Ore solution chemistry VII. Stabilities of chloride and bisulfide complexes of zinc to 350°C. *Economic Geology* **82,** 1839-1863.

Broadbent D., Lewis G.G., and Wetton E.A.M. (1978) The chemistry of high temperature phosphate solutions in relation to steam generation *Proc. BNES Conf. Water Chem. Nuclear Reactor Systems* (London) pp. 53-62.

Broadbent D., Lewis G.G., and Wetton E.A.M. (1977) Phase equilibria in aqueous sodium phosphate solutions at elevated temperatures. *J. Chem. Soc. Dalton Trans.* **5**, 464-468.

Broadbent D., Mackenzie J.P., and Wetton E.A.M. (1978) High-temperature phosphate chemistry, Part IV Corrosion of mild steel in sodium phosphate solutions at 250°, 300° and 350°C. *Central Electricity Generating Board Research Report NW/SSD/RR/67/78.*

Burgmayer P. (1989) Where's all that copper in your boiler coming from? *Materials Performance* Sept., 75-89.

Caminiti R. (1982) Nickel and cadmium phosphates in aqueous solution. Cation-anion complex formation and phosphate-H_2O interactions. *J. Chem. Phys.* **77**, 5682-5686.

Castle J.E., and Masterson H.G. (1966) The role of diffusion in the oxidation of mild steel in high temperature aqueous solutions. *Corrosion Sci.* **6**, 93-104.

Cerreta M.K., and Berglund K.A. (1987) The structure of aqueous solutions of some dihydrogen orthophosphates by laser raman spectroscopy. *J. Cryst. Growth* **84**, 577-588.

Chen, M.C., Shalvoy R.S., and Gould G.C. (1984) The effects of phosphate environments on turbine materials. *EPRI Report CS-3541.*

Childs C.W. (1970) A potentiometric study of equilibria in Aqueous Divalent Metal orthophosphate solutions. *Inorg. Chem.* **9**, 2465-2469.

Childs C.W. (1969) Equilibria in dilute aqueous solutions of orthophosphates. *J. Phys. Chem.* **73**, 2956 - 2960.

Childs C.W., Downes C.J., and Platford R.F. (1973) Thermodynamics of aqueous sodium and potassium dihydrogen orthophosphate solutions at 25°. *Aust. J. Chem.* **26**, 863-866.

Cohen P. (1970) Chemistry of additives and contaminants in high pressure boilers. *Trans. ASME J. Eng. Power* Jan., 89-94.

Cohen P., Taylor G.R., and Picon L.F. (1962) A radiotracer test facility for hide-out measurements under boiler conditions. *ASME Paper No. 62-WA-253.*

Connor W.M., and Panson A.J (1983) Investigation of phosphate-sludge interactions. *EPRI Report NP-2963.*

Corbridge D.E.C. (1980) Phosphorus: *An Outline of its Chemistry, Biochemistry, and Technology* Elsevier, Amsterdam.

Costa S.I., and Brestel L.O. (1989) Managing a captive-alkalinity boiler-treatment program. *Power* March, 21-28.

Cotton F.A., and Wilkinson G. (1988) *Advanced Inorganic Chemistry, Fifth Edition* John Wiley & Sons, New York.

Daniele P.G., Rigano C., and Sammartano S. (1985) Ionic strength dependence of formation constants. Alkali metal complexes of ethylenediaminetetraacetate, nitrilotriacetate, diphosphate, and tripolyphosphate in aqueous solution. *Anal. Chem.* **57**, 2956-2960.

Daniele P.G., De Robertis A., De Stefava C., Gianguzza A., and Sammartano S. (1991) Salt effects on the protonation of ortho-phosphate between 10 and 50°C in aqueous solution. A complex formation model. *J. Solution Chem.* **20**, 495-515.

Dibble W.E., and Tiller W.A. Jr. (1981) Non-equilibrium water/rock interactions - I. Model for interface-controlled reactions. *Geochim. Cosmochim. Acta* **45**, 79-92.

Dick I.B. (1963) Experience with hydrogen embrittlement in the consolidated Edison system. *ASME Paper No. 63-PWR-13.*

Dooley R B. (1994) Cycle guidelines for fossil plants: Phosphate treatment for drum units *EPRI Report TR-103665.*

Dooley B., and Broske D., eds. (1987) *Proc. EPRI Conf. Boiler Tube Failures in Fossil Power Plants.* (Atlanta, GA.).

Economy G., Panson A.J., Liu Chia-tsun, Esposito J.N., and Lindsay W.T. Jr. (1975) Sodium phosphate solutions at boiler conditions: Solubility, phase equilibria and interactions with magnetite. *Proc. 36th Int. Water Conf.* (Pittsburgh, PA.) pp. 161 - 173.

Edwards J.W., and Herzog A.H. (1957) The mechanism of formation of sodium triphosphate from orthophosphate mixtures. *J. Amer. Chem. Soc.* **79**, 3647-3650.

Elmore K.L., Hatfield J.D., Dunn R.L., and Jones A.D. (1965) Dissociation of phosphoric acid solutions at 25°. *J. Phys. Chem.* **69**, 3520-3525.

Eysseltova J. (1988) IUPAC Solubility Data Series, S. Kertes, ed., Vol. 31.

Filatova L.N. (1974) Complex Formation by Iron(III) with Orthophosphate in Weakly Acidic Aqueous Solutions. *Russian J. Inorg. Chem.* **19**, 3335-3339.

Filatova L.N., Shelyakina M.A., Plachinda A.S., and Makarov E.F. (1976) Dimerization of iron(III) in aqueous solution in the presence of phosphate ions. *Russian J. Inorg. Chem.* **21**, 2715-2720.

Galonian G.E., Ziemniak S.E., and Opalka E.P. (1982) Possible local chemistry conditions for attack of Ni Cr Fe alloy steam generator tubes *Proc. EPRI Contractors Meeting on Intergranular Corrosion* (Clearwater Beach, FL).

Goldman S., and Bates R.G. (1972) Calculation of thermodynamic functions for ionic hydration. *J. Am. Chem. Soc.* **94**, 1476-1484.

Goldstrohm D.D., and Robertson T.W. (1989) Low phosphate - low sodium hydroxide treatment in 2600 psig boilers of Salt River Projects's Coronado Station. *Proc. 50th Int. Water Conf.* (Pittsburgh, PA.) pp. 493-499.

Gorman J.A., and Partridge M.J. (1988) Proc. 1987 EPRI Workshop on Secondary-Side Intergranular Corros. Mech. *EPRI Report NP-5971.*

Greenberg J.P., and Moller N. (1989) The prediction of mineral solubilities in natural waters: A chemical equilibrium model for the Na-K-Ca-Cl-SO_4-H_2O systems to high concentration from 0 to 250°C. *Geochim. Cosmochim. Acta.* **53,** 2503-2518.

Griffith E.J., and Buxton R.L. (1968) Selected aqueous phase diagrams of condensed phosphate systems. *J. Chem. Eng. Data* **13,** 145-148.

Haar L., Gallagher J.S., and Kell G.S. (1984) NBS/NRC Steam Tables. Thermodynamic and Transport Properties and Computer Programs for Vapour and Liquid States of Water in SI Units. Hemisphere Publishing Corporation.

Hall R.E. (1944) A new approach to the problem of conditioning water for steam generation. *Trans. ASME* **66,** 457-474.

Hall R.E. (1927) Physico-chemical study of scale formation and boiler water conditioning. *Mining and Metallurgical Investigations, Carnegie Institute of Technology Bulletin* **24,** 72-73.

Harada K., Arai T., Shimada M., Kawai N., and Kurosawa T. (1978) Corrosion of Inconel 600 in high temperature water. Part I: Design and construction of high temperature experimental apparatus under boiling heat transfer condition and corrosion behavior in sodium triphosphate solution. *Central Research Institute of Electric Power Industry (Japan), Report EEL-E277010.*

Hayward A., Hearn B., Hunt, and M.R. (1967) Solubility of cupric oxide in pure water at temperatures up to 550°C. *Nature* **215,** 730.

Hearn B., Hunt M.R., and Hayward A. (1969) Solubility of cupric oxide in pure subcritical and supercritical water. *J. Chem. Eng. Data* **14,** 442.

Helgeson H.C., Delaney J.M., Nesbitt H.W., and Bird D.K. (1978) Summary and critique of the thermodynamic properties of rock-forming minerals. *Am. J. Sci.* **278A,** 1-229.

Helgeson H.C., and Kirkham D.H. (1976) Theoretical prediction of the thermodynamic properties of aqueous electrolytes at high pressures and temperatures. III. Equation of state for aqueous species at infinite dilution. *Am. J. Sci.* **276,** 97-240.

Helgeson H.C., Kirkham D.H., and Flowers G.C. (1981) Theoretical prediction of the thermodynamic properties of aqueous electrolytes at high pressures and temperatures: IV. Calculation of activity coefficients, osmotic coefficients, and apparent molal and standard and relative molal properties to 600°C and 5kb. *Am. J. Sci.* **281,** 1249-1493.

Hershey J.P., Fernandez M., and Millero F.J. (1989) The dissociation of phosphoric acid in NaCl and NaMgCl solutions at 25°C. *J. Solution Chem.* **18,** 875-891.

Högfeldt E. (1982) *Stability constants of metal-ion complexes. Part A: Inorganic*

ligands. IUPAC Chemical Data Series, No. 21. Permagon, New York, N.Y.

Holmes H.F., and Mesmer R.E. (1983) Thermodynamic properties of aqueous solutions of the alkali metal chlorides to 250°C. *J. Phys. Chem.* **87,** 1242-1255.

Holroyd A., and Salmon J.E. (1956) Ion-exchange studies of phosphates. Part I. Ion-exchange sorption an pH-titration methods for detection of complex formation. *J. Chem. Soc.* 269.

Jameson R.F., and Salmon J.E. (1954) Complexes involving tervalent iron and orthophosphoric acid. Part III. The system ferric oxide-phosphoric oxide-water at 25°C. *J. Chem. Soc.* 28-34.

JCPDS (1991) Powder Diffraction File. *JCPDS Int. Center for Diffraction Data* Swarthmore, PA.

Johnson J.W., Oelkers E.H., and Helgeson H.C. (1992) Supert92: A software package for calculating the standard molal thermodynamic properties of minerals, gases, aqueous species and reactions from 1 to 5000 bar and 0 to 1000°C. *Computers and Geoscience* **18(7),** 899-947.

Jonas O. (1981) Transport of ionic impurities in fossil and PWR cycles new observations. *Proc. 42nd Int. Water Conf.* Paper IWC-81-40 pp. 125 - 139.

Jonas O. (1985) Transport of chemicals in steam cycles. *NACE Corrosion 85* (Boston, MA) Paper 245.

Jonas O. (1985b) Transport of ionic impurities in fossil and PWR cycles new observations. *Pure & Appl. Chem.* **57,** 283-301.

Jonas O. (1988) Chemical data for steam generating cycles. *J. Solution Chem.* **17,** 791 - 804.

Jonas O., Lindsay Jr. W.T., and Evans, N.A. (1980) Turbine steam purity - 1979 Update. *Water and Steam -Their Properties and current Industrial Applications.* J. Straub and K. Scheffler, eds., Pergamon Press, Oxford. pp 595-607.

Jonas O., and Layton K.F. (1988) Phosphate boiler water treatment for high pressure boilers. *Proc. Second EPRI Fossil Plant Cycle Chemistry Conf.* (Seattle, WA.)

Jonas O., Blood F., Connick B., Lehner K., and Homan W.R. (1987) Water, steam, and turbine Deposit Chemistries in Phosphate-Treated Drum Boiler Units", *EPRI Report CS-5275, Project No. 1986-9.*

Kelly J.A., Bain D.I., and Thompson H.W. (1988) Recent experience with phosphate pH control programs. *Corrosion 88* (St. Louis, MI) Paper 204.

Kharaka Y.K., Gunter W.D., Aggarwal P.K., Perkins E.H., and DeBraal J.D. (1988) SOLMINEQ.88: A computer program for geochemical modeling of water-rock interactions. *US Geological Survey, Water-Resources Investigations Report 88-4227.*

Khodakovsky I.L., and Yelkin A.E. (1975) Experimental determination of zincite solubility in water and aqueous NaOH solutions at temperatures of 100, 150, and 200°C. *Geokhimiya* **10,** pp. 1490-1495; *Geochemistry Int.* **12,** 127-133.

Kiehl, S.J., and Wallace G.H. (1927) The dissociation pressures of monopotassium and monosodium orthophosphates and of dipotassium and disodium dihydrogen pyrophosates. Phosphate IV. *J. Amer. Chem. Soc.* **49,** 375-386.

Kielman H.S., and Leyte J.C. (1975) Nuclear magnetic relaxation of ^{31}P in aqueous orthophosphate solutions. *Ber. Buns. Phys. Chem.* **79,** 1201-1205.

Kirsch H. (1964) Phosphate containing deposits in high pressure steam generators. *Mitteilung* **VGB 89,** 80-88.

Klein H.A. (1962) Use of coordinated phosphate treatment to prevent caustic corrosion in high pressure boilers. *Combustion* **Oct.,** 45-52.

Kunig R.H., and Sandler Y.L. (1986) Solubility of simulated PWR primary circuit corrosion products", *EPRI Report NP-4248.*

Kunig R.H., and Sandler Y.L. (1981) The solubility of nickel ferrite in aqueous boric acid solution. *Nucl. Sci. Eng.* **77,** 211-218.

Kunig R.H., and Sandler Y.L. (1977) The solubility of nonstoichiometric nickel ferrite in high-temperature aqueous solution. *Nucl. Sci. Eng.* **64,** 866-874.

Larson J.W., Zeeb K.G., and Hepler L.G. (1982) Heat capacities and volumes of dissociation of phosphoric acid (1st, 2nd, and 3rd), bicarbonate ion, and bisulfate ion in aqueous solution. *Can. J. Chem.* **60,** 2141-2190.

Layton K.F. (1987) Water side corrosion in the water wall tubes of Hunter Unit 3. *Proc. EPRI Conf. on Boiler Tube Failure in Fossil Plants* (Atlanta, GA.)

LePage Y., and Dornay G. (1977) The crystal structure of the new mineral maricite, $NaFePO_4$. *Canadian Mineralogist* **15,** 518-521.

Lindsay W.T. Jr. (1979) Behavior of impurities in steam turbines. *Power Eng.* May, 68-72.

Lindsay W.T. Jr. (1989) Computer modeling of aqueous systems in power cycles. in *Properties of Water and Steam* M. Pichal and O. Sifner, eds. Hemisphere Publishing, New York, NY. pp. 29-38.

Lindsay W.T. Jr., and Lee P.K. (1981) Condensation of low-volatility impurities in steam turbines. *Proc. Conf. Corros. Fatique of Steam Turbine Blades, EPRI Report.*

Macbeth R.V., Trenberth R., and Wood R.W.(1971) An investigation into the effect of "crud" deposits on surface temperature, dry-out, and pressure drop with forced convection boiling of water at 69 bar in an annular test section. *UKEA Report No. AEEW-R705* Winfrith, Dorchester, UK.

MacNeil C.K., and Silbert M.D. (1988) A new look at phosphate vs AVT for nuclear steam generators. *Proc. 49th Int. Water Conf.* (Pittsburgh PA.) Paper IWC-88-34.

Maier C.G., and Kelley K.K. (1932) An equation for the representation of high temperature heat content data. *J. Am. Chem. Soc.* **54**, 3243-3246.

Mair A.D. (1976) Dimorphism of trisodium phosphate. *N.Z. J. Sci.* **19**, 61-67

Malinowski D.D., and Fletcher W.D. (1978) Update of operations with Westinghouse steam generators. *Nuclear Technology* 103-110.

Marcy V.M., and Halstead S.L. (1964) Improved basis for coordinated phosphate-pH control of boiler water. *Combustion* **Jan.**, 45-47.

Marshall W.L. (1985) Aqueous inorganic phase equilibria at high temperatures: Some experimental, theoretical, and applied aspects. *Pure and Appl. Chem.* **57**, 283-301.

Marshall W.L. (1982) Two-liquid-phase boundaries and critical phenomena at 275-400°C for high-temperature aqueous potassium phosphate and sodium phosphate solutions. Potential applications for steam generators. *J. Chem. Eng. Data* **27**, 175-180.

Marshall W.L., and Begun G.M. (1989) Raman spectroscopy of aqueous phosphate solutions at temperatures up to 450°C. *J. Chem. Soc., Faraday Trans. 2* **85**, 1963-1978.

Martell A.E., Motekaitis R.J., Fried A.R., Wilson J.S., and MacMillan D.T. (1975) Thermal decomposition of EDTA, NTA, and nitrilotrimethylenephosphonic acid in aqueous solution. *Can. J. Chem.* **53**, 3471-3476.

Martynova O.I., and Rogatskin B.S. (1970) Deposition of salts and corrosion products in supercritical turbine flow sections. *Teploenergetika* **17**, 50-54.

Martynova N.K., Akol'zin P.A., Ibragimov M.Kh., and Avdonkin M.A. (1990) Investigating the interaction between phosphate solutions and carbonate scale. *Thermal Eng.* **37**, 86-89.

Matijevic E. (1986) Monodispersed colloids: Art and science. *Langmuir* **2**, 12-20

McDonald A.C., and Tracy, B.L. (1988) Phosphate hideout in high-pressure solutions. *Proc. 49th Int. Water Conf.* (Pittsburgh, PA.) Paper IWC-88-41.

Melendres C.A., Camillone N., and Tipton T. (1989) Laser raman spectroelectrochemical studies of anodic corrosion and film formation on iron in phosphate solutions. *Electrochimica Acta* **34**, 281-286

Meissner H.P. (1980) Prediction of activity coefficients of strong electrolytes in aqueous systems. *Thermodynamics of Aqueous Systems with Industrial Applications*. Symposium Series No. 133. Newman S.A. ed. Washington, D.C. American Chemical Society, 495-511.

Mesmer R.E., and Baes C.F. Jr. (1974) Phosphoric acid dissociation equilibria in aqueous

solutions to 300°C. *J. Solution Chem.* **3**, 307-322.

Mesmer R.E., Marshall W.L., Palmer D.A., Simonson J.M., and Holmes H.F. (1988) Thermodynamics of aqueous association and ionization reactions at high temperatures and pressures. *J. Solution Chem.* **17**, 307-321.

Miller J.C. and Miller J.N. (1988) *Statistics for Analytical Chemistry*. 2nd edition, Ellis Horwood Ltd., John Wiley and Sons, Chapter 2, pp. 46, 1988.

Millero F.J.(1976) Effects of pressure and temperature on activity coefficients. in *Activity Coefficients in Electrolyte Solutions*, R.M. Pytkowicz, ed., CRC Press, Boca Raton, Florida.

Morey G.W. (1953) The system H_2O-$NaPO_3$. *J. Amer. Chem. Soc.* **75**, 5794-5797.

Moore P.B. (1970) Crystal chemistry of the basic iron phosphate. *Amer. Mineralogist* **55**, 135-169.

Palazzi M., and Remy F. (1971) Polymorphism of anhydrous trisodium arsenate and phosphate. *Radiocrystallorgraphic Study, Bull. Soc. Chim. France* 2795-2798.

Panson A.J., Economy G., Liu Chia-tsun, Bulischeck T.S., and Lindsay W.T. Jr. (1975) Sodium phosphate solubility and phase relations basis for invariant point chemistry control. *J. Electrochem. Soc.* **122**, 915 - 918.

Parr S.W. (1917) The embrittling action of sodium hydroxide on soft steel. *University of Illinois Bulletin 93.*

Parr S.W., and Straub F.G. (1928) Embrittlement of boiler steel. *Midwest Power Conference* (Chicago, IL) (Cited by Bohnsack, in prep.)

Partridge E.P., and Hall R.E. (1939) Attack on steel in high-capacity boilers as a result of overheating due to steam blanketing. *Trans. ASME* **10**, 597-627.

Patel P.R., Gregory T.M., and Brown W.E. (1974) Solubility of $CaHPO_4 \cdot 2H_2O$ in the quaternary system $Ca(OH)_2$- H_3PO_4 - NaCl - H_2O at 25°C. *J. Res. National Bureau of Standards* **78A**, 675-681.

Pessall N., Dunlap A.B., and Feldman D.W. (1977) The corrosion resistance of inconel alloy 600 in high temperature phosphate solutions. *Corrosion* **33**, 130-144.

Phutela R.C., Pitzer K.S., and Saluja P.S. (1987) Thermodynamics of aqueous magnesium chloride, calcium chloride, and strontium chloride at elevated temperatures. *J. Chem. Eng. Data* **32**, 76-80.

Pitzer K.S. (1991) *Activity Coefficients in Electrolyte Solutions*. 2nd ed, CRC Press, Boca Raton, FL.

Pitzer K.S. (1984) Ionic fluids. *J. Phys. Chem.* **88**, 2689-2697.

Pitzer K.S., and Simonson J.M. (1986) Thermodynamics of multicomponent, miscible, ionic systems: Theory and equations. *J. Phys. Chem.* **90**, 3005-3009.

Plummer L.N., Parkhurst D.L., Fleming G.W., and Dunkle S.A. (1988) A computer program incorporating Pitzer's equations for calculation of geochemical reactions in brines. *U.S. Geolog. Survey WRI Report 88-4153, 310pp.*

Plyasunov A.V., Belonozhko A.B., Ivanov I.P., and Khodakovskiy I.L. (1988) Solubility of zinc oxide in alkaline solutions at 200-300°C under saturated steam pressure. *Geochem. Int.* **3**, 77-84.

Pocock F.J. (1983) Waterside corrosion and its control in fossil utility steam generators. *Proc. Symp. Thermal Utilities Boiler Reliability* (Toronto) pp. 159-196.

Pollard A.J., and Edwards A.J. (1963) An investigation of the effects of alkaline phosphate solutions at elevated temperature on compounds prepared at room temperature *U.S. Naval Research Laboratory Report NRL 5865.*

Potter E.C., and Mann G.M.W. (1965) *Brit. Corros. J.* **1**, 26.

Potter E.C. (1964) Large scale steam generation of steel surfaces: A physicochemical enquiry. *Proc. 25th Int. Water Conf.* (Pittsburgh, PA.) pp. 7-21.

Preston C.M., and Adams W.A. (1979) A laser raman spectroscopic study of aqueous orthophosphate salts. *J. Phys. Chem.* **83**, 814-821.

Pryor M.J., and Cohen M. (1951) The mechanism of the inhibition of the corrosion of iron by solutions of sodium orthophosphate. *J. Electrochem. Soc.* **98**, 263-272.

Purcell T.E., and Whirl S.F. (1943) Protection against caustic embrittlement by coordinated phosphate - pH control. *Trans. Electrochem. Soc.* **83**, 343-359.

Ravich M.I., Borovaya F.E., and Ketkovich V.Ya. (1953) Izv. Sektora Fiz. -Khim. Anal. Inst. Obshch. Neorg. Khim. Akad. Nauk SSSR, **22**, 225.

Ravich M.I., Borovaya F.E., and Ketkovich V.Ya. (1953) Izv. Sektora Fiz. -Khim. Anal. Inst. Obshch. Neorg. Khim. Akad. Nauk SSSR, **22**, 250.

Ravich M.I., and Borovaya F.E. (1955) Izv. Sektora Fiz. -Khim. Anal. Inst. Obshch. Neorg. Khim. Akad. Nauk SSSR, **26**, 229.

Ravich M.I., and Scherbakova L.A. (1955) Nature of the solid phase which crystallizes from aqueous solutions of trisodium orthophosphate at high temperatures. *Izvest. Sektora Fiz. Khim. Anal., Inst. Obshchei Neorg. Khim. Akad. Nauk SSSR* **26**, 248-258.

Ravich M.I., and Yastrebova L.F. (1959) The solid phases crystallizing in the system $Na_3PO_4/Na_2SO_4/H_2O$ at high temperatures. *Russ. J. Inorg. Chem.* **4**, 69-74.

Rivers H.M. (1951) Concentrating films - Their role in boiler scale and corrosion problems. *Proc. 12th Int. Water Conf.* (Pittsburgh, PA.) pp. 131-137.

Roesmer J., Dole L.R., Mesmer R.E., and Feldman D.W. (1975) Experimental and theoretical pH values of phosphate solutions between 25 and 285°C. *Proc. 36th Int. Water Conf.* (Pittsburgh, PA.) Paper IWC-75-24, 149-160.

Ruaya J.R., and Seward T.M. (1986) The stability of chlorozinc (II) complexes in hydrothermal solutions up to 350°C. *Geochim. Cosmochim. Acta* **50,** 651-661.

Rummery T.E., and Macdonald D.D. (1975) Prediction of corrosion product stability in high-temperature aqueous systems. *J. Nucl. Materials* **55,** 23.

Salmon J.E., and Terry H. (1950) The systems zinc oxide - phosphorous oxide - water and manganous oxide - phosphoric acid - water at temperatures between 25° and 100°C. *J. Chem. Soc.* 2813-2824.

Scatchard G., and Breckenridge R.C. (1954) Isotonic solutions. II. The chemical potential of water in aqueous solutions of potassium and sodium phosphates and arsenates at 25°. *J. Phys. Chem.* **58,** 596-602.

Scheerer C.C., and Maxwell J.K. (1990) Minimize phosphate hideout by chemical cleaning. *Power* Oct., 13-16.

Scheerer C.C., and Maxwell J.K. (1990) Phosphate hideout: An on-line indication of boiler cleanliness. *Proc. Amer. Power Conf.*

Schroeder W.C., and Berk A.A. (1942) Intercrystalline cracking of boiler steel and its prevention. *U.S. Bur. Mines Bull.* 44B; abstracted in *Power* **86,** 103.

Schroeder W.C., Berk A.A., and Gabriel A. (1937) Solubility of equilibria of sodium sulfate at temperatures from 150 to 350°. III. Effect of sodium hydroxide and sodium phosphate. *J. Amer. Chem. Soc.* **59,** 1783-1790

Selvaratnam M., and Spiro M. (1965) Transference numbers of orthophosphoric acid and the limiting equivalent conductance of the $H_2PO_4^-$ ion in water at 25°C. *Trans. Faraday Soc.* **61,** 360-373.

Shcherbakova L.G. (1953) Thesis, Inst. Obshch. Neorg. Khim. Akad. Nauk SSSR.

Shock E.L., Helgeson H.C. (1988) Calculation of the thermodynamic and transport properties of aqueous species at high temperatures and pressures: Correlation algorithms for ionic species and equation of state predictions to 5 kbar and 1000°C. *Geochim. Cosmochim. Acta* **52,** 2009-2036.

Shock E.L., Oelkers E.H., Johnson J.W., Sverjensky D.A., and Helgeson H.C. (1992) Calculation of the thermodynamic properties of aqueous species at high pressures and temperatures. Effective electrostatic radii, dissociation constants and standard partial molar properties to 1000°C and 5 kbar. *J. Chem. Soc. Faraday Trans.* **88,** 803-826.

Silbert M.D., and MacNeil C.K. (1990) Point Lepreau phosphate control - 600 MW Candu experience. *Proc. ASME Workshop on Laboratory and Field Experiences with Phosphate in Power Utility Drum Boilers* (Pittsburgh, PA.)

Smith R.M., and Alberty R.A. (1955) The apparent stability constants of ionic complexes of various adenosine phosphates with monovalent cations. *J. Phys. Chem.* **60**, 180-184.

Smith R.M., and Martell A.E. (1976) *Critical Stability Constants. Volume 4: Inorganic Complexes*. Plenum, New York, NY.

Splittgerber A. (1938) Die bedeutung der wasserstoffionenkonzentration im kesselbetrieb (Hydrogen ion concentration and its importance for boiler operation). *Mitt.* **VGB 70**, 335-341.

Splittgerber A. (1928) Ober den derzeitigen stand der kesselspeisewasserpflege mit besonderer berüsichtigung der speisung von höchstdruckkesseln (Present state of the art of boiler water chemistry with emphasis on feeding maximum pressure boilers). *Jahrbuch vom Wasser* **II**, 98-12.

Sprague B.C. (1927) Overcoming boiler water troubles with trisodium phosphate. *Power* **65**, 321-322.

Stodola J. (1985) Phosphate and other hide-out. *Proc. Fossil Plant Water Chemistry Symposium, EPRI Report CS-4950.*

Stodola J. (1986) Review of boiler water alkalinity control. *Proc. 47th Int. Water Conf.* (Pittsburgh, PA) pp.1-9.

Stodola J. (1991) Rationale for equilibrium phosphate treatment *Proc. EPRI Conf. on Cycle Chemistry in Fossil Plants* (Baltimore, MD) pp. ?-?.

Straub F.G. (1950) Hideout of sodium phosphate in high-pressure boilers *Trans. ASME* **72**, 479-489.

Stumm W., and Morgan J.J. (1970) *Aquatic Chemistry*. Wiley-Interscience, New York, NY.

Styrikovich M.A., Reznikov M.I., and Tolmacheva I.K. (1973) *Teploenergetika* **20**, 81; *Transl. Thermal Eng.* **20**, 114.

Sweeton F.H., Mesmer R.E., and Baes C.F. (1974) Acidity measurements at elevated temperature VII. Dissociation of water. *J. Solution Chem.* **3**, 191-214.

Tanger J.C., and Helgeson H.C. (1988) Calculation of the thermodynamic and transport properties of aqueous species at high temperatures and pressures. Revised equation of state for the standard partial molar properties of ions and electrolytes. *Am. J. Sci.* **288**, 19-98.

Taylor P., Tremaine P.R., and Bailey M.G. (1979) Sodium oxide-phosphorus (V) oxide-water phase diagram near 300°C: equilibrium solid phases *Inorganic Chem.* **11**, 2947-2953.

Thiel A., and Luckmann H. (1928) Ober Korrosionserscheinungen (Corrosion Phenomena). *Korrosion und Metallschutz* **4**, 169-177.

Thilo E. (1965) The structural chemistry of condensed inorganic phosphates. *Agnew.*

Chem. Internat. **4**, 1061-1071.

Treloar N.C. (1973) Raman study of phosphate equilibria in aqueous solutions from 25 to 150°C. *CERL Laboratory Note RD/L/N 270/73* Central Electricity Research Laboratories, Leatherhead, Surrey.

Tremaine P.R., Gray L.G.S., Wiwchar B., Stodola J., and Taylor P. (1992) Sodium phosphate chemistry under high pressure utility drum boiler conditions. *Can. Electrical Assoc. R & D Agreement 913G730, Final Report* Vol I, 104 pp; Vol II, 196 pp; Vol III, 183 pp.

Tremaine P.R., Gray L.G.S., Wiwchar B., Stodola J., and Taylor P. (1993). Phosphate interactions with metal oxides under high-pressure boiler hideout conditions, *Proc. 54th Int. Water Conf.* Paper IWC-93-35.

Tremaine P.R., Sway K., and Barbero J.A. (1986) The apparent molar heat capacity of aqueous hydrochloric acid from 10-140°C. *J. Phys Chem.* **15**, 1-22.

Van Wazer, J.R. (1958): *Phosphorus and Its Compounds*. Interscience, N.Y.

Walker S.M. Thornton E.W. (1989) Reanalysis of oxide solubility data. *Proc. Fifth Conf. Water Chem. of Nuclear Reactor Systems* BNES, London. pp. 89-95.

Weingärtner H. (1989) Thermodynamics of aqueous electrolyte solutions with liquid-liquid phase separation. *Ber. Bunsenges. Phys. Chem.* **93**, 1058-1065.

Wendrow B., and Kobe K.A. (1955) The system sodium oxide-phosphorus pentoxide-water, *Ind. Eng. Chem.* **44**, 1439-1448.

Weres O., and Tsao L. (1986) Activity of water mixed with molten salts at 317°C. *J. Phys. Chem.* **90**, 3014-3018.

Wetton E.A.M. (1980) High-temperature phosphate chemistry in relation to the phosphate treatment of boilers. *Central Electricity Generating Board Research Report No. NW SSD/RM/58/80.*

Wetton E.A.M., MacKenzie J.P. (1980) High-temperature phosphate chemistry, Part V Corrosion of mild steel, 1% and 9% Cr steels in sodium phosphate solutions at 300°C. *Central Electricity Generating Board Research Report NW/SSD/RR/99/80.*

Wetton E.A.M. (in preparation) High temperature phosphate chemistry. Part VI Interaction of aqueous sodium phosphates with iron compounds at 300°C.

Wetton E.A.M. (1981) Phase equilibria in aqueous sodium phosphate solutions at 350°C. *Power Industry Research* **1**, 151-158.

Wetton E.A.M. (1981b) Solubility equilibria and oxidation-reduction reactions in aqueous sulfate systems at 350°C. *Power Industry Research* **1**, 329-345.

Wilhelmy R.B., Patel R.C., and Matijevic E. (1985) Thermodynamics and kinetics of

aqueous ferric phosphate complex formation. *Inorg. Chem.* **24**, 3290-3329.

Wood R.H., Platford R.F. (1975) Free energies of aqueous mixtures of NaH_2PO_4 and $NaClO_4$: Evidence for the species $(H_2PO_4)_2^{2-}$. *J. Solution Chem.* **4**, 977-982.

Xiao C., and Tremaine P.R. (1994) Standard partial molar heat capacities and volumes of aqueous divalent and trivalent ions from measurements near 25°C. *Proc. 12th Int. Conf. on Properties of Water and Steam* (Orlando, Fl..).

Ziemniak S.E. (1991) Metal oxide solubility behavior in high-temperature aqueous solutions. *Proc. 2nd. Int. Sympos. on Chemistry in High-Temperature Water.* (EPRI - to be published). *Knolls Atomic Power Lab. Report KAPL - 4727.*

Ziemniak S.E., Jones M.E., and Combs K.E.S. (1990) Zinc(II) oxide solubility and phase behaviour in aqueous sodium phosphate solutions at elevated temperatures *Knolls Atomic Power Laboratory Report KAPL - 4716.*

Ziemniak S.E., Jones M.E., and Combs K.E.S. (1989) Solubility and phase behavior of nickel oxide in aqueous sodium phosphate solutions at elevated temperatures *J. Solution Chem.* **18,** 1133-1152.

Ziemniak S.E., and Opalka E.P. (1988) Nickel oxide stability in aqueous sodium phosphate solutions at elevated temperatures. *Proc. Int. Symp. on Environmental Degradation of Materials in Nuclear Power Systems-Water Reactors* Theus, G.J., and Weeks, J.R., eds pp.153-156.

Ziemniak S.E., and Opalka E.P. (1992) Magnetite stability in aqueous sodium phosphate solution at elevated temperatures. *Knolls Atomic Power Lab Report KAPL-4735.*

Ziemniak S.E., and Opalka E.P. (1993) *Proc. Sixth Int. Symposium on Environmental Degradation of Materials in Nuclear Power Systems - Water Reactors* Gold R.E., and Simonen E.P., eds. (Warrendale, PA.) pp. 929-935.

Ziemniak S.E., Stalnaker N.D., Jones M.E., and Grossman, B. (1981) Chemical interactions between high temperature aqueous solutions of sodium phosphate and magnetite. *EPRI Workshop* (Minneapolis., MN, June 1981) Abstract.

7.0 APPENDIX I

Introduction

The following report is a summary of x-ray diffraction data of relevant species in the reactions of iron phosphate hematite, magnetite, iron (III) nitrilotriacetate, and iron powder with sodium phosphate solutions.

Description of samples

1. Unreacted iron (III) phosphate, $FePO_4$, starting material. (Johnson Matthey, $FePO_4 \cdot xH_2O$ ~ 17% H_2O). XRD file: Z00026.RAW.

2. Unreacted hematite, Fe_2O_3, starting material. (BDH, ~97%). XRD file: Z00043.RAW.

3. Unreacted hematite, Fe_2O_3, starting material. (Aldrich, 99+%). XRD file: Z00042.RAW.

4. Unreacted magnetite, Fe_3O_4, starting material. (Aldrich, 98%). XRD file: Z00027.RAW.

5. Filtered reaction product of iron (III) phosphate and 1.4 mol kg^{-1} $Na_{2.15}H_{0.85}PO_4$ solution at 250°C for three weeks in 45 mL Teflon lined pressure vessel. (SQ30E). XRD file: Z00021.RAW

6. Filtered reaction product of hematite and 0.9 mol kg^{-1} $Na_{2.15}H_{0.85}PO_4$ solution at 250°C for three weeks in 45 mL Teflon lined pressure vessel. (SQ30C). XRD file: Z00022.RAW.

7. Filtered reaction product of magnetite and 1.9 mol kg^{-1} $Na_{2.15}H_{0.85}PO_4$ solution at 250°C for three weeks in 45 mL Teflon lined pressure vessel. (SQ30A). XRD file: Z00023.RAW.

8. Reaction product of hematite and 0.5 mol kg^{-1} $Na_{2.5}H_{0.5}PO_4$ solution at 200-250°C for one week in 450 mL Hastelloy pressure vessel. Solid was found attached to sampling tube out of contact with liquid phase. (SQ79D). XRD file: Z00036.RAW.

9. Filtered reaction product of ammonium ferric sulfate, $NH_4Fe(III)(SO_4)\cdot 12H_2O$ and nitrilotriacetic acid, H_3NTA, boiled in aqueous solution for one hour to give Fe(III)NTA to be used as a starting material for subsequent pressure vessel reactions (SQ2A). XRD file. SQ2A.MDI.

10 Filtered reaction product of iron (III) nitrilotriacetate, Fe(III)NTA, (SQ2A), starting material and 0.6 mol kg^{-1} $Na_{2.15}H_{0.85}PO_4$ solution at 250°C for two weeks in 45 mL Teflon lined pressure vessel. (SQ4A) XRD file Z00058.RAW

11. Filtered reaction product of iron (III) nitrilotriacetate, Fe(III)NTA, (SQ2A), starting material, 0.6 mol kg^{-1} $Na_{2.15}H_{0.85}PO_4$ solution with 0.4 g of CuO at 250°C for four days in 45 mL Teflon lined pressure vessel (2SQ6C). XRD file 2SQ6C.MDI

12. Filtered reaction product of iron (III) nitrilotriacetate, Fe(III)NTA, (SQ2A), starting material, 0.6 mol kg^{-1} $Na_{2.15}H_{0.85}PO_4$ solution with 6 mL 1m $NaNO_3$ solution at 250°C for six days in 45 mL Teflon lined pressure vessel (2SQ5A) XRD file 2SQ5A2.MDI.

13. Filtered reaction product of iron powder and 0.9 mol kg^{-1} NaH_2PO_4 solution at 250°C for three weeks in 45 mL Teflon lined pressure vessel (SQ39D) XRD file Z00057.RAW.

14. Filtered reaction product of hematite and 0.9 mol kg^{-1} $Na_{2.5}H_{0.5}PO_4$ solution at 250°C for three weeks in 45 mL Teflon lined pressure vessel (SQ35A-E) XRD file Z00045.RAW.

15. Filtered reaction product of hematite and 0.9 mol kg^{-1} $Na_{2.5}H_{0.5}PO_4$ solution at 250°C for three weeks in 45 mL Teflon lined pressure vessel with 1% hematite by mass (SQ35A-E). XRD file: Z00048.RAW.

16. Filtered reaction product of hematite and 0.9 mol kg^{-1} $Na_{2.5}H_{0.5}PO_4$ solution at 250°C for three weeks in 45 mL Teflon lined pressure vessel with 1% hematite by mass (SQ35A-E). XRD file: Z00049.RAW.

17. Filtered reaction product of hematite and 0.9 mol kg^{-1} $Na_{2.5}H_{0.5}PO_4$ solution at 250°C for three weeks in 45 mL Teflon lined pressure vessel with 5% hematite by mass (SQ35A-E). XRD file: Z00050.RAW.

18 Filtered reaction product of hematite and 0.9 mol kg^{-1} $Na_{2.5}H_{0.5}PO_4$ solution at 250°C for three weeks in 45 mL Teflon lined pressure vessel with 5% hematite by mass. (SQ35A-E) XRD file: Z00051.RAW.

19 Filtered reaction product of hematite and 0.9 mol kg^{-1} $Na_{2.5}H_{0.5}PO_4$ solution at 250°C for three weeks in 45 mL Teflon lined pressure vessel with 10% hematite by mass. (SQ35A-E) XRD file. Z00052.RAW.

20 Filtered reaction product of hematite and 0.9 mol kg^{-1} $Na_{2.5}H_{0.5}PO_4$ solution at 250°C for three weeks in 45 mL Teflon lined pressure vessel with 10% hematite by mass. (SQ35A-E) XRD file Z00053.RAW

Results of X-Ray Diffractometry

1 Sample #1, Iron phosphate sample.
The search-match program identified the solid as the mineral phosphosiderite, with the formula $FePO_4 \cdot 2H_20$. The match is not perfect, since a few peaks are slightly off, but the results are satisfactory. This may be due to poor sample preparation, or the unknown number of waters of hydration.

2. Sample # 2 Unreacted hematite
The search-match program correctly identified this sample as hematite. The pattern fits perfectly. There was no trace of magnetite in the sample.

3. Sample #3 Unreacted hematite, second supply
This pattern was identified as hematite, but the peaks are all at slightly lower values of 2θ than expected. This is almost certainly due to poor sample preparation. If the sample is too thick, the entire powder pattern is often shifted. Once again, there was no trace of magnetite.

4. Sample #4 Unreacted magnetite
This powder pattern had slightly lower values of 2θ than the JCPDS file. This may be due to sample preparation, as in #3. However, the match is satisfactory.

5. Sample #5 Iron phosphate reaction product
The powder pattern for this sample did not match any minerals or other inorganic compound in the JCPDS file, but was a match to previously reported patterns for the

SIHP. There was no trace of hematite, magnetite, maghemite, or maricite in the sample.

6. Sample #6 Hematite reaction product

Again, there was no match found by the search-match program, but the pattern did match SIHP, and the above sample. There was a trace of hematite as shown by the peaks at 2θ = 33.1° and 35.5°. Neither magnetite nor maghemite were detected in the sample. The largest hematite peak overlaps a strong SIHP peak, but there are enough large peaks in the hematite powder pattern that it is not difficult to identify traces of hematite in the sample.

7. Sample #7 Magnetite reaction product

This product matches the previous two powder patterns well, and as such, was identified as SIHP. There was no trace of magnetite, hematite, or maghemite in the sample. The problem with detecting magnetite in the SIHP, is the overlap of a strong SIHP peak with the largest magnetite peak at 2θ = 35.5°. The second and third largest peaks are then used to check for magnetite.

8. Sample #8 Hematite reaction product from 450 mL reaction vessel

This sample matches the previous SIHP powder patterns, but has a large contribution from hematite, since such a large excess was used in the reaction vessel. The pattern confirms the presence of SIHP in the reaction vessel.

9. Sample #9 FeNTA starting material

This pattern was typical of organic solids. There were many sharp peaks, but the search-match program could not identify the pattern.

10. Sample #10 FeNTA reaction product

This powder pattern was identified as maricite. The differences in the patterns were within experimental error except for one peak at a 2θ value of 26.5°. This peak was thought to be from $Na_4P_2O_7$, as determined by the software.

11. Sample #11 FeNTA, CuO reaction product

This pattern could not be found in the JCPDS file, but seemed to be a mixture of Cu_2O with traces of CuO, Cu, and maricite

12. Sample #12 FeNTA, $NaNO_3$ reaction product

This sample was difficult to identify, but it appeared to be a mixture of maricite, magnetite and hematite.

13. Sample #13 Fe powder reaction product

The search-match program identified this sample as maricite. This pattern was not of high quality, since it had a large hump in the baseline, and the count was low, but the match to maricite was good nonetheless. When the sample was run again, a similar pattern was obtained.

14 Samples #14-20 Hematite reaction product

These samples were identified as the SIHP in the first sample, but in subsequent samples more hematite · ·ed. The strongest hematite peak at $2\theta = 35.4°$ increases substantially with small amounts added. These runs were used to determine the amount of hematite in the reaction product. The range of 2θ used for these samples was reduced to the region containing the strong hematite and SIHP ($2\theta = 33.3°$) peaks - 32.0-36.5°.

Table 7.1 XRD powder patterns of selected samples of SHP and previous work

Calculated Ziemniak and Opalka (1992)		Ziemniak and Opalka (1992)		This work, synthesized from $FePO_4$		This work, synthesized from Fe_2O_3		This work, synthesized from Fe_3O_4	
hkl	d_{calc}	d_{obs}	I/I_{100}	d_{obs}	I/I_{100}	d_{obs}	I/I_{100}	d_{obs}	I/I_{100}
100	7.728	7.71	15	7.769	78	7.777	32	7.779	58
010	7.348	7.31	35	7.367	73	7.367	57	7.361	53
110	5.325	5.31	25	5.343	32	5.344	49	5.342	47
020	3.654			3.637	7	3.637	26		
210	3.421	3.42	5	3.432	15	3.433	22	3.431	18
120	3.305	3.31	15	3.323	19	3.321	21	3.321	16
012	3.200	3.20	5			3.204	11		
220	2.660	2.663	100	2.668	100	2.668	100	2.668	100
202	2.621	2.618	30	2.624	6	2.623	21	2.626	7
022	2.552	2.552	20	2.557	8	2.557	24	2.557	7
030	2.436	2.443	5	2.450	13	2.450	11	2.448	6
222	2.129	2.112	10	2.116	5	2.134	8	2.114	5
320	2.108			2.116	5	2.115	9	2.072	7
230	2.062	2.075	5	2.081	8	2.071	10		
231	1.980			1.940	60				
400	1.935	1.938	20	1.935	34	1.940	15	1.940	26
123	1.928								
410	1.871	1.872	5	1.876	4	1.875	7	1.876	4
040	1.830	1.835	40	1.837	38	1.837	18	1.836	12
411	1.809			1.832	23	1.837	18		

Calculated Ziemniak and Opalka (1992)		Ziemniak and Opalka (1992)		This work, synthesized from $FePO_4$		This work, synthesized from Fe_2O_3		This work, synthesized from Fe_3O_4	
hkl	d_{calc}	d_{obs}	I/I_{100}	d_{obs}	I/I_{100}	d_{obs}	I/I_{100}	d_{obs}	I/I_{100}
232	1.784	1.788	5						
004	1.779	1.778	10	1.779	4	1.780	10	1.777	5
313	1.699	1.696	5			1.691	6		
024	1.600	1.599	5			1.597	7		
422	1.543	1.545	10	1.546	5	1.545	13	1.546	4
242	1.499	1.505	35	1.505	4	1.504	9	1.505	4
224	1.479					1.481	6		
251	1.343			1.334	5	1.333	6	1.334	5
404	1.310								
350	1.272								

Table 7.2 XRD powder patterns for selected maricite samples and previous work

Tremaine et al (1992)		This work, synthesized from FeNTA		This work, synthesized from Fe powder	
d_{obs}	I/I_{100}	d_{obs}	I/I_{100}	d_{obs}	I/I_{100}
4.50	5	4.514	45	4.512	49
4.40	20	4.417	31	4.409	53
3.757	10	3.768	13	3.775	54
3.705	40	3.714	18	3.721	63
2.729	90	2.730	28	2.728	84
2.707	80	2.710	36	2.713	85
2.574	100	2.582	100	2.579	100
2.525	30	2.527	17	2.522	43
2.431	15	2.432	23	2.431	30
2.401	10			2.401	28
2.244	1	2.203	8	2.254	22
2.096	10	2.098	10	2.096	30
2.062	2	2.062	6	2.027	49
1.881	30	1.883	15	1.880	41
1.853	60	1.854	21	1.852	35
1.714	15	1.717	13	1.717	23
1.696	1	1.697	10	1.690	22
1.678	2			1.681	21
1.654	5	1.654	7	1.653	21
1.519	10			1.520	28
1.508	15			1.509	27

8.0 APPENDIX II: X-RAY CRYSTAL STRUCTURE OF SODIUM IRON (III) HYDROXY PHOSPHATE (SIHP) AND MARICITE

Single Crystal X-Ray Diffraction Structure Report for SIHP

J. Bridson and D. Miller

Dept. Of Chemistry

Memorial University of Newfoundland

November 9, 1995

TABLE OF CONTENTS

1. Introduction

2. Description of Experimental Procedures

    1. Data Collection

    2. Data Reduction

    3. Structure Solution and Refinement

3. References

4. Tables

    1. Experimental Details

        1. Crystal Data
        2. Intensity Measurements
        3. Structure Solution and Refinement

5. Figures - PLUTO[1] and ORTEP[2] representations

An excellent data set was collected on a reasonable crystal with no apparent flaws. The cell geometry was established with ease and Laue symmetry checks confirmed an orthorhombic spacegroup. At this stage there was no evidence for a long-range order/superlattice phenomenon although when powder data was made available later this became a possibility.

Absences and statistical analysis suggested the spacegroup should be Ibam but initial attempts to extract a solution in this spacegroup proved fruitless. An overall idea of the structure was developed in P-1 and with this in hand a systematic attack on the problem in I222 gave an essentially complete solution which was transferred to the correct spacegroup (Ibam) for finishing.

The main structural feature is a chain of alternating irons and oxygens with additional linking of the irons by two phosphates. The bridging oxygen has an associated proton in some instances and a sodium ion in others. Refinement of the sodium occupancy suggests a ratio of Na:H = 55:45 - the tempting 50:50 ratio fitted the data less well. Attempting to find less than one hydrogen atom in a difference map is not likely to be successful. However a peak at the correct position was found and its designation as hydrogen did improve the refinement. Furthermore, the hydrogen remained in a sensible position when allowed to refine positionally. While doubt may be cast upon the crystallographic reliability of this, in chemical terms the hydrogen is both required to be present and expected at the assigned location.

Five other sites in the lattice are occupied by sodium ions, none having simple coordination geometry. In one of these sites a very much flattened tetrahedral array of oxygens holds a sodium which is disordered over two sites - each having an almost linear O-Na-O arrangement. The two sodium images are close to the 222 symmetry special position and are on one axis. Placing the sodium at the 222 position significantly worsened the least-squares fit.

As the disordered sites are close there is clearly a possiblity that they are not strictly disordered at all but that some correlation exists between the two. This probably accounts for the superlattice found in the powder work.

EXPERIMENTAL

DATA COLLECTION

A red irregular crystal of $Na_{4.55}HH_{0.45}O_9P_2Fe$ having approximate dimensions of 0.100 X 0.050 X 0.400 mm was mounted on a glass fiber. All measurements were made on a Rigaku AFC6S diffractometer with graphite monochromated Mo Kα radiation and a 2KW sealed tube generator.

Cell constants and an orientation matrix for data collection, obtained from a least-squares refinement using the setting angles of 19 carefully centered reflections in the range $44.29 < 2\theta < 49.21°$ corresponded to an orthorhombic cell with dimensions:

$a = 14.698\ (3)Å$
$b = 15.522\ (4)Å$
$c = 7.114\ (4)Å$
$V = 1623\ (1)Å^3$

For $Z = 8$ and F.W. = 366.85, the calculated density is 3.002 g/cm^3. Based on the systematic absences of:

hkl: $h+k+l \neq 2n$
0kl: $k \neq 2n$
h0l: $h \neq 2n$

packing considerations, a statistical analysis of intensity distribution, and the successful solution and refinement of the structure, the space group was determined to be:

Ibam (#72)

The data were collected at a temperature of 26 ± 1°C using the ω-2θ scan technique to a maximum 2θ value of 50.1°. Omega scans of several intense reflections, made prior to data collection, had an average width at half-height of 0.33° with a take-off angle of 6.0°. Scans of (1.31 + 0.35 tan θ)° were made at a speed of 4.0°/min (in omega). The weak reflections ($I < 10.0\sigma(I)$) were rescanned (maximum of 2 rescans) and the counts were accumulated to assure good counting statistics. Stationary background counts were recorded on each side of the reflection. The ratio of peak counting time to background counting time was 2:1. The diameter of the incident beam collimator was 1.0 mm and the crystal to detector distance was 400.0 mm.

DATA REDUCTION

A total of 848 reflections was collected. The intensities of three representative reflections which were measured after every 150 reflections remained constant throughout data collection indicating crystal and electronic stability (no decay correction was applied).

The linear absorption coefficient for Mo Kα is 25.1 cm^{-1}. An empirical absorption correction, based on azimuthal scans of several reflections, was applied which resulted in transmission factors ranging from 0.87 to 1.00. The data were corrected for Lorentz and polarization effects. A correction for secondary extinction was applied (coefficient = 0.30529E-06).

STRUCTURE SOLUTION AND REFINEMENT

The structure was solved by direct methods[3]. The non-hydrogen atoms were refined anisotropically. The final cycle of full-matrix least-squares refinement[4] was based on 593 observed reflections ($I > 2.00\sigma(I)$) and 97 variable parameters and converged (largest parameter shift was 0.00 times its esd) with unweighted and weighted agreement factors of:

$$R = \Sigma \, ||Fo| - |Fc|| \, / \, \Sigma \, |Fo| = 0.034$$

$$R_w = [(\Sigma \, w \, (|Fo| - |Fc|)^2 \, / \, \Sigma \, w \, Fo^2)]^{1/2} = 0.036$$

The standard deviation of an observation of unit weight[5] was 2.48. The weighting scheme was based on counting statistics and included a factor ($p = 0.01$) to downweight the intense reflections. Plots of $\Sigma \, w \, (|Fo| - |Fc|)^2$ versus $|Fo|$, reflection order in data collection, $\sin \theta/\lambda$, and various classes of indices showed no unusual trends. The maximum and minimum peaks on the final difference Fourier map corresponded to 0.45 and -0.74 $e^-/Å^3$, respectively.

Neutral atom scattering factors were taken from Cromer and Waber[6]. Anomalous dispersion effects were included in Fcalc[7]; the values for $\Delta f'$ and $\Delta f''$ were those of Cromer[8]. All calculations were performed using the TEXSAN[9] crystallographic software.

References

(1) PLUTO:
Motherwell,S. & Clegg,W.; PLUTO. Program for plotting molecular and crystal structures. Univ. of Cambridge, England (1978).

(2) Structure Solution Methods:
MITHRIL
Gilmore,C.J.; MITHRIL - an integrated direct methods computer program. J. Appl. Cryst. 17, 42-46, Univ. of Glasgow, Scotland, (1984).
DIRDIF
Beurskens,P.T.; DIRDIF: Direct Methods for Difference Structures - an automatic procedure for phase extension and refinement of difference structure factors. Technical Report 1984/1 Crystallography Laboratory, Toernooiveld, 6525 Ed Nijmegen, Netherlands.

(3) Least-Squares:
Function minimized: $\Sigma\, w\,(|Fo| - |Fc|)^2$
where: $w = 4Fo^2/\sigma^2(Fo^2)$
$\sigma^2(Fo^2) = [S^2(C+R^2B) + (pFo^2)^2]/Lp^2$
S = Scan rate
C = Total Integrated Peak Count
R = Ratio of Scan Time to background counting time.
B = Total Background Count
Lp = Lorentz-polarization factor
p = p-factor

(4) Standard deviation of an observation of unit weight:

$$[\Sigma\, w(|Fo| - |Fc|)^2/(No - Nv)]^{1/2}$$

where: No = number of observations
Nv = number of variables

(5) Cromer,D.T. & Waber,J.T.; "International Tables for X-ray Crystallography", Vol. IV, The Kynoch Press, Birmingham, England, Table 2.2 A (1974).

(6) Ibers,J.A. & Hamilton,W.C.; Acta Crystallogr., 17, 781 (1964).

(7) D.T. Cromer, "International Tables for X-ray Crystallography", Vol/ IV, The Kynoch Press. Birmingham, England. Table 2.3.1 (1974).

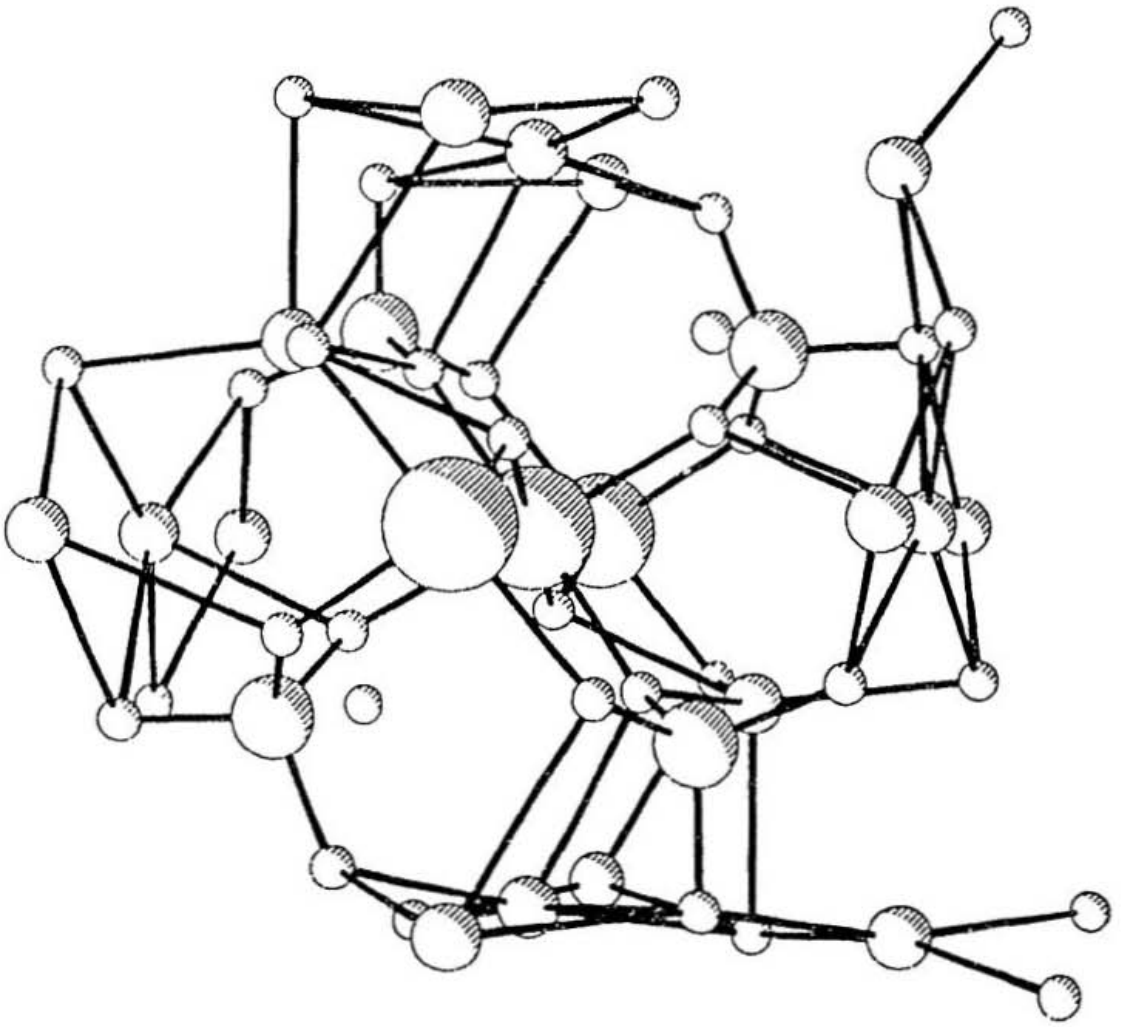
EXPERIMENTAL DETAILS

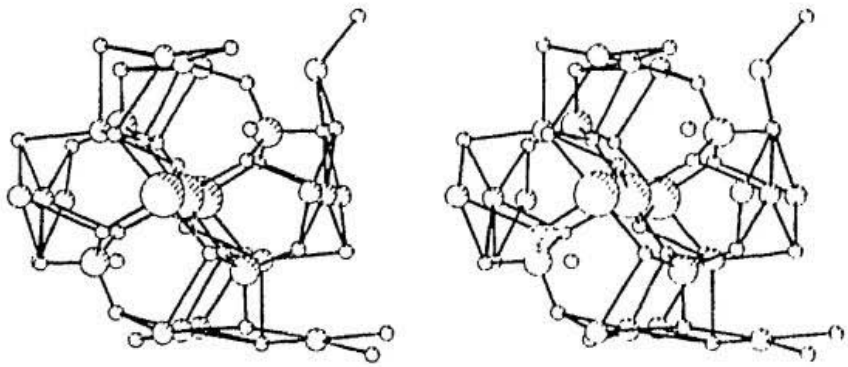
Empirical Formula	$Na_{4.55}HHO_{9.45}O_9P_2Fe$
Formula Weight	366.85
Crystal Color	red, irregular
Crystal Dimensions (mm)	0.100 x 0.050 x 0.400
Crystal System	Orthorhombic
No. Reflections Used for Unit Cell Determination (2θ range)	19 (44.3-49.2°)
Omega Scan Peak Width at half height	0.33
Lattice Parameters a=14.698Å V=1623Å	b=15.522Å c=7.114Å
Space Group	Ibam (#72)
z value	8
D_{calc}	3.002 g cm^{-3}
F_{000}	1428
μ(MoKα)	25.11 cm^{-1}
Diffractometer	Rigaku AFC6S
Radiation	MoKα (λ=0.71069 Å)
Temperature	26°C
Take off Angle	6.0°C
Detector Aperture	4.5 mm horizontal 3.0 mm vertical
Crystal to Detector Distance	40 cm

Scan Type	ω-2θ
Scan Rate	4.0°/min (in omega) (2 rescans)
Scan Width	(1.31 + 0.35 tanθ)°
$2\theta_{max}$	50.1°
No. of Reflections Measured	Total: 848
Corrections	Lorentz-polarization Absorption (trans. factors: 0.87 - 1.00) Secondary Extinction (coefficient: 0.30529E-06)

C. Structure Solution and Refinement

Structure Solution	Direct Methods
Refinement	Full-matrix least-squares
Function Minimized	Σ w (|Fo| - |Fc|)^2
Least-squares Weights	$4Fo^2/\sigma^2(Fo^2)$
p-factor	0.01
Anomalous Dispersion	All non-hydrogen atoms
No. Observations (I>2.00σ(I)) No. Variables Reflection/Parameter Ratio	593 97 6.11
Residuals: R; R_w	0.034; 0.036
Goodness of Fit Indicator	2.48
Max Shift/Error in Final Cycle	0.00
Maximum Peak in Final Diff. Map Minimum Peak in Final Diff. Map	0.45 $e^-/Å^3$ -0.74 $e^-/Å^3$





Single-Crystal X-Ray Diffraction Structure Report for Maricite

J. Bridson and D. Miller
Dept. of Chemistry
Memorial University of Newfoundland

January 29, 1996

TABLE OF CONTENTS

1. Introduction

2. Description of Experimental Procedures

    1. Data Collection

    2. Data Reduction

    3. Structure Solution and Refinement

3. References

4. Tables

    1. Experimental Details

        1. Crystal Data
        2. Intensity Measurements
        3. Structure Solution and Refinement

5. Figures - PLUTO[1] and ORTEP[2] representations

INTRODUCTION

The simple $NaFePO_4$ structure was solved rapidly and with excellent refinement results. Chains of Fe atoms are linked by a bidentate phosphate and the single O's of two other PO_4 groups. The remaining oxygens of the phosphates are involved in other Fe chains thus producing a 3-D lattice. Parallel to the Fe chains are Na - O - Na - O .... chains in which Na ions lie directly between the monodentate O's.

EXPERIMENTAL

DATA COLLECTION

A colorless plate crystal of $NaFePO_4$ having approximate dimensions of 0.400 X 0.300 X 0.100 mm was mounted on a glass fiber. All measurements were made on a Rigaku AFC6S diffractometer with graphite monochromated Mo Kα radiation and a 2KW sealed tube generator.

Cell constants and an orientation matrix for data collection, obtained from a least-squares refinement using the setting angles of 14 carefully centered reflections in the range $47.54 < 2\theta < 49.50°$ corresponded to an orthorhombic cell with dimensions:

$a = 8.990\ (3)\text{Å}$
$b = 6.862\ (4)\text{Å}$
$c = 5.047\ (3)\text{Å}$
$V = 311.3\ (5)\text{Å}^3$

For $Z = 4$ and F.W. = 173.81, the calculated density is 3.708 g/cm^3. Based on the systematic absences of:

$0kl: k+l \neq 2n$
$hk0: h \neq 2n$

packing considerations, a statistical analysis of intensity distribution, and the successful solution and refinement of the structure, the space group was determined to be:

Pnma (#62)

The data were collected at a temperature of 26 ± 1°C using the ω-2θ scan technique to a maximum 2θ value of 50.0°. Omega scans of several intense reflections, made prior to data collection, had an average width at half-height of 0.39° with a take-off angle of 6.0°. Scans of $(1.84 + 0.35 \tan\theta)°$ were made at a speed of 4.0°/min (in omega). The weak reflections ($I < 10.0\sigma(I)$) were rescanned (maximum of 4 rescans) and the counts were accumulated to assure good counting statistics. Stationary background counts were recorded on each side of the reflection. The ratio of peak counting time to background counting time was 2:1. The diameter of the incident beam collimator was 1.0 mm and the crystal to detector distance was 400.0 mm.

DATA REDUCTION

A total of 358 reflections was collected. The intensities of three representative reflections which were measured after every 150 reflections remained constant throughout data collection indicating crystal and electronic stability (no decay correction was applied).

The linear absorption coefficient for Mo Kα is 53.2 cm^{-1}. An empirical absorption correction, based on azimuthal scans of several reflections, was applied which resulted in transmission factors ranging from 0.53 to 1.00. The data were corrected for Lorentz and polarization effects. A correction for secondary extinction was applied (coefficient = 0.30964E-05).

STRUCTURE SOLUTION AND REFINEMENT

The structure was solved by direct methods[3]. The non-hydrogen atoms were refined anisotropically. The final cycle of full-matrix least-squares refinement[4] was based on 272 observed reflections ($I > 2.00\sigma(I)$) and 41 variable parameters and converged (largest parameter shift was 0.00 times its esd) with unweighted and weighted agreement factors of:

$$R = \Sigma \, ||Fo| - |Fc|| \, / \, \Sigma \, |Fo| = 0.026$$

$$R_w = [(\Sigma \, w \, (|Fo| - |Fc|)^2 \, / \, \Sigma \, w \, Fo^2)]^{1/2} = 0.031$$

The standard deviation of an observation of unit weight[5] was 2.69. The weighting scheme was based on counting statistics and included a factor ($p = 0.01$) to downweight the intense reflections. Plots of $\Sigma \, w \, (|Fo| - |Fc|)^2$ versus $|Fo|$, reflection order in data collection, $\sin\theta/\lambda$, and various classes of indices showed no unusual trends. The maximum and minimum peaks on the final difference Fourier map corresponded to 0.61 and -0.51 $e^-/Å^3$, respectively.

Neutral atom scattering factors were taken from Cromer and Waber[6]. Anomalous dispersion effects were included in Fcalc[7]; the values for $\Delta f'$ and $\Delta f''$ were those of Cromer[8]. All calculations were performed using the TEXSAN[9] crystallographic software package of Molecular Structure Corporation.

References

(1) PLUTO:
Motherwell,S. & Clegg,W.; PLUTO. Program for plotting molecular and crystal structures. Univ. of Cambridge, England (1978).

(2) ORTEP:
Johnson,C.K.; ORTEPII. Report ORNL-5138. Oak Ridge National Laboratory, Oak Ridge, Tennessee (1976).

(3) Structure Solution Methods:
MITHRIL
Gilmore,C.J.; MITHRIL - an integrated direct methods computer program. J. Appl. Cryst. 17, 42-46, Univ. of Glasgow, Scotland, (1984).
DIRDIF
Beurskens,P.T.; DIRDIF: Direct Methods for Difference Structures - an automatic procedure for phase extension and refinement of difference structure factors. Technical Report 1984/1 Crystallography Laboratory, Toernooiveld, 6525 Ed Nijmegen, Netherlands.

(4) Least-Squares:
Function minimized: $\Sigma\, w\, (|Fo| - |Fc|)^2$
where: $w = 4Fo^2/\sigma^2(Fo^2)$
$\sigma^2(Fo^2) = [S^2(C+R^2B) + (pFo^2)^2]/Lp^2$
S = Scan rate
C = Total Integrated Peak Count
R = Ratio of Scan Time to background counting time.
B = Total Background Count
Lp = Lorentz-polarization factor
p = p-factor

(5) Standard deviation of an observation of unit weight:

$$[\Sigma\, w(|Fo| - |Fc|)^2/(No - Nv)]^{1/2}$$

where: No = number of observations
Nv = number of variables

(6) Cromer,D.T. & Waber,J.T.; "International Tables for X-ray Crystallography", Vol. IV, The Kynoch Press, Birmingham, England, Table 2.2 A (1974).

(7) Ibers,J.A. & Hamilton,W.C.; Acta Crystallogr., 17, 781 (1964).

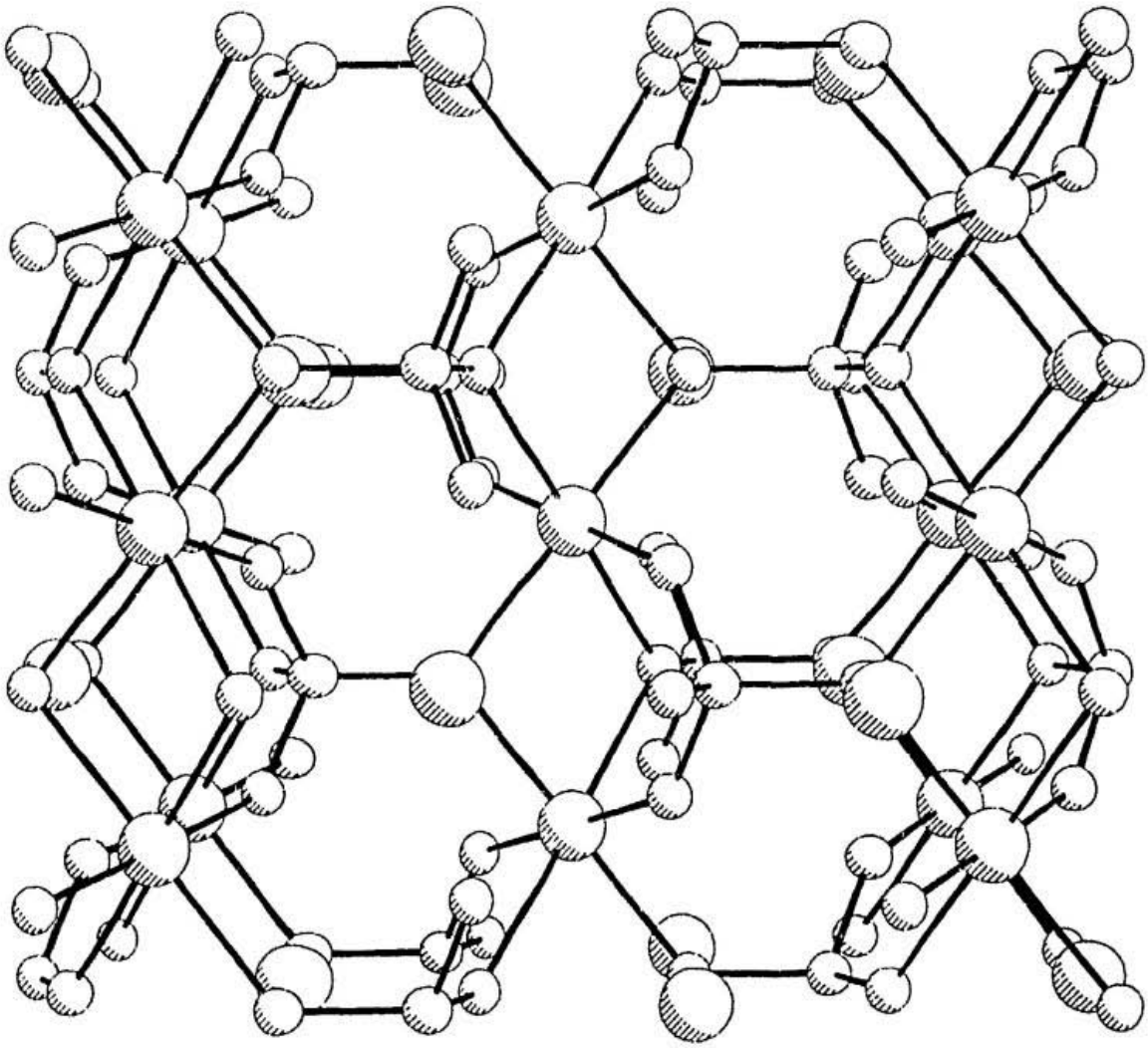
EXPERIMENTAL DETAILS

Empirical Formula	$NaFePO_4$
Formula Weight	173.81
Crystal Color	colorless, plate
Crystal Dimensions (mm)	0.400 x 0.300 x 0.100
Crystal System	Orthorhombic
No. Reflections Used for Unit Cell Determination (2θ range)	14 (47.5-49.5°)
Omega Scan Peak Width at half height	0.39
Lattice Parameters a=8.990 Å V=311.3 Å	b=6.862 Å c=5.047Å
Space Group	Pnma (#62)
z value	4
D_{calc}	3.708 g cm^{-3}
F_{000}	336
μ(MoKα)	53.17 cm^{-1}
Diffractometer	Rigaku AFC6S
Radiation	MoKα (λ=0.71069 Å)
Temperature	26°C
Take off Angle	6.0°C
Detector Aperture	4.3 mm horizontal 3.0 mm vertical
Crystal to Detector Distance	40 cm

Scan Type	ω-2θ
Scan Rate	4.0°/min (in omega) (4 rescans)
Scan Width	(1.84 + 0.35 tanθ)°
$2\theta_{max}$	50.0°
No. of Reflections Measured	Total: 358
Corrections	Lorentz-polarization Absorption (trans. factors: 0.53 - 1.00) Secondary Extinction (coefficient: 0.30964E-05)

C. Structure Solution and Refinement

Structure Solution	Direct Methods
Refinement	Full-matrix least-squares
Function Minimized	Σ w (|Fo| - |Fc|)^2
Least-squares Weights	$4Fo^2/\sigma^2(Fo^2)$
p-factor	0.01
Anomalous Dispersion	All non-hydrogen atoms
No. Observations (I>2.00σ(I))	272
No. Variables	41
Reflection/Parameter Ratio	6.63
Residuals: R; R_w	0.026; 0.031
Goodness of Fit Indicator	2.69
Max Shift/Error in Final Cycle	0.00
Maximum Peak in Final Diff. Map	0.61 $e^-/Å^3$
Minimum Peak in Final Diff. Map	-0.51 $e^-/Å^3$



9.0 APPENDIX III: KINETIC AND SOLUBILITY DATA FOR SODIUM IRON HYDROXY PHOSPHATE FORMATION EQUILIBRIA WITH HEMATITE

TABLE A III 1 Summary of ICP ES Results for Standard Solutions

run name	stock sol'n	$m(HPO_4^{2-})_{tot}$ mol kg^{-1}	% dev	$m(Na^+)_{tot}$ mol kg^{-1}	% dev
run 1	SQ64A	0.4867	0.34	1.201	1.61
	-	0 4759	2.56	1.189	2.56
	-	0.4783	2.07	1 129	7.50
run 2	SQ64A	0.4745	2.85	1.231	0.81
	-	0.4732	3.13	1.220	0.09
	-	0 4719	3.38	1.216	0.40
	SQ72A	0 6157	1.55	1.369	1.82
	-	0 6178	1.23	1.373	2.13
	-	0 6287	0.52	1.384	2.92
	SQ71A	1 1094	0.08	2 833	2 23
	-	1 1203	1.07	2 764	0.25
	-	1 1230	1.31	2.714	2.06
run 3	SQ71A	1 0959	1.13	2.969	7.12
	-	1 1018	0 60	2.972	7.21
kinetic 2	SQ37A	1 0696	0.94	1 058	0 11
	-	1.0633	0 34	1.045	1.36
	-	1.0611	0.13	1 048	1.11
	SQ86A	0.5582	0 32	1.434	2.13
	-	0.5613	0.25	1.455	3 62
	-	0 5660	1.09	1 480	5.42
kinetic 3	SQ72A	0.6354	1.59	1.380	2.60
	-	0.6394	2 22	1.397	3.88
	-	0 6418	2.62	1.388	3.21
kinetic 4	SQ97C	0.5316	0.23	1.335	0.55
	-	0.5282	0.42	1 352	1.80
	-	0 5306	0.03	1.353	1.89
kinetic 5	SQ97C	0.5183	2.29	1.331	0.22
	-	0.5158	2.75	1.327	0.07
	-	0 5151	2.88	1.324	0 33
nap 3	N/A	-	-	-	-
nap 3 run 2	SQ54A				
	-				
	-				

TABLE A.III.2 Kinetic Data

Time hr	$m(Na^+)$ mol kg^{-1}	$m(HPO_4^{2-})_{exp}$ mol kg^{-1}	$m(HPO_4^{2-})_{calc}$ mol kg^{-1}
	Precipitation at 250°C		
1.9	0.725	0.242	0.244
1.9	0.737	0.253	0.244
2.3	0.725	0.254	0.230
2.3	0.654	0.222	0.230
5.8	0.511	0.167	0.177
5.8	0.499	0.162	0.177
5.8	0.450	0.150	0.177
5.8	0.485	0.160	0.177
11.7	0.492	0.164	0.148
11.7	0.445	0.146	0.148
12.5	0.465	0.152	0.146
12.5	0.454	0.150	0.146
24.1	0.476	0.156	0.127
24.1	0.456	0.148	0.127
95.5	0.302	0.0947	0.102
95.5	0.332	0.105	0.102
117.4	0.306	0.0943	0.0993
117.4	0.317	0.0990	0.0993
170.3	0.292	0.0861	0.0955
170.3	0.297	0.0891	0.0955

TABLE A III 2 (Continued)

Time hr	$m(Na^+)$ mol kg^{-1}	$m(HPO_4^{2-})_{exp}$ mol kg^{-1}	$m(HPO_4^{2-})_{calc}$ mol kg^{-1}
		Precipitation at 225°C	
3 2	1 048	0.391	0.437
3 2	1 029	0.382	0 437
4 0	1.321	0.522	0 423
4 0	1 298	0.518	0.423
6 0	0 854	0 308	0.398
6 0	0.856	0 311	0.398
23 0	0 920	0.328	0.327
23 0	0 967	0 345	0 327
24 0	0 793	0.292	0.326
24 0	0.959	0.352	0.326
47 0	0 918	0.339	0 301
47 0	1 007	0.364	0 301
95 0	0 863	0.316	0.281
95 0	0.885	0.322	0.281
119 3	0 815	0.299	0.276
119.3	0.889	0.322	0.276
142 8	0.802	0.294	0.272
142 8	0.865	0 314	0.272
143 7	0 808	0.278	0.272
143 7	0.792	0.274	0.272
166 8	0 819	0.299	0.269
166 8	0.760	0.278	0.269

TABLE A.III.2 (Continued)

Time	$m(Na^+)$	$m(HPO_4^{2-})_{exp}$	$m(HPO_4^{2-})_{calc}$
hr	mol kg^{-1}	mol kg^{-1}	mol kg^{-1}
		Precipitation at 225°C	
167.3	0.769	0.262	0.269
167.3	0.782	0.268	0.269
190.8	0.788	0.286	0.267
190.8	0.704	0.255	0.267
192.0	0.718	0.244	0.267
192.0	0.753	0.256	0.267
219.0	0.799	0.290	0.265
219.0	0.798	0.288	0.265
240.0	0.647	0.218	0.263
240.0	0.697	0.234	0.263
262.3	0.725	0.242	0.262
288.8	0.674	0.220	0.261
288.8	0.697	0.227	0.261
309.8	0.685	0.223	0.260
309.8	0.728	0.237	0.260
		Redissolution at 225°C	
2.6	0.403	0.127	0.119
6.8	0.429	0.139	0.137
9.4	0.482	0.155	0.146
23.7	0.509	0.166	0.179
45.1	0.565	0.188	0.204

TABLE A.III 2 (Continued)

Time	$m(Na^+)$	$m(HPO_4^{2-})_{exp}$	$m(HPO_4^{2-})_{calc}$
hr	mol kg^{-1}	mol kg^{-1}	mol kg^{-1}
	Redissolution at 225°C		
1.9	0.475	0.143	0.115
6.9	0.521	0.163	0.138
28.9	0.595	0.194	0.187
53.2	0.589	0.191	0.210
76.3	0.634	0.211	0.221
164.0	0.713	0.237	0.239
192.0	0.778	0.253	0.242
192.0	0.770	0.257	0.242

TABLE A.III.3 Experimental Data for the Reaction

$$3Fe_2O_3(s) + 26Na^+ + 12HPO_4^{2-}(aq) + 2OH^-(aq) \rightleftharpoons 6Na_3Fe(PO_4)_2\cdot(Na_{4/3}H_{2/3}O)(s) + 5H_2O(l)$$

	Experimental Results			Results from Kinetic Correction			
T	$m(HPO_4^{2-})$	$m(Na^+)$	t	$m(HPO_4^{2-})$	$m(Na^+)$	$m(OH^-)$	ln Q
°C	mol kg^{-1}	mol kg^{-1}	hr	mol kg^{-1}	mol kg^{-1}	mol kg^{-1}	
			Na/P=2.5, run I				
220.0	0.412	1.017	24	0.299	0.773	0.175	4.106
220.0	0.410	1.025	24	0.297	0.781	0.186	4.056
220.0	0.413	1.017	24	0.301	0.772	0.171	4.108
220.0	0.422	1.025	24	0.311	0.810	0.188	3.802
220.0	0.420	1.016	24	0.309	0.797	0.180	3.902
220.0	0.421	1.051	24	0.310	0.808	0.189	3.822
240.0	0.279	1 039	24	0.214	0.588	0.160	5.990
240.0	0 280	1.049	24	0.216	0.586	0.153	6.008
240.0	0.254	0.727	24	0.189	0.549	0.172	6.520
240.0	0.255	0.724	24	0.190	0.553	0 174	6.463
250.0	0.163	0.690	24	0 114	0 357	0.128	9.490

TABLE A.III.3 (Continued)

	Experimental Results			Results from Kinetic Correction			
T	$m(HPO_4^{2-})$	$m(Na^+)$	t	$m(HPO_4^{2-})$	$m(Na^+)$	$m(OH^-)$	ln Q
°C	mol kg^{-1}	mol kg^{-1}	hr	mol kg^{-1}	mol kg^{-1}	mol kg^{-1}	
			Na/P=2.5, run 1				
250.0	0.190	0.694	24	0.142	0.440	0.155	8.083
250.0	0.189	0.542	24	0 142	0.439	0.156	8.097
250.0	0.188	0.541	24	0.141	0.438	0.157	8.113
260.0	0.118	0.353	48	0.0929	0.298	0.112	10.723
260.0	0.119	0.357	48	0.0942	0.302	0.114	10.633
260.0	0.120	0.359	48	0.0947	0.304	0.115	10.591
260.0	0.141	0.420	48	0.118	0.369	0.134	9.260
260.0	0.140	0.412	48	0.116	0.361	0.128	9.399
260.0	0.141	0.413	48	0.118	0.362	0.127	9.367
267.0	0.0972	0.294	18	0.0675	0.230	0.0946	12.552
267.0	0.0972	0.300	18	0.0675	0.236	0.101	12.408
267.0	0.0973	0.300	18	0.0677	0.236	0.101	12.410

TABLE A.III.3 (Continued)

	Experimental Results			Results from Kinetic Correction			
T	$m(HPO_4^{2-})$	$m(Na^+)$	t	$m(HPO_4^{2-})$	$m(Na^+)$	$m(OH^-)$	ln Q
°C	mol kg^{-1}	mol kg^{-1}	hr	mol kg^{-1}	mol kg^{-1}	mol kg^{-1}	
			Na/P=2.5, run 1				
267.0	0.0970	0.303	18	0.0673	0.238	0.104	12.367
270.0	0.0862	0.267	18	0.0618	0.214	0.0900	13.058
270.0	0.106	0.320	18	0.101	0.311	0.108	10.378
270.0	0.106	0.321	18	0.102	0.311	0.108	10.363
270.0	0.105	0.322	18	0.101	0.314	0.112	10.332
282.0	0.0610	0.188	46	0.0465	0.145	0.0626	15.424
282.0	0.0719	0.215	46	0.0584	0.175	0.0680	14.121
282.0	0.0721	0.214	46	0.0585	0.174	0.0669	14.140
290.0	0.0481	0.148	48	0.0370	0.111	0.0488	17.107
290.0	0.0519	0.159	48	0.0414	0.125	0.0527	16.353
290.0	0.0518	0.162	48	0.0413	0.128	0.0560	16.237
293.0	0.0344	0.114	24	0.0268	0.0831	0.0424	19.074

TABLE A.III.3 (Continued)

	Experimental Results			Results from Kinetic Correction			
T	$m(HPO_4^{2-})$	$m(Na^+)$	t	$m(HPO_4^{2-})$	$m(Na^+)$	$m(OH^-)$	ln Q
°C	mol kg^{-1}	mol kg^{-1}	hr	mol kg^{-1}	mol kg^{-1}	mol kg^{-1}	
			Na/P=2.5, run 1				
293.0	0.0366	0.124	24	0.0291	0.0944	0.0487	18.309
293.0	0.0365	0.124	24	0.0290	0.0946	0.0491	18.303
303.0	0.0203	0.0767	24	0.0150	0.0518	0.0341	22.360
303.0	0.0248	0.101	24	0.0195	0.0776	0.0499	19.947
303.0	0.0251	0.101	24	0.0199	0.0777	0.0493	19.909
313.0	0.0148	0.0644	48	0.0110	0.0511	0.0339	23.044
313.0	0.0180	0.0849	48	0.0147	0.0736	0.0480	20.762
313.0	0.0183	0.0839	48	0.0150	0.0729	0.0466	20.774
325.0	0.0108	0.0530	48	0.00790	0.0429	0.0306	24.493
325.0	0.00926	0.0534	48	0.00691	0.0429	0.0341	24.725
325.0	0.00920	0.0533	48	0.00684	0.0427	0.0341	24.759

TABLE A.III.3 (Continued)

	Experimental Results			Results from Kinetic Correction			
T	$m(HPO_4^{2-})$	$m(Na^+)$	t	$m(HPO_4^{2-})$	$m(Na^+)$	$m(OH^-)$	ln Q
°C	mol kg^{-1}	mol kg^{-1}	hr	mol kg^{-1}	mol kg^{-1}	mol kg^{-1}	
			Na/P=2.5, run 2				
200.0	0.452	1.123	48	0.378	0.962	0.207	2.640
200.0	0.451	1.090	48	0.373	0.921	0.175	2.905
200.0	0.469	1.132	48	0.400	0.982	0.183	2.477
225.0	0.443	1.061	18	0.336	0.829	0.157	3.614
225.0	0.441	1.073	18	0 334	0.840	0.173	3.532
225.0	0.442	1.089	18	0 334	0.856	0 187	3.422
250.0	0.172	0.486	24	0.122	0.378	0.133	9.092
250.0	0.180	0.486	24	0.130	0.378	0.118	9.011
250.0	0.172	0.480	24	0.122	0.372	0.127	9.181
250 0	0.172	0.473	24	0.122	0 365	0.120	9.277
250.0	0.173	0.478	24	0 123	0.370	0.123	9.197
250.0	0 174	0.481	24	0.124	0.372	0.124	9.155
275.0	0 0866	0.203	24	0.0616	0.149	0.0261	15.032

TABLE A.III.3 (Continued)

	Experimental Results			Results from Kinetic Correction			
T	$m(HPO_4^{2-})$	$m(Na^+)$	t	$m(HPO_4^{2-})$	$m(Na^+)$	$m(OH^-)$	ln Q
°C	mol kg^{-1}	mol kg^{-1}	hr	mol kg^{-1}	mol kg^{-1}	mol kg^{-1}	
			Na/P=3.0 run 1				
200.0	0.439	1.381	48	0.356	1.201	0.490	1.511
200.0	0.471	1.497	48	0.364	1.266	0.537	1.204
210.0	0.497	1.571	71	0.416	1.397	0.564	0.496
210.0	0.489	1.547	71	0.407	1.368	0.553	0.637
219.0	0.506	1.618	47	0.433	1.460	0.594	0.207
219.0	0.493	1.563	47	0.416	1.398	0.566	0.489
230.0	0.467	1.484	50	0.414	1.370	0.542	0.600
230.0	0.479	1.550	50	0.430	1.444	0.584	0.272
241.0	0.197	0.847	71	0.159	0.765	0.446	5.103
241.0	0.207	0.900	71	0.169	0.817	0.479	4.670
250.0	0.127	0.618	47	0.0930	0.544	0.358	7.731
250.0	0.143	0.712	47	0.1098	0.640	0.420	6.642
261.0	0.113	0.626	52	0.0882	0.572	0.396	7.582

TABLE A.III.3 (Continued)

	Experimental Results			Results from Kinetic Correction			
T	$m(HPO_4^{2-})$	$m(Na^+)$	t	$m(HPO_4^{2-})$	$m(Na^+)$	$m(OH^-)$	ln Q
°C	mol kg^{-1}	mol kg^{-1}	hr	mol kg^{-1}	mol kg^{-1}	mol kg^{-1}	
			Na/P=3.0 run 1				
261.0	0.119	0.662	52	0.0947	0.609	0.419	7.155
273.0	0.0893	0.593	70	0.0747	0.561	0.412	7.986
273.0	0.0894	0.598	70	0.0748	0.566	0.416	7.945
			Na/P=3.0 run 2				
281.0	0.0684	0.492	96	0.0580	0.469	0.353	9.320
291.0	0.0469	0.433	46	0.0353	0.408	0.337	10.935
291.0	0.0476	0.443	46	0.0360	0.418	0.346	10.780
303.0	0.0307	0.374	48	0.0222	0.356	0.311	12.480
303.0	0.0330	0.412	48	0.0246	0.394	0.344	11.810

TABLE A.III.4 Equilibrium Constant Calculation From the Model System

$$3Fe_2O_3(s) + 26Na^+ + 12HPO_4^{2-}(aq) + 2OH^-(aq) \rightleftharpoons 6Na_3Fe(PO_4)_2\cdot(Na_{4.3}H_{2.3}O)(s) + 5H_2O(l)$$

T °C	ln Q	I mol kg^{-1}	$\gamma_\pm$(NaCl)	$\gamma_\pm(HPO_4^{2-})$	$\gamma_\pm(Na^+)$	$\gamma_\pm(OH^-)$	a(H_2O)	ln K
				Na/P=2.5 run 1				
220.0	4.106	1.073	0.440	0.0374	0.440	0.440	0.968	14.484
220.0	4.057	1.078	0.440	0.0373	0.440	0.440	0.097	14.443
220.0	4.108	1.074	0.440	0.0374	0.440	0.440	0.968	14.488
220.0	3.802	1.122	0.437	0.0365	0.437	0.437	0.966	14.257
220.0	3.902	1.106	0.438	0.0368	0.438	0.438	0.967	14.334
220.0	3.822	1.118	0.437	0.0366	0.437	0.437	0.967	14.270
240.0	5.989	0.803	0.420	0.0310	0.420	0.420	0.977	16.973
240.0	6.001	0.802	0.420	0.0310	0.420	0.420	0.977	16.988
240.0	6.520	0.738	0.426	0.0330	0.426	0.426	0.979	17.308
240.0	6.463	0.744	0.425	0.0327	0.425	0.425	0.978	17.272
250.0	9.490	0.471	0.444	0.0390	0.444	0.444	0.986	19.749
250.0	8.083	0.582	0.426	0.0328	0.426	0.426	0.983	18.890

TABLE A.III.4 (Continued)

T °C	ln Q	I mol kg^{-1}	$\gamma_{\pm}$(NaCl)	$\gamma_{\pm}$(HPO_4^{2-})	$\gamma_{\pm}$(Na^+)	$\gamma_{\pm}$(OH^-)	a(H_2O)	ln K
				Na/P=2.5 run 1				
250.0	8.096	0.581	0.426	0.0329	0.426	0.426	0.983	18.897
250.0	8.113	0.580	0.426	0.0329	0.426	0.426	0.983	18.908
260.0	10.723	0.391	0.442	0.0382	0.442	0.442	0.989	21.050
260.0	10.633	0.396	0.441	0.0378	0.441	0.441	0.989	20.997
260.0	10.591	0.399	0.440	0.0376	0.440	0.440	0.986	20.973
260.0	9.260	0.487	0.421	0.0314	0.421	0.421	0.986	20.204
260.0	9.399	0.478	0.423	0.0320	0.423	0.423	0.986	20.285
260.0	9.367	0.480	0.423	0.0320	0.423	0.423	0.986	20.257
267.0	12.552	0.297	0.456	0.0432	0.456	0.456	0.991	22.492
267.0	12.407	0.304	0.453	0.0423	0.453	0.453	0.991	22.411
267.0	12.410	0.304	0.454	0.0424	0.454	0.454	0.991	22.411
267.0	12.367	0.306	0.453	0.0421	0.453	0.453	0.992	22.390
270.0	13.058	0.275	0.458	0.0440	0.458	0.458	0.988	22.945
270.0	10.378	0.412	0.416	0.0300	0.416	0.416	0.988	21.478

TABLE A.III.4 (Continued)

T °C	ln Q	I mol kg^{-1}	$\gamma_{\pm}$(NaCl)	$\gamma_{\pm}$(HPO_4^{2-})	$\gamma_{\pm}$(Na^+)	$\gamma_{\pm}$(OH^-)	a(H_2O)	ln K
				Na/P=2.5 run 1				
270.0	10.363	0.413	0.416	0.0299	0.416	0.416	0.988	21.470
270.0	10.332	0.415	0.415	0.0298	0.415	0.415	0.988	21.450
282.0	15.424	0.197	0.477	0.0516	0.477	0.477	0.995	25.049
282.0	14.121	0.238	0.453	0.0420	0.453	0.453	0.994	24.317
282.0	14.140	0.238	0.453	0.0421	0.453	0.453	0.994	24.326
290.0	17.107	0.154	0.491	0.0580	0.491	0.491	0.996	26.454
290.0	16.353	0.172	0.476	0.0513	0.476	0.476	0.995	26.021
290.0	16.237	0.175	0.474	0.0504	0.474	0.474	0.995	25.959
293.0	19.074	0.116	0.524	0.0752	0.524	0.524	0.997	27.816
293.0	18.309	0.130	0.508	0.0667	0.508	0.508	0.997	27.360
293.0	18.303	0.130	0.508	0.0667	0.508	0.508	0.998	27.359
303.0	22.360	0.0729	0.596	0.126	0.596	0.596	0.997	29.968
303.0	19.947	0.103	0.517	0.0714	0.517	0.517	0.997	28.992
303.0	19.910	0.103	0.516	0.0710	0.516	0.516	0.997	28.952

TABLE A.III.4 (Continued)

T °C	ln Q	I mol kg^{-1}	$\gamma_{\pm}$(NaCl)	$\gamma_{\pm}$(HPO_4^{2-})	$\gamma_{\pm}$(Na^+)	$\gamma_{\pm}$(OH^-)	a(H_2O)	ln K
				Na/P=3.0 run 1				
200.0	1.512	1.557	0.462	0.0456	0.462	0.462	0.952	11.246
200.0	1.204	1.630	0.461	0.0450	0.461	0.461	0.949	10.977
210.0	0.496	1.813	0.436	0.0362	0.436	0.436	0.944	10.960
210.0	0.637	1.775	0.437	0.0364	0.437	0.437	0.946	11.081
219.0	0.207	1.893	0.415	0.0295	0.415	0.415	0.943	11.309
219.0	0.489	1.814	0.416	0.0300	0.416	0.416	0.945	11.548
230.0	0.660	1.785	0.392	0.0235	0.392	0.392	0.947	12.426
230.0	0.272	1.875	0.390	0.0230	0.390	0.390	0.944	12.164
241.0	5.103	0.924	0.407	0.0274	0.407	0.407	0.973	16.467
241.0	4.670	0.987	0.402	0.0262	0.402	0.402	0.971	16.178
250.0	7.731	0.636	0.418	0.0305	0.418	0.418	0.982	18.770
250.0	6.642	0.750	0.404	0.0267	0.404	0.404	0.979	18.098
261.0	7.582	0.661	0.391	0.0235	0.391	0.391	0.981	19.447
261.0	7.155	0.703	0.386	0.0222	0.386	0.386	0.980	19.193

TABLE A.III.4 (Continued)

T °C	ln Q	I mol kg^{-1}	$\gamma_\pm$(NaCl)	$\gamma_\pm$(HPO_4^{2-})	$\gamma_\pm$(Na^+)	$\gamma_\pm$(OH^-)	a(H_2O)	ln K
				Na/P=2.5 run 2				
250.0	9.011	0.508	0.438	0.0367	0.438	0.438	0.986	19.464
250.0	9.181	0.493	0.440	0.0375	0.440	0.440	0.986	19.561
250.0	9.277	0.487	0.441	0.0380	0.441	0.441	0.986	19.624
250.0	9.197	0.493	0.440	0.0376	0.440	0.440	0.986	19.572
250.0	9.154	0.496	0.440	0.0374	0.440	0.440	0.987	19.547
275.0	15.032	0.211	0.477	0.0517	0.477	0.477	0.994	24.406
275.0	15.160	0.203	0.481	0.0537	0.481	0.481	0.994	24.418
275.0	15.067	0.206	0.480	0.0529	0.480	0.480	0.994	24.370

TABLE A.III 4 (Continued)

T °C	ln Q	I mol kg^{-1}	$\gamma_\pm$(NaCl)	$\gamma_\pm$(HPO_4^{2-})	$\gamma_\pm$(Na^+)	$\gamma_\pm$(OH^-)	a(H_2O)	ln K
				Na/P=2.5 run 1				
313.0	23.044	0.0644	0.548	0 0904	0.548	0.548	0.998	31 134
313.0	20.762	0.0901	0.500	0.0625	0.500	0.500	0.998	29 809
313.0	20.775	0.0896	0.500	0.0627	0.500	0.500	0.998	29.798
325.0	24.492	0.0525	0.544	0.0873	0.544	0.544	0.999	32.716
325.0	24.725	0.0523	0.549	0.0906	0.549	0.549	0.999	33.237
325.0	24.759	0.0521	0.549	0.0909	0 549	0.549	0.999	33.273
				Na/P=2.5 run 2				
200.0	2.640	1.340	0 468	0 0478	0.468	0.468	0.959	12.230
200.0	2.905	1.295	0.469	0.0484	0.469	0.469	0.960	12.458
200.0	2.477	1.382	0.467	0.0473	0.467	0.467	0.957	12.099
225.0	3.615	1.164	0.425	0.0326	0.425	0.425	0.965	14.429
225.0	3.532	1.174	0.424	0.0324	0.424	0.424	0.965	14.362
225.0	3.423	1.190	0.423	0.0322	0.423	0.423	0.965	14.276
250.0	9.092	0.500	0.439	0.0372	0.439	0.439	0.986	19.505

TABLE A.III.4 (Continued)

T °C	ln Q	I mol kg^{-1}	$\gamma_\pm$(NaCl)	$\gamma_\pm$(HPO_4^{2-})	$\gamma_\pm$(Na^+)	$\gamma_\pm$(OH^-)	a(H_2O)	ln K
				Na/P=3.0 run 1				
273 0	7.986	0.636	0 368	0.0184	0.368	0.368	0.982	20.630
273.0	7.945	0.641	0 367	0.0182	0.367	0.367	0 982	20.613
				Na/P=3 0 run 2				
281.0	9.320	0.527	0 367	0 0181	0.367	0.367	0.986	22 002
291.0	10 934	0 443	0 360	0 0168	0.360	0 360	0.988	23 852
291 0	10.780	0.454	0 358	0 0164	0 358	0.358	0 988	23.784
303 0	12 480	0 378	0.346	0 0143	0 346	0.346	0 990	25 906
303 0	11 810	0 418	0 336	0 0127	0 336	0 336	0 989	25 626

TABLE A III.5 Thermochemical Data for SIHP

$$3Fe_2O_3(s) + 26Na^+ + 12HPO_4^{2-}(aq) + 2OH^-(aq) \rightleftharpoons 6Na_3Fe(PO_4)_2{\cdot}(Na_{4.3}H_{2.3}O)(s) + 5H_2O(l)$$

T °C	ln K	$\Delta_r G°$(experimental) cal mol^{-1}	$\Sigma\Delta_f G^{app}$(other species) cal mol^{-1}	$\Delta_f G^{app}$(SIHP, exp) cal mol^{-1}
		Na/P=2.5 run 1		
220.0	14.484	-14194	850169	-864362
220.0	14.443	-14153	850169	-864322
220.0	14.488	-14198	850169	-864366
220.0	14.257	-13971	850169	-864139
220.0	14.334	-14046	850169	-864215
220.0	14.270	-13985	850169	-864153
240.0	16.973	-17308	849839	-867146
240.0	16.988	-17323	849839	-867161
240.0	17.308	-17649	849839	-867487
240.0	17.272	-17612	849839	-867450
250.0	19.749	-20530	849564	-870093
250.0	18.890	-19638	849564	-869201

TABLE A.III.5 (Continued)

T °C	ln K	$\Delta_f G°$(experimental) cal mol^{-1}	$\Sigma\Delta_f G^{app}$(other species) cal mol^{-1}	$\Delta_f G^{app}$(SIHP, exp) cal mol^{-1}
		Na/P=2.5 run 1		
250.0	18.897	-19645	849564	-869209
250.0	18.908	-19656	849564	-869219
260.0	21.050	-22302	849201	-871502
260.0	20.997	-22245	849201	-871445
260 0	20.973	-22220	849201	-871420
260.0	20.204	-21405	849201	-870605
260.0	20.285	-21491	849201	-870692
260.0	20 257	-21461	849201	-870662
267.0	22 492	-24142	848889	-873029
267.0	22.411	-24056	848889	-872943
267 0	22.411	-24055	848889	-872942
267 0	22.390	-24032	848889	-872919
270 0	22.945	-24756	848738	-873503
270 0	21 478	-23182	848738	-871919

TABLE A.III.5 (Continued)

T °C	ln K	$\Delta_r G^\circ$(experimental) cal mol^{-1}	$\Sigma\Delta_f G^{3PP}$(other species) cal mol^{-1}	$\Delta_f G^{3PP}$(SIHP, exp) cal mol^{-1}
		Na/P=2.5 run 1		
270.0	21.470	-23173	848738	-871910
270.0	21.450	-23152	848738	-871889
282.0	25.049	-27369	848731	-875664
282.0	24.317	-26643	848731	-874856
282.0	24.326	-26655	848731	-874866
290.0	26.454	-29229	847456	-877059
290.0	26.021	-28818	847456	-876574
290.0	25.959	-28748	847456	-876505
293.0	27.816	-30674	847217	-878509
293.0	27.360	-30241	847217	-877996
293.0	27.359	-30237	847217	-877995
303.0	29.968	-33103	846316	-880625
303.0	28.992	-32405	846316	-879508
303.0	28.952	-32382	846316	-879462

TABLE A.III.5 (Continued)

T °C	ln K	$\Delta_f G°$(experimental) cal mol^{-1}	$\Sigma\Delta_f G^{app}$(other species) cal mol^{-1}	$\Delta_f G^{app}$(SIHP, exp) cal mol^{-1}
		Na/P=2.5 run 1		
313.0	31.134	-35706	845235	-881498
313.0	29.809	-34408	845235	-879955
313.0	29.798	-34410	845235	-879941
325.0	32.716	-38289	843640	-882527
325.0	33.237	-38427	843640	-883146
325.0	33.273	-38453	843640	-883188
		Na/P=2.5 run 2		
200.0	12.230	-11499	850266	-861764
200.0	12.458	-11714	850266	-861979
200.0	12.099	-11376	850266	-861641
225.0	14.429	-14284	850111	-864394
225.0	14.362	-14217	850111	-864327
225.0	14.276	-14131	850111	-864242
250.0	19.505	-20277	849564	-869840

TABLE A.III.5 (Continued)

T °C	ln K	$\Delta_r G°$(experimental) cal mol^{-1}	$\Sigma\Delta_f G^{app}$(other species) cal mol^{-1}	$\Delta_f G^{app}$(SIHP, exp) cal mol^{-1}
		Na/P=2.5 run 2		
250.0	19.464	-20235	849564	-869798
250.0	19.561	-20336	849564	-869899
250.0	19.624	-20401	849564	-869964
250.0	19.572	-20347	849564	-869910
250.0	19.547	-20321	849564	-869884
275.0	24.406	-26584	848465	-875048
275.0	24.418	-26598	848465	-875062
275.0	24.370	-26546	848465	-875010

TABLE A.III.5 (Continued)

T °C	ln K	$\Delta_f G°$(experimental) cal mol^{-1}	$\Sigma\Delta_f G^{app}$(other species) cal mol^{-1}	$\Delta_f G^{app}$(SIHP, exp) cal mol^{-1}
		Na/P=3.0 run 1		
200.0	11.246	-10574	850266	-860839
200.0	10.977	-10321	850266	-860587
210.0	10.960	-10523	850243	-860765
210.0	11.081	-10639	850243	-860882
219.0	11.309	-11060	850179	-861239
219.0	11.548	-11294	850179	-861473
230.0	12.426	-12424	850038	-862461
230.0	12.164	-12162	850038	-862199
241.0	16.467	-16825	849815	-866639
241.0	16.178	-16530	849815	-866344
250.0	18.770	-19514	849564	-869077
250.0	18.098	-18814	849564	-868378
261.0	19.447	-20643	849159	-869801
261.0	19.193	-20372	849159	-869531

TABLE A.III.5 (Continued)

T °C	ln K	$\Delta_r G^\circ$(experimental) cal mol^{-1}	$\Sigma\Delta_f G^{app}$(other species) cal mol^{-1}	$\Delta_f G^{app}$(SIHP, exp) cal mol^{-1}
		Na/P=3.0 run 1		
273.0	20.630	-22390	848578	-870967
273.0	20.613	-22372	848578	-870948
		Na/P=3.0 run 2		
281.0	22.002	-24228	848097	-872324
291.0	23.852	-26739	847378	-874116
291.0	23.784	-26664	847378	-874041
303.0	25.900	-29654	846316	-875968
303.0	25.626	-29340	846316	-875655

TABLE A.III.6 Experimental and Fitted Values for SIHP

T /°C	ln K		$\Delta_r G^{app}$(SIHP) /cal mol^{-1}	
	experimental	model	experimental	model
		Na/P=2.5	run 1	
220.0	14.484	13.761	-14194	-13485
220.0	14.443	13.761	-14153	-13485
220.0	14.488	13.761	-14198	-13485
220.0	14.257	13.761	-13971	-13485
220.0	14.334	13.761	-14046	-13485
220.0	14.270	13.761	-13985	-13485
240.0	16.973	16.983	-17308	-17318
240.0	16.988	16.983	-17323	-17318
240.0	17.308	16.983	-17649	-17318
240.0	17.272	16.983	-17612	-17318
250.0	19.749	18.620	-20530	-19357
250.0	18.890	18.620	-19638	-19357
250.0	18.897	18.620	-19645	-19357
250.0	18.908	18.620	-19656	-19357
260.0	21.050	20.286	-22302	-21492
260.0	20.997	20.286	-22245	-21492
260.0	20.973	20.286	-22220	-21492
260.0	20.204	20.286	-21405	-21492
260.0	20.285	20.286	-21491	-21492
260.0	20.257	20.286	-21461	-21492

TABLE A III 6 (Continued)

T /°C	ln K		$\Delta_f G^{app}$(SIHP) /cal mol^{-1}	
	experimental	model	experimental	model
		Na/P=2.5 run 1		
267.0	22.492	21.474	-24142	-23049
267.0	22.411	21.474	-24056	-23049
267.0	22.411	21.474	-24055	-23049
267.0	22.390	21.474	-24032	-23049
270.0	22.945	21.990	-24766	-23734
270.0	21.478	21.990	-23182	-23734
270.0	21.470	21.990	-23173	-23734
270.0	21.450	21.990	-23152	-23734
282.0	25.049	24.099	-27369	-26585
282.0	24.317	24.099	-26643	-26585
282.0	24.326	24.099	-26655	-26585
290.0	26.454	25.553	-29229	-28595
290.0	26.021	25.553	-28818	-28595
290.0	25.959	25.553	-28748	-28595
293.0	27.816	26.109	-30674	-29374
293.0	27.360	26.109	-30241	-29374
293.0	27.359	26.109	-30237	-29374
303.0	29.968	28.015	-33103	-32075
303.0	28.992	28.015	-32405	-32075
303.0	28.952	28.015	-32382	-32075
313.0	31.134	30.016	-35706	-34962
313.0	29.809	30.016	-34408	-34962

TABLE A.III.6 (Continued)

T /°C	ln K		$\Delta_f G^{app}$(SHHP) /cal mol^{-1}	
	experimental	model	experimental	model
		Na/P=2.5	run 1	
313.0	29.798	30.016	-34410	-34962
325.0	32.716	32.584	-38289	-38730
325.0	33.237	32.584	-38427	-38730
325.0	33.273	32.584	-38453	-38730
		Na/P=2.5	run 2	
200.0	12.230	10.552	-11499	-9921
200.0	12.458	10.552	-11714	-9921
200.0	12.099	10.552	-11376	-9921
225.0	14.429	14.562	-14284	-14415
225.0	14.362	14.562	-14217	-14415
225.0	14.276	14.562	-14131	-14415
250.0	19.505	18.620	-20277	-19357
250.0	19.464	18.620	-20235	-19357
250.0	19.561	18.620	-20336	-19357
250.0	19.624	18.620	-20401	-19357
250.0	19.572	18.620	-20347	-19357
250 0	19.547	18.620	-20321	-19357
275.0	24.406	22.859	-26584	-24899
275.0	24.418	22.859	-26598	-24899
275.0	24.370	22.859	-26546	-24899

TABLE A III 6 (Continued)

T /°C	ln K		$\Delta_f G^{app}$(SIHP) /cal mol^{-1}	
	experimental	model	experimental	model
		Na/P=3 0	run 1	
200 0	11.246	10.552	-10574	-9921
200.0	10.977	10.552	-10321	-9921
210.0	10 960	12.158	-10523	-11673
210.0	11.081	12.158	-10639	-11673
219.0	11.309	13 600	-11060	-13301
219.0	11.548	13.600	-11294	-13301
230 0	12 426	15.366	-12424	-15364
230.0	12.164	15.366	-12162	-15364
241.0	16.467	17.146	-16825	-17518
241 0	16.178	17.146	-16530	-17518
250 0	18.770	18 620	-19514	-19357
250.0	18.098	18.620	-18814	-19357
261.0	19.447	20.454	-20643	-21711
261.0	19.193	20.454	-20372	-21711
273.0	20.630	22.510	-22390	-24429
273.0	20.613	22.510	-22372	-24429
		Na/P=3.0	run 2	
281.0	22.002	23.920	-24228	-26340
291.0	23.852	25.737	-26739	-28853
291.0	23.784	25.737	-26664	-28853
303.0	25.900	28.015	-29654	-32075
303 0	25.626	28.015	-29340	-32075

TABLE A.III.4 (Continued)

T °C	ln Q	I mol kg^{-1}	$\gamma_\pm$(NaCl)	$\gamma_\pm$(HPO_4^{2-})	$\gamma_\pm$(Na^+)	$\gamma_\pm$(OH^-)	a(H_2O)	ln K
				Na/P=2.5 run 2				
250.0	9.011	0.508	0.438	0.0367	0.438	0.438	0.986	19.464
250.0	9.181	0.493	0.440	0.0375	0.440	0.440	0.986	19.561
250.0	9.277	0.487	0.441	0.0380	0.441	0.441	0 986	19.624
250 0	9.197	0.493	0.440	0 0376	0.440	0.440	0.986	19.572
250 0	9 154	0.496	0 440	0 0374	0 440	0.440	0.987	19 547
275 0	15.032	0.211	0 477	0.0517	0.477	0 477	0.994	24.406
275 0	15.160	0.203	0 481	0 0537	0.481	0.481	0.994	24 418
275 0	15 067	0.206	0 480	0 0529	0 480	0 480	0.994	24.370

TABLE A.III.4 (Continued)

T °C	ln Q	I mol kg^{-1}	$\gamma_\pm$(NaCl)	$\gamma_\pm$(HPO_4^{2-})	$\gamma_\pm$(Na^+)	$\gamma_\pm$(OH^-)	a(H_2O)	ln K
				Na/P=2.5 run 1				
313.0	23.044	0.0644	0.548	0.0904	0.548	0.548	0.998	31.134
313.0	20.762	0.0901	0.500	0.0625	0.500	0.500	0.998	29.809
313.0	20.775	0.0896	0.500	0.0627	0.500	0.500	0.998	29.798
325.0	24.492	0.0525	0.544	0.0873	0.544	0.544	0.999	32.716
325.0	24.725	0.0523	0.549	0.0906	0.549	0.549	0.999	33.237
325.0	24.759	0.0521	0.549	0.0909	0.549	0.549	0.999	33.273
				Na/P=2.5 run 2				
200.0	2.640	1.340	0.468	0.0478	0.468	0.468	0.959	12.230
200.0	2.905	1.295	0.469	0.0484	0.469	0.469	0.960	12.458
200.0	2.477	1.382	0.467	0.0473	0.467	0.467	0.957	12.099
225.0	3.615	1.164	0.425	0.0326	0.425	0.425	0.965	14.429
225.0	3.532	1.174	0.424	0.0324	0.424	0.424	0.965	14.362
225.0	3.423	1.190	0.423	0.0322	0.423	0.423	0.965	14.276
250.0	9.092	0.500	0.439	0.0372	0.439	0.439	0.986	19.505

TABLE A.III.4 (Continued)

T °C	ln Q	I mol kg^{-1}	$\gamma_\pm$(NaCl)	$\gamma_\pm$(HPO_4^{2-})	$\gamma_\pm$(Na^+)	$\gamma_\pm$(OH^-)	a(H_2O)	ln K
				Na/P=3.0 run 1				
273.0	7.986	0.636	0.368	0.0184	0.368	0.368	0.982	20.630
273.0	7.945	0.641	0.367	0.0182	0.367	0.367	0.982	20.613
				Na/P=3.0 run 2				
281.0	9.320	0.527	0.367	0.0181	0.367	0.367	0.986	22.002
291.0	10.934	0.443	0.360	0.0168	0.360	0.360	0.988	23.852
291.0	10.780	0.454	0.358	0.0164	0.358	0.358	0.988	23.784
303.0	12.480	0.378	0.346	0.0143	0.346	0.346	0.990	25.900
303.0	11.810	0.418	0.336	0.0127	0.336	0.336	0.989	25.626

TABLE A.III.5 Thermochemical Data for SIHP

$$3Fe_2O_3(s) + 26Na^+ + 12HPO_4^{2-}(aq) + 2OH^-(aq) \rightleftharpoons 6Na_3Fe(PO_4)_2\cdot(Na_{4.3}H_{2.3}O)(s) + 5H_2O(l)$$

T °C	ln K	$\Delta_r G°$(experimental) cal mol^{-1}	$\Sigma\Delta_f G^{app}$(other species) cal mol^{-1}	$\Delta_f G^{app}$(SIHP, exp) cal mol^{-1}
		Na/P=2.5 run 1		
220.0	14.484	-14194	850169	-864362
220.0	14.443	-14153	850169	-864322
220.0	14.488	-14198	850169	-864366
220.0	14.257	-13971	850169	-864139
220.0	14.334	-14046	850169	-864215
220.0	14.270	-13985	850169	-864153
240.0	16.973	-17308	849839	-867146
240.0	16.988	-17323	849839	-867161
240.0	17.308	-17649	849839	-867487
240.0	17.272	-17612	849839	-867450
250.0	19.749	-20530	849564	-870093
250.0	18.890	-19638	849564	-869201

TABLE A.III.5 (Continued)

T °C	ln K	$\Delta_f G°$(experimental) cal mol^{-1}	$\Sigma\Delta_f G^{app}$(other species) cal mol^{-1}	$\Delta_f G^{app}$(SIHP, exp) cal mol^{-1}
		Na/P=2.5 run 1		
250.0	18.897	-19645	849564	-869209
250.0	18.908	-19656	849564	-869219
260.0	21.050	-22302	849201	-871502
260.0	20.997	-22245	849201	-871445
260.0	20.973	-22220	849201	-871420
260.0	20.204	-21405	849201	-870605
260.0	20.285	-21491	849201	-870692
260.0	20.257	-21461	849201	-870662
267.0	22.492	-24142	848889	-873029
267.0	22.411	-24056	848889	-872943
267.0	22.411	-24055	848889	-872942
267.0	22.390	-24032	848889	-872919
270.0	22.945	-24756	848738	-873503
270.0	21.478	-23182	848738	-871919

TABLE A.III.5 (Continued)

T °C	ln K	$\Delta_f G°$(experimental) cal mol^{-1}	$\Sigma\Delta_f G^{app}$(other species) cal mol^{-1}	$\Delta_f G^{app}$(SIHP, exp) cal mol^{-1}
		Na/P=2.5 run 1		
270.0	21.470	-23173	848738	-871910
270.0	21.450	-23152	848738	-871889
282.0	25.049	-27369	848731	-875664
282.0	24.317	-26643	848731	-874856
282.0	24.326	-26655	848731	-874866
290.0	26.454	-29229	847456	-877059
290.0	26.021	-28818	847456	-876574
290.0	25.959	-28748	847456	-876505
293.0	27.816	-30674	847217	-878509
293.0	27.360	-30241	847217	-877996
293.0	27.359	-30237	847217	-877995
303.0	29.968	-33103	846316	-880625
303.0	28.992	-32405	846316	-879508
303.0	28.952	-32382	846316	-879462

TABLE A.III.5 (Continued)

T °C	ln K	$\Delta_r G°$(experimental) cal mol^{-1}	$\Sigma\Delta_t G^{app}$(other species) cal mol^{-1}	$\Delta_f G^{app}$(SIHP, exp) cal mol^{-1}
		Na/P=2.5 run 1		
313.0	31.134	-35706	845235	-881498
313.0	29.809	-34408	845235	-879955
313.0	29.798	-34410	845235	-879941
325.0	32.716	-38289	843640	-882527
325.0	33.237	-38427	843640	-883146
325.0	33.273	-38453	843640	-883188
		Na/P=2.5 run 2		
200.0	12.230	-11499	850266	-861764
200.0	12.458	-11714	850266	-861979
200.0	12.099	-11376	850266	-861641
225.0	14.429	-14284	850111	-864394
225.0	14.362	-14217	850111	-864327
225.0	14.276	-14131	850111	-864242
250.0	19.505	-20277	849564	-869840

TABLE A.III.5 (Continued)

T °C	ln K	$\Delta_r G^\circ$(experimental) cal mol^{-1}	$\Sigma\Delta_f G^{app}$(other species) cal mol^{-1}	$\Delta_f G^{app}$(SIHP, exp) cal mol^{-1}
		Na/P=2.5 run 2		
250.0	19.464	-20235	849564	-869798
250.0	19.561	-20336	849564	-869899
250.0	19.624	-20401	849564	-869964
250.0	19.572	-20347	849564	-869910
250.0	19.547	-20321	849564	-869884
275.0	24.406	-26584	848465	-875048
275.0	24.418	-26598	848465	-875062
275.0	24.370	-26546	848465	-875010

TABLE A.III.5 (Continued)

T °C	ln K	$\Delta_f G°$(experimental) cal mol^{-1}	$\Sigma\Delta_f G^{app}$(other species) cal mol^{-1}	$\Delta_f G^{app}$(SIHP, exp) cal mol^{-1}
		Na/P=3.0 run 1		
200.0	11.246	-10574	850266	-860839
200.0	10.977	-10321	850266	-860587
210.0	10.960	-10523	850243	-860765
210.0	11.081	-10639	850243	-860882
219.0	11.309	-11060	850179	-861239
219.0	11.548	-11294	850179	-861473
230.0	12.426	-12424	850038	-862461
230.0	12.164	-12162	850038	-862199
241.0	16.467	-16825	849815	-866639
241.0	16.178	-16530	849815	-866344
250.0	18.770	-19514	849564	-869077
250.0	18.098	-18814	849564	-868378
261.0	19.447	-20643	849159	-869801
261.0	19.193	-20372	849159	-869531

TABLE A.III.5 (Continued)

T °C	ln K	$\Delta_f G^\circ$(experimental) cal mol^{-1}	$\Sigma\Delta_f G^{app}$(other species) cal mol^{-1}	$\Delta_f G^{app}$(SIHP, exp) cal mol^{-1}
		Na/P=3.0 run 1		
273.0	20.630	-22390	848578	-870967
273.0	20.613	-22372	848578	-870948
		Na/P=3.0 run 2		
281.0	22.002	-24228	848097	-872324
291.0	23.852	-26739	847378	-874116
291.0	23.784	-26664	847378	-874041
303.0	25.900	-29654	846316	-875968
303.0	25.626	-29340	846316	-875655

TABLE A.III.6 Experimental and Fitted Values for SIHP

T /°C	ln K		$\Delta_f G^{app}$(SIHP) /cal mol^{-1}	
	experimental	model	experimental	model
		Na/P=2.5	run 1	
220.0	14.484	13.761	-14194	-13485
220.0	14.443	13.761	-14153	-13485
220.0	14.488	13.761	-14198	-13485
220.0	14.257	13.761	-13971	-13485
220.0	14.334	13.761	-14046	-13485
220.0	14.270	13.761	-13985	-13485
240.0	16.973	16.983	-17308	-17318
240.0	16.988	16.983	-17323	-17318
240.0	17.308	16.983	-17649	-17318
240.0	17.272	16.983	-17612	-17318
250.0	19.749	18.620	-20530	-19357
250.0	18.890	18.620	-19638	-19357
250.0	18.897	18.620	-19645	-19357
250.0	18.908	18.620	-19656	-19357
260.0	21.050	20.286	-22302	-21492
260.0	20.997	20.286	-22245	-21492
260.0	20.973	20.286	-22220	-21492
260.0	20.204	20.286	-21405	-21492
260.0	20.285	20.286	-21491	-21492
260.0	20.257	20.286	-21461	-21492

TABLE A.III 6 (Continued)

T /°C	ln K		$\Delta_f G^{app}$(SIHP) /cal mol^{-1}	
	experimental	model	experimental	model
		Na/P=2.5 run 1		
267.0	22.492	21.474	-24142	-23049
267.0	22.411	21.474	-24056	-23049
267.0	22.411	21.474	-24055	-23049
267.0	22.390	21.474	-24032	-23049
270.0	22.945	21.990	-24766	-23734
270.0	21.478	21.990	-23182	-23734
270.0	21.470	21.990	-23173	-23734
270.0	21.450	21.990	-23152	-23734
282.0	25.049	24.099	-27369	-26585
282.0	24.317	24.099	-26643	-26585
282.0	24.326	24.099	-26655	-26585
290.0	26.454	25.553	-29229	-28595
290.0	26.021	25.553	-28818	-28595
290.0	25.959	25.553	-28748	-28595
293.0	27.816	26.109	-30674	-29374
293.0	27.360	26.109	-30241	-29374
293.0	27.359	26.109	-30237	-29374
303.0	29.968	28.015	-33103	-32075
303.0	28.992	28.015	-32405	-32075
303.0	28.952	28.015	-32382	-32075
313.0	31.134	30.016	-35706	-34962
313.0	29.809	30.016	-34408	-34962

TABLE A.III.6 (Continued)

T /°C	ln K		$\Delta_f G^{app}$(SHIP) /cal mol^{-1}	
	experimental	model	experimental	model
		Na/P=2.5	run 1	
313.0	29.798	30.016	-34410	-34962
325.0	32.716	32.584	-38289	-38730
325.0	33.237	32.584	-38427	-38730
325.0	33.273	32.584	-38453	-38730
		Na/P=2.5	run 2	
200.0	12.230	10.552	-11499	-9921
200.0	12.458	10.552	-11714	-9921
200.0	12.099	10.552	-11376	-9921
225.0	14.429	14.562	-14284	-14415
225.0	14.362	14.562	-14217	-14415
225.0	14.276	14.562	-14131	-14415
250.0	19.505	18.620	-20277	-19357
250.0	19.464	18.620	-20235	-19357
250.0	19.561	18.620	-20336	-19357
250.0	19.624	18.620	-20401	-19357
250.0	19.572	18.620	-20347	-19357
250 0	19.547	18.620	-20321	-19357
275.0	24.406	22.859	-26584	-24899
275.0	24.418	22.859	-26598	-24899
275.0	24.370	22.859	-26546	-24899

TABLE A III.6 (Continued)

T /°C	ln K		$\Delta_f G^{app}$(SHP) /cal mol^{-1}	
	experimental	model	experimental	model
		Na/P=3.0	run 1	
200.0	11.246	10.552	-10574	-9921
200.0	10.977	10.552	-10321	-9921
210.0	10.960	12.158	-10523	-11673
210.0	11.081	12.158	-10639	-11673
219.0	11.309	13 600	-11060	-13301
219.0	11.548	13.600	-11294	-13301
230 0	12 426	15.366	-12424	-15364
230.0	12.164	15.366	-12162	-15364
241.0	16.467	17.146	-16825	-17518
241 0	16.178	17.146	-16530	-17518
250 0	18.770	18 620	-19514	-19357
250.0	18.098	18.620	-18814	-19357
261.0	19.447	20.454	-20643	-21711
261.0	19.193	20.454	-20372	-21711
273.0	20.630	22.510	-22390	-24429
273.0	20.613	22.510	-22372	-24429
		Na/P=3.0	run 2	
281.0	22.002	23.920	-24228	-26340
291.0	23.852	25.737	-26739	-28853
291.0	23.784	25.737	-26664	-28853
303.0	25.900	28.015	-29654	-32075
303 0	25.626	28.015	-29340	-32075